

THESIS

2
(1999)



This is to certify that the

dissertation entitled

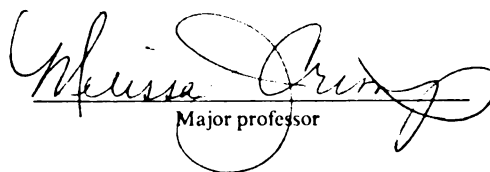
COLLOIDAL PROCESSING OF SiCw/Al₂O₃ CERAMIC MATRIX COMPOSITES

presented by

Mingli Zhang

has been accepted towards fulfillment
of the requirements for

DOCTOR OF PHILOSOPHY degree in MATERIALS SCIENCE
AND MECHANICS



Major professor

Date November 25, 1998

PLACE IN RETURN BOX to remove this checkout from your record.
TO AVOID FINES return on or before date due.
MAY BE RECALLED with earlier due date if requested.

DATE DUE	DATE DUE	DATE DUE
<hr/>	<hr/>	<hr/>
<hr/>	<hr/>	<hr/>
<hr/>	<hr/>	<hr/>
<hr/>	<hr/>	<hr/>
<hr/>	<hr/>	<hr/>

COLLOIDAL PROCESSING OF SiC_w/Al₂O₃ CERAMIC MATRIX COMPOSITES

By

Mingli Zhang

A DISSERTATION

**Submitted to
Michigan State University
in partial fulfillment of the requirements
for the degree of**

DOCTOR OF PHILOSOPHY

Department of Materials Science and Mechanics

1998

ABSTRACT

COLLOIDAL PROCESSING OF SiC_w/Al₂O₃ CERAMIC MATRIX COMPOSITES

By

Mingli Zhang

By manipulating the interparticle forces of ceramic colloidal systems, suspensions of different dispersing abilities were obtained. Changing the concentration of ionic species, pH, polyelectrolyte and the solution altered the net interparticle force. The zeta potentials of single component suspensions of varying concentration of ionic species, polyelectrolyte addition, pH and solution (electrolyte, ethanol, or a mixture of electrolyte and ethanol) were measured. The stability ratio, W , which measures the effectiveness of the potential barrier in preventing the particles from coagulation, and the interaction between the components were discussed. SiC whisker reinforced Al₂O₃ suspensions were slip cast at different processing conditions (SiC whisker volume fraction, solids loading, ball milling, sintering aids, polyelectrolyte and pH). Green specimens were cold-isostatically pressed and pressureless sintered in a flowing nitrogen atmosphere.

Homogeneous SiC_w/Al₂O₃ green bodies with densities of 2.55 ± 0.07 g/cm³ (~65% theoretical density) were obtained. Bulk densities of 3.80 ± 0.06 g/cm³ (96% theoretical density), 3.79 ± 0.06 g/cm³ (97% theoretical density), and 3.40 ± 0.07 g/cm³ (89% theoretical density) were obtained at 1600°C for composite samples containing 5, 10 and 20 vol% SiC whiskers, respectively. Bulk densities of the 10 vol% SiC_w/Al₂O₃ composites were 3.79 ± 0.06 g/cm³ at pH 11 and 3.66 ± 0.07 g/cm³ at pH 4, respectively. pH 11 was determined to be the optimum processing pH for SiC_w/Al₂O₃ composites with

sintering aids (2 wt% Y_2O_3 and 0.5 wt% MgO) and 2.5 vol% polyelectrolyte (Ammonia salt of a polymeric carboxylic acid). The final microstructure revealed homogeneous and near fully densified composites. Compositions of the composites were characterized using Energy Dispersive X-ray Spectrum (EDX).

The effect of the aspect ratio of SiC whisker, the Y_2O_3 content and the choice of polyelectrolyte were examined. The whisker aspect ratio reduction had a more dramatic effect on achieving dense composites in 20 vol% SiC whisker when compared to 5 or 10 vol% SiC whisker composites. High densities with 10 vol% SiC whisker were attainable without aspect ratio reduction. Sintered densities increased with increasing Y_2O_3 content. For 10 vol% SiC_w/ Al₂O₃, the densities remained almost constant at Y_2O_3 additions greater than 0.5 wt%. 2.5 vol% polyelectrolyte stabilized the suspension and resulted in high composite densities. However, further addition of polyelectrolyte, past the adsorption saturation limit, served to leave excess polyelectrolyte in suspension. This excess polyelectrolyte lowered the composite density due to depletion flocculation. Sintered densities of 10 vol% SiC_w/Al₂O₃ composites slip cast from a mixture of ethanol and water were only $2.92 \pm 0.08 \text{ g/cm}^3$ (75% theoretical density).

The fracture toughness of Al₂O₃ was remarkably improved with increasing whisker content. The fracture toughness of 20 vol% SiC_w/Al₂O₃ composite was twice the fracture toughness of the unreinforced Al₂O₃ matrix.

**To my mother and my daughter,
whose love and support is the source of my strength**

ACKNOWLEDGMENTS

I wish to express my sincere appreciation to Dr. M. J. Crimp, my advisor, for her guidance throughout my doctoral studies and reviews of my dissertation. I would also like to thank Dr. E. D. Case for his guidance in hardness and fracture toughness measurements and sample preparation, his generosity for letting me use his Indentation Tester and his encouragement. I would also like to thank Dr. H. Eick for his corrections on my dissertation and his suggestion to have a committee meeting to discuss my dissertation and to provide an opportunity for me to get help from all the committee members. I would also like to thank Dr. P. Kwon for being my committee member. I appreciate all the committee members, for their precious time on reviewing my dissertation, attending the comprehensive and oral examinations.

I also wish to thank the following group of people: D. Oppermann for providing help in CIP and furnace equipment, B. Wilson for his help in ESA and EDX measurements, Michelle for her proofreading the last part of my dissertation, and all the help and friendship from other fellow graduate students.

TABLE OF CONTENTS

LIST OF TABLES.....	ix
LIST OF FIGURES.....	x
INTRODUCTION.....	1
CHAPTER 1 LITERATURE REVIEW.....	6
1.1 Theory of Colloidal Stability.....	6
1.1.1 Electrostatic Repulsion.....	6
1.1.2 Van Der Waals Attraction.....	10
1.1.3 Stability Ratio.....	11
1.1.4 Refinements of DLVO Theory.....	13
1.2 Processing Techniques of Ceramic Matrix Composites.....	16
CHAPTER 2 EXPERIMENTAL PROCEDURES.....	25
2.1 Materials.....	25
2.2 Zeta Potential Measurement.....	25
2.3 Viscosity Measurement.....	28
2.4 Sedimentation Experiment.....	28
2.5 Stability Ratio Calculation.....	28
2.6 Dispersion and Slip Casting.....	29
2.7 Sintering.....	31
2.8 Microstructure and Composition.....	31
2.9 Density Measurement.....	32
2.10 Hardness and Fracture Toughness Measurement.....	32

CHAPTER 3 RESULTS AND DISCUSSION.....	34
3.1 Summary and Overview of Research Approaches.....	34
3.2 Colloidal Stability and Suspension Parameters of SiC_w/Al₂O₃ in Aqueous and Nonaqueous System.....	37
3.2.1 Zeta Potential.....	37
3.2.2 Stability Ratio.....	43
3.2.3 Viscosity.....	50
3.2.4 Sedimentation Bulk Density.....	50
3.2.5 Microstructure.....	53
3.2.6 Conclusions.....	53
3.3 Colloidal Processing of SiC_w/Al₂O₃ Composites.....	57
3.3.1 Monolithic Alumina.....	57
3.3.2 Processing of SiC _w /Al ₂ O ₃ Composites in Aqueous System.....	59
3.3.3 Processing of SiC _w /Al ₂ O ₃ Composites in Nonaqueous System.....	65
3.3.4 Discussion and New Approaches.....	71
3.4 Densification of SiC_w/Al₂O₃ Composites through Improved Processing Approaches.....	72
3.4.1 Colloidal Processing Combined with Mechanical Methods.....	72
3.4.2 Sintering Aids.....	78
3.4.3 Polyelectrolyte.....	82
3.4.4 Discussion.....	92

3.5 Improved Properties of SiC _w /Al ₂ O ₃ Composites.....	93
3.5.1 Sintered Density.....	93
3.5.2 Microstructure and EDX Analysis.....	98
3.5.3 Hardness and Fracture Toughness.....	110
CHAPTER 4 CONCLUSIONS.....	125
REFERENCES.....	128

LIST OF TABLES

Table 1 Composite processing and mechanical properties.....	20
Table 2 Major characteristics of Tokai TWS-100 SiC whisker, Sumitomo AKP-30 and AKP-50 alumina powder and Y ₂ O ₃ powder [44].....	27
Table 3 Stable pH range in various media.....	49
Table 4 Compatibility of stable pH range for different components in aqueous media	83
Table 5 Compatibility of stable pH range for different components in 99% ethanol and 1% electrolyte.....	83
Table 6 Comparison of polyelectrolyte addition to iep and ζ-potential for Al ₂ O ₃	86
Table 7 Comparison of iso-electric point of Al ₂ O ₃ between this research and published data [26,30]	86
Table 8 EDX composition of 10 and 20 vol% SiC _w /Al ₂ O ₃ composites.....	98
Table 9 Different grain sizes for the 5 and 20 vol% SiC _w loading.....	105

LIST OF FIGURES

Figure 1 A schematic diagram of an agglomerate in an array of particles [4]	2
Figure 2 Defects originating from agglomerates caused by a) agglomerate sintering faster than the matrix and b) matrix sintering faster than the agglomerate [5].....	3
Figure 3 Incompatible shrinkage between the matrix and dispersed whiskers [4]	4
Figure 4 Model of charged spherical particles in a liquid indicating potential distribution $\Phi(r)$, where r is distance [12].....	8
Figure 5 Schematic of the interaction energy as a function of separation between two particles in suspension [11].....	12
Figure 6 Model for treating the effect of adsorbed polymer on zeta-potential. The model allows for the possibility of a shift in the shear plane as well as a modified ion distribution in the diffuse layer [25].....	15
Figure 7 Plot of ζ versus pH showing the location of the iso-electric point (i.e.p.) and the regions of stability [29].....	18
Figure 8 The properties of ceramic product [40].....	24
Figure 9 Relationship between different parts of the ceramic process [43].....	24
Figure 10 A flow chart of experimental procedures.....	26
Figure 11 The processing approach of high performance ceramic composites. Improved performance is achieved through controlled processing approaches. *Density, Fracture Toughness, Hardness.....	36
Figure 12 Zeta potential of Al_2O_3 versus pH at different electrolyte strengths.....	38
Figure 13 Zeta potential of SiC_w versus pH at different electrolyte strengths.....	39
Figure 14 Zeta potential versus pH for SiC_w at varying ratios of ethanol to electrolyte under 0.001N KNO_3 and 0.5 vol% solids content.....	41
Figure 15 Zeta potential versus pH for Al_2O_3 at varying ratios of ethanol to electrolyte under 0.001N KNO_3 and 0.5 vol% solids content.....	42

Figure 16 Stability ratio versus pH for SiC _w /Al ₂ O ₃ in 0.001N KNO ₃ and ethanol:electrolyte (0:1).....	44
Figure 17 Stability ratio versus pH for SiC _w /Al ₂ O ₃ in 0.001N KNO ₃ and ethanol:electrolyte (1:4).....	45
Figure 18 Stability ratio versus pH for SiC _w /Al ₂ O ₃ in 0.001N KNO ₃ and ethanol:electrolyte (1:1).....	46
Figure 19 Stability ratio versus pH for SiC _w /Al ₂ O ₃ in 0.001N KNO ₃ and ethanol:electrolyte (4:1).....	47
Figure 20 Stability ratio versus pH for SiC _w /Al ₂ O ₃ in 0.001N KNO ₃ and ethanol:electrolyte (99:1).....	48
Figure 21 Viscosity of 10 vol% SiC _w /Al ₂ O ₃ with 40 wt% solids content at varying ratios of ethanol to electrolyte.....	51
Figure 22 Sedimentation bulk density versus pH for Al ₂ O ₃ and SiC _w in electrolyte and ethanol, respectively (0.001N KNO ₃).....	52
Figure 23 SEM photomicrographs of 10 vol% SiC _w /Al ₂ O ₃ green body in a) electrolyte, b) ethanol:electrolyte (1:1), and c) ethanol:electrolyte (99:1) (0.001N KNO ₃ , non-ball-milled, pH 4, no polyelectrolyte and sintering aids).....	54
Figure 24 SEM photomicrographs of 10 vol% SiC _w /Al ₂ O ₃ partially sintered samples: a) electrolyte, b) ethanol:electrolyte (1:1) (0.001N KNO ₃ , non-ball-milled, pH 4, no polyelectrolyte and sintering aids, sintered at 1650°C for 1h, nitrogen atmosphere).....	56
Figure 25 Colloidal processing approaches.....	58
Figure 26 SEM photomicrographs of green microstructures of 10 vol% SiC _w /Al ₂ O ₃ composite processed from different pHs: a) pH 2, b) pH 3, c) pH 4, d) pH 8, e) pH 10, and f) pH 11 (0.001N KNO ₃ , non-ball-milled, no polyelectrolyte and sintering aids).....	60
Figure 27 SEM photomicrographs of sintered microstructures: a) 5 vol% SiC _w /Al ₂ O ₃ and b) 10 vol% SiC _w /Al ₂ O ₃ . Sintered at 1650°C for 1h, nitrogen atmosphere (0.001N KNO ₃ , non-ball-milled, pH 4, no polyelectrolyte and sintering aids).....	63
Figure 28 Green density versus whisker loading (0.001N KNO ₃ , non-ball-milled, pH 4, no polyelectrolyte and sintering aids).....	64

Figure 29 SEM photomicrographs showing the green microstructures of 10 vol% SiC _w /Al ₂ O ₃ composites: a) 100% electrolyte, b) ethanol:electrolyte (1:4), c) ethanol:electrolyte (1:1), d) ethanol:electrolyte (4:1) and e) ethanol:electrolyte (99:1) (0.001N KNO ₃ , non-ball-milled, pH 4, no polyelectrolyte and sintering aids)	66
Figure 30 SEM photomicrographs of sintered microstructures of 10 vol% SiC _w /Al ₂ O ₃ . a) electrolyte and b) ethanol:electrolyte (1:1) (0.001N KNO ₃ , non-ball-milled, pH 4, no polyelectrolyte and sintering aids, sintered at 1650°C for 1h, N ₂)	69
Figure 31 Green density variation of 10 vol% SiC _w /Al ₂ O ₃ at different ratios of ethanol to electrolyte (0.001N KNO ₃ , non-ball-milled, pH 4, no polyelectrolyte and sintering aids)	70
Figure 32 Green density of 5 and 10 vol% SiC _w /Al ₂ O ₃ as a function of ball milling time (0.001N KNO ₃ , ball-milled, pH 4, no polyelectrolyte and sintering aids)	73
Figure 33 Sintered density of 5 and 10 vol% SiC _w /Al ₂ O ₃ as a function of ball milling hour (0.001N KNO ₃ , ball-milled, pH 4, no polyelectrolyte and sintering aids, sintered at 1600°C for 1h, nitrogen atmosphere)	74
Figure 34 Green density of 5 and 10 vol% SiC _w /Al ₂ O ₃ as a function of solids loading (0.001N KNO ₃ , non-ball-milled, pH 4, no polyelectrolyte and sintering aids)	76
Figure 35 Sintered density of 5 and 10 vol% SiC _w /Al ₂ O ₃ as a function of solids loading (0.001N KNO ₃ , non-ball-milled, pH 4, no polyelectrolyte and sintering aids, sintered at 1600°C for 1h, nitrogen atmosphere)	77
Figure 36 The Al ₂ O ₃ -Y ₂ O ₃ -SiO ₂ phase diagram [63]	79
Figure 37 Green density of 5 and 10 vol% SiC _w /Al ₂ O ₃ as a function of Y ₂ O ₃ content (0.001N KNO ₃ , ball-milled, pH 11, 2.5 vol% polyelectrolyte)	80
Figure 38 Sintered density of 5 and 10 vol% SiC _w /Al ₂ O ₃ as a function of Y ₂ O ₃ content (0.001N KNO ₃ , ball-milled, pH 11, 2.5 vol% polyelectrolyte, sintered at 1600°C for 1h, nitrogen atmosphere)	81
Figure 39 Zeta potential for Al ₂ O ₃ versus pH at different polyelectrolyte concentrations (0.001N KNO ₃)	85

Figure 40 Green density of 10 and 20 vol% SiC _w /Al ₂ O ₃ as a function of polyelectrolyte concentration (0.001N KNO ₃ , ball-milled, pH 11, 0.5 wt% MgO and 2 wt% Y ₂ O ₃).....	88
Figure 41 Sintered density of 10 and 20 vol% SiC _w /Al ₂ O ₃ as a function of polyelectrolyte concentration (0.001N KNO ₃ , ball-milled, pH 11, 0.5 wt% MgO and 2 wt% Y ₂ O ₃ , sintered at 1600°C for 1h, nitrogen atmosphere).....	89
Figure 42 Green density of 10 and 20 vol% SiC _w /Al ₂ O ₃ as a function of ball milling hour (0.001N KNO ₃ , ball-milled, pH 11, 2.5 vol% polyelectrolyte, 0.5 wt% MgO and 2 wt% Y ₂ O ₃).....	90
Figure 43 Sintered density of 10 and 20 vol% SiC _w /Al ₂ O ₃ as a function of ball milling hour (0.001N KNO ₃ , ball-milled, pH 11, 2.5 vol% polyelectrolyte, 0.5 wt% MgO and 2 wt% Y ₂ O ₃ , sintered at 1600°C for 1h, nitrogen atmosphere).....	91
Figure 44 Green and sintered density of 10 vol% SiC _w /Al ₂ O ₃ as a function of pH (0.001N KNO ₃ , ball-milled, 2.5 vol% polyelectrolyte, 0.5 wt% MgO and 2 wt% Y ₂ O ₃ , sintered at 1600°C for 1h, nitrogen atmosphere).	94
Figure 45 Comparison of sintered density of SiC _w /Al ₂ O ₃ composites between this research and other published results [3,54,73]	95
Figure 46 The sinterd density versus the green density (5-20 vol% SiC _w /Al ₂ O ₃ , 0.001N KNO ₃ , ball-milled, pH 11, 2.5 vol% polyelectrolyte, 0.5 wt% MgO and 2 wt% Y ₂ O ₃ , sintered at 1600°C for 1h, nitrogen atmosphere).....	97
Figure 47 EDX composition spectra: a) 10 vol% SiC _w /Al ₂ O ₃ , b) 20 vol% SiC _w /Al ₂ O ₃ (0.001N KNO ₃ , ball-milled, pH 11, 2.5 vol% polyelectrolyte, 0.5 wt% MgO and 2 wt% Y ₂ O ₃ , sintered at 1600°C for 1h, nitrogen atmosphere).....	99
Figure 48 SEM photomicrograph of the fracture surface of 5 vol% SiC _w /Al ₂ O ₃ (0.001N KNO ₃ , non-ball-milled, pH 4, no polyelectrolyte and sintering aids, sintered at 1600°C for 1h, nitrogen atmosphere).....	101
Figure 49 SEM photomicrograph of fracture surface of 10 vol% SiC _w /Al ₂ O ₃ (0.001N KNO ₃ , ball-milled, pH 11, 2.5 vol% polyelectrolyte, 0.5 wt% MgO and 2 wt% Y ₂ O ₃ , sintered at 1600°C for 2h, nitrogen atmosphere).....	102
Figure 50 SEM photomicrograph of fracture surface of 20 vol% SiC _w /Al ₂ O ₃ (0.001N KNO ₃ , ball-milled, pH 11, 2.5 vol% polyelectrolyte, 0.5 wt% MgO and 2 wt% Y ₂ O ₃ , sintered at 1600°C for 4h, nitrogen flow)	103

Figure 51 SEM photomicrograph of fracture surface of 20 vol% SiC _w /Al ₂ O ₃ (0.001N KNO ₃ , non-ball-milled, pH 11, 2.5 vol% polyelectrolyte, 0.5 wt% MgO and 2 wt% Y ₂ O ₃ , sintered at 1600°C for 4h, nitrogen atmosphere).....	104
Figure 52 SEM photomicrograph of the fracture surface of 5 vol% SiC _w /Al ₂ O ₃ (0.001N KNO ₃ , non-ball-milled, pH 4, no polyelectrolyte and sintering aids, sintered at 1600°C for 1h, nitrogen atmosphere).....	106
Figure 53 SEM photomicrograph of the fracture surface of 20 vol% SiC _w /Al ₂ O ₃ (0.001N KNO ₃ , ball-milled, pH 11, 2.5 vol% polyelectrolyte, 0.5 wt% MgO and 2 wt% Y ₂ O ₃ , sintered at 1600°C for 4h, nitrogen atmosphere).....	107
Figure 54 SEM photomicrograph of the fracture surface of 20 vol% SiC _w /Al ₂ O ₃ (0.001N KNO ₃ , ball-milled, pH 11, 2.5 vol% polyelectrolyte, 0.5 wt% MgO and 2 wt% Y ₂ O ₃ , sintered at 1600°C for 4h, nitrogen flow)	108
Figure 55 SEM photomicrograph of the fracture surface of 20 vol% SiC _w /Al ₂ O ₃ (0.001N KNO ₃ , non-ball-milled, pH 11, 2.5 vol% polyelectrolyte, 0.5 wt% MgO and 2 wt% Y ₂ O ₃ , sintered at 1600°C for 4h, nitrogen atmosphere).....	109
Figure 56 K _{IC} of composites versus whisker loading showing the comparison between this research and other published results [3, 74].....	111
Figure 57 Hardness of composites versus whisker loading (0.001N KNO ₃ , ball-milled, pH 11, 2.5 vol% polyelectrolyte, 0.5 wt% MgO and 2 wt% Y ₂ O ₃ , sintered at 1600°C for 1h, nitrogen atmosphere).....	112
Figure 58 Comparison of K _{IC} of 20 vol% SiC _w composites with ball milling and without ball milling (0.001N KNO ₃ , pH 11, 2.5 vol% polyelectrolyte, 0.5 wt% MgO and 2 wt% Y ₂ O ₃ , sintered at 1600°C for 1h, nitrogen atmosphere).....	113
Figure 59 Comparison of Hardness of 10 and 20 vol% SiC _w composites with ball milling and without ball milling (0.001N KNO ₃ , pH 11, 2.5 vol% polyelectrolyte, 0.5 wt% MgO and 2 wt% Y ₂ O ₃ , sintered at 1600°C for 1h, nitrogen atmosphere).....	114
Figure 60 SEM photomicrographs of the fracture surface of 10 vol% SiC _w /Al ₂ O ₃ showing (a) long whisker protruding length and (b) deep whisker pullout holes (0.001N KNO ₃ , ball-milled, pH 11, 2.5 vol% polyelectrolyte, 0.5 wt% MgO and 2 wt% Y ₂ O ₃ , sintered at 1600°C for 1h, nitrogen atmosphere).....	116

Figure 61 Hardness of 10 vol% SiC _w /Al ₂ O ₃ as a function of pH (0.001N KNO ₃ , ball-milled, no polyelectrolyte and sintering aids at pH 4 and 2.5 vol% polyelectrolyte and 2 wt% Y ₂ O ₃ at pH 11, sintered at 1600°C for 1h, nitrogen atmosphere).....	117
Figure 62 Hardness of 10 vol% SiC _w /Al ₂ O ₃ as a function of Y ₂ O ₃ content (0.001N KNO ₃ , ball-milled, pH 11, 2.5 vol% polyelectrolyte, sintered at 1600°C for 1h, nitrogen atmosphere).....	118
Figure 63 Hardness of 10 vol% SiC _w /Al ₂ O ₃ as a function of density (0.001N KNO ₃ , ball-milled, pH 11, 2.5 vol% polyelectrolyte, 0.5 wt% MgO and 2 wt% Y ₂ O ₃ , sintered at 1600°C for 1h, nitrogen atmosphere).....	119
Figure 64 Hardness of 10 vol% SiC _w /Al ₂ O ₃ as a function of ball milling time (0.001N KNO ₃ , ball-milled, pH 4, no polyelectrolyte and sintering aids, sintered at 1600°C for 1h, nitrogen atmosphere).....	120
Figure 65 Hardness of 10 vol% SiC _w /Al ₂ O ₃ as a function of polyelectrolyte concentration (0.001N KNO ₃ , ball-milled, pH 11, 0.5 wt% MgO and 2 wt% Y ₂ O ₃ , sintered at 1600°C for 1h, nitrogen atmosphere).....	122
Figure 66 Hardness of 10 vol% SiC _w /Al ₂ O ₃ as a function of solids loading (0.001N KNO ₃ , non-ball-milled, pH 4, no polyelectrolyte and sintering aids, sintered at 1600°C for 1h, nitrogen atmosphere).....	123
Figure 67 K _{IC} and hardness of sintered composites versus the green density of their green bodies, respectively (5-20 vol% SiC _w /Al ₂ O ₃ , 0.001N KNO ₃ , ball-milled, pH11, 2.5 vol% polyelectrolyte, 0.5 wt% MgO and 2 wt% Y ₂ O ₃ , sintered at 1600°C for 1h, nitrogen atmosphere)	124

INTRODUCTION

The brittleness of alumina ceramics limits their application as structural materials. Reinforcement of alumina with SiC whiskers can improve the fracture toughness [1-3]. The most common consolidation method for ceramic powders is via dry pressing. Since dry powders are naturally agglomerated, these agglomerates produce large, crack-like voids during densification, which can be a major strength degrading flaw. The agglomerates pack together during consolidation to produce compacts with differentials in packing density leading to poor densification.

Figure 1 is a schematic showing an agglomerate in an array of particles [4]. The differential shrinkage during sintering results in defects originating from agglomerates (circumferential cracks and radial cracks in Figure 2). For whisker or fiber reinforced composites, the incompatible sintering between the matrix and dispersed whiskers or fibers is more serious (pore, crack and whisker bending in Figure 3). Since it is considerably difficult to obtain homogeneous matrix packing between whiskers, there will commonly be inhomogeneous shrinkage between whiskers resulting in bending (exaggerated) of one or both whiskers [4].

Often combined with dry processing, dry milling is used to help mix and add various organics such as binders. The dry milling process introduces contaminates, large inclusions and whisker damage. The elimination of polymer binders is not only time consuming (days) but can also produce disruptive phenomena. Conventional powder processing also causes poorly distributed second phases and particle packing that encourages abnormal grain growth. Furthermore, the resultant components that have been received

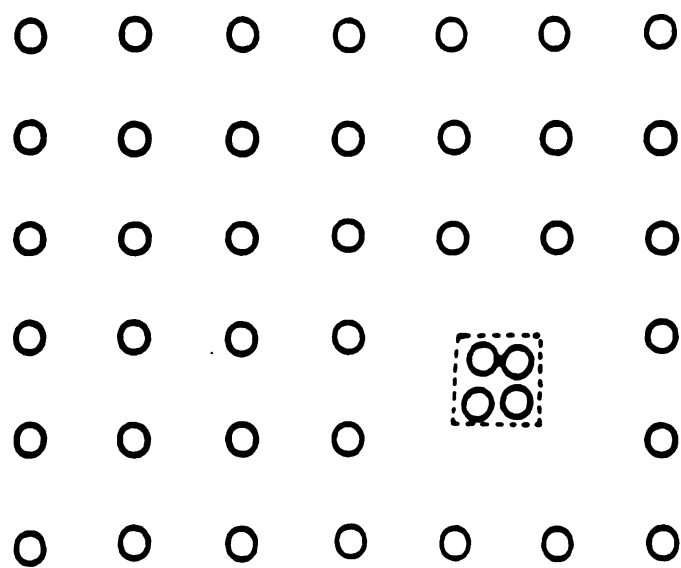
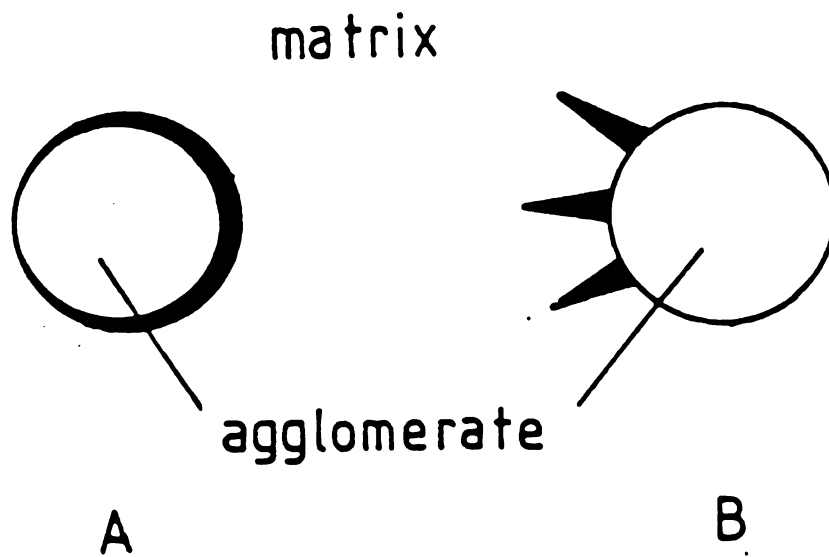


Figure 1 A schematic diagram of an agglomerate in an array of particles [4].



**Figure 2 Defects originating from agglomerates caused by
a) agglomerate sintering faster than the matrix and
b) matrix sintering faster than the agglomerate [5].**

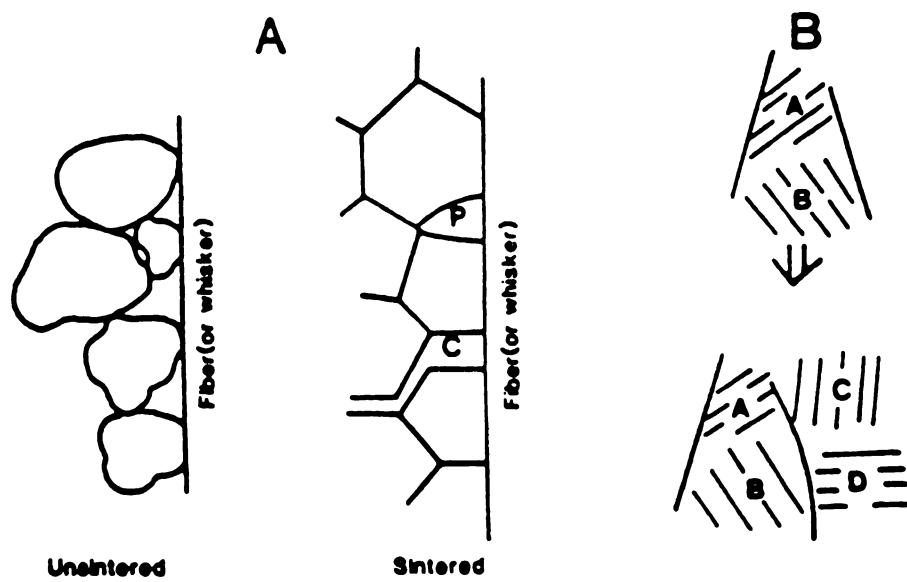


Figure 3 Incompatible shrinkage between the matrix and dispersed whiskers [4].

hot-pressed have anisotropic properties due to the partial planar whisker orientation developed during the hot pressing [6].

The purpose of this research was to determine the optimum conditions for particle/whisker codispersion, consolidation and sintering densification of optimized green bodies. By colloidal processing, stable, binder free, homogeneous suspensions and green bodies at various processing parameters (SiC whisker volume fraction, solids loading, ball milling time, sintering aid content, polyelectrolyte content and pH) are produced. These homogeneous green bodies are pressurelessly sintered at relatively low sintering temperatures and short sintering times. The final microstructure and composition are characterized. The final ceramic matrix composites exhibit improved mechanical properties.

CHAPTER 1 LITERATURE REVIEW

1.1 Theory of Colloidal Stability

DLVO theory (developed by Deryagin and Landau [7] and, independently, by Verwey and Overbeek [8,9]) is accepted as the basic theory of colloidal stability [10]. According to the DLVO theory, the interaction between colloidal particles is a superposition of electrostatic repulsion and van der Waals attraction.

1.1.1 Electrostatic Repulsion

The surface charge required for stability can be the result of one of the following four processes [10].

(a) Dissociation of surface groups. This is the charge-determining mechanism for several oxides. Silica, for example, can acquire a negative charge by dissociation of surface silanol groups.

(b) Adsorption of potential-determining ions. An example is adsorption of Ag^+ and I^- ions on AgI, rendering the AgI particles positive or negative, respectively.

(c) Adsorption of ionized surfactants. Carbon black dispersions, for example, can become negatively charged by adsorption of anionic surfactants.

(d) Isomorphic substitution. This mechanism is common in clay minerals, e.g., isomorphic substitution in the octahedral Al_2O_3 layers and the resultant charge-balancing by exchangeable counterions.

Charged particles attract oppositely charged ions (i.e., counter-ions) around the particles. The charged surface and the surrounding counter-ions form the electric

double layer. When the particle moves in the liquid, some ions “shear off” [11], and the resultant potential between the surface and the shear layer plane is the zeta potential. The zeta potential is identified with the value of the double-layer potential at the outer edge of the Stern layer of fluid that remains attached to the particle during the relative motion of the particles and liquid during electrophoresis (Figure 4). The region extending outwards from the Stern layer is termed the diffuse region, in which electrostatic forces are opposed by those of thermal agitation, and the potential decays approximately exponentially. In Figure 4, Φ_z represents the electrokinetic (zeta) potential and Φ_{DL} the Nernst (double-layer) potential, which is the potential at the surface of the particle relative to a remote point in the liquid. The higher the zeta potential, the thicker the double layer, and the more stable are the particles against coagulation.

In the DLVO theory, the distribution in a diffuse double layer is assumed to obey the Poisson-Boltzmann distribution [13,14]

$$\epsilon_r \epsilon_o \nabla^2 \Psi = -e \sum Z_i c_i \exp\left(-\frac{Z_i e \Psi}{kT}\right) \quad (1)$$

where Ψ is the electrostatic potential, ϵ_o and ϵ_r are the dielectric constants of water and solvent, respectively, Z_i is the valence of the ion i , c_i is the local concentration of ion i , T is the absolute temperature, e is elementary charge, and k is Boltzmann’s constant. Two boundary conditions plus a reference point for the surface potential are required to solve equation (1).

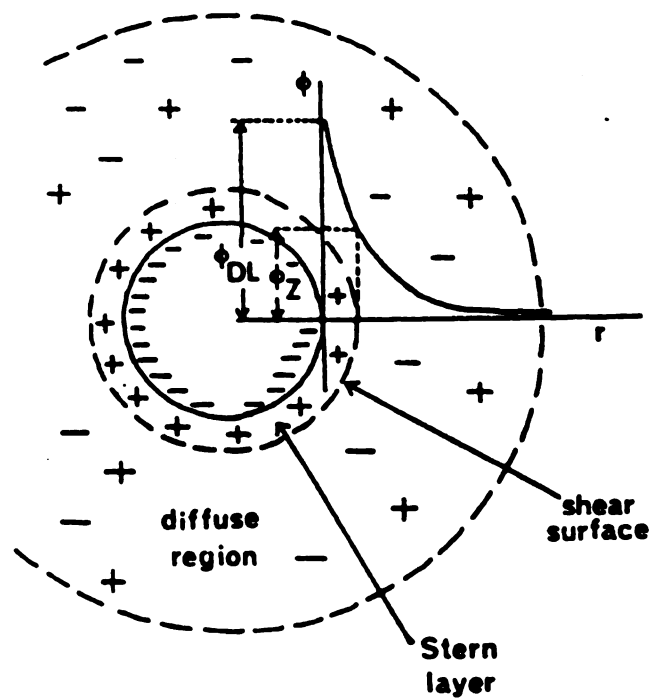


Figure 4 Model of charged spherical particles in a liquid indicating potential distribution $\Phi(r)$, where r is distance [12].

Applying the Debye-Huckel approximation to equation (1) gives:

$$\Psi(x) = \Psi_o \exp(-\kappa x) \quad (2)$$

where $1/\kappa$ is the Debye screening length or the characteristic double-layer thickness and is given by

$$1/\kappa = \left(\frac{\epsilon_r \epsilon_o kT}{\sum (Z_i e)^2 c_o} \right)^{1/2} \quad (3)$$

where Ψ_o is the surface potential, x the distance from surface, and c_o is the bulk ionic concentration. The exponential decay of the potential requires low-potential conditions; i.e., it is valid only sufficiently far from the surface that the potential approaches zero. This solution is not valid near the particle surface where the potential is high.

Hogg, Healy and Fuerstenau [15] developed a theory for nonidentical particles. In the HHF theory [16], the two different particles are treated as two plates having a constant potential, separated by a distance $2d$ with the boundary conditions

$$\Psi = \Psi_o, \quad \text{as } x \rightarrow 0 \quad \text{and} \quad \Psi = \Psi_o, \quad \text{as } x \rightarrow 2d. \quad (4)$$

The solution gives

$$\Psi = \Psi_o \cosh(\kappa x) + \left(\frac{\Psi_o - \Psi_o \cosh(2\kappa d)}{\sinh(2\kappa d)} \right) \sinh(\kappa x) \quad (5)$$

When two particles approach each other, double layer overlap occurs. Two cases can be distinguished, and may be denoted as the constant potential and the constant charge interactions [10].

In the first case, it is assumed that during the encounter of two colloidal particles the

surface potential remains constant, and as a result of double layer overlap, the surface charge should decrease. In the second case it is assumed that during the encounter the surface charge remains constant, in which case double layer overlap leads to an increase in the surface potential Ψ_o [10].

The free energy of the double layer increases [10] upon interaction. Work must be performed to bring the particles closer together. The repulsive energy $V_R(d)$ is the work required to bring the particle surfaces from infinity to a distance d . The free energy should be calculated as a function of d . If $F(\infty)$ represents the free energy at infinite separation, V_R follows as [10]

$$V_R(d) = 2[F(d) - F(\infty)]. \quad (6)$$

For two identical spherical particles at small potentials

$$V_R = \frac{\epsilon \Psi_o^2}{2} \ln(1 + e^{\kappa(R-2a)}) \quad (7)$$

where a is the particle radius, and R is the distance between the centers of the particles.

For two nonidentical spherical particles, the repulsive energy is [17,18]

$$V_R = \epsilon_r \epsilon_o \pi \left(\frac{a_i a_j}{a_i + a_j} \right) \left(\Psi_{o_i}^2 + \Psi_{o_j}^2 \right) \left(\frac{2 \Psi_{o_i} \Psi_{o_j}}{\Psi_{o_i}^2 + \Psi_{o_j}^2} \ln \left(\frac{1 + \exp(-\kappa x)}{1 - \exp(-\kappa x)} \right) + \ln(1 - \exp(-2\kappa x)) \right). \quad (8)$$

1.1.2 Van Der Waals Attraction

The attractive forces existing between colloidal particles are called London-van der Waals forces [19]. The attractive potential energy between two colloidal particles is large enough to compete with double layer repulsion. The attractive energy is [11]

$$V_A = -\frac{A}{6x} \frac{a_i a_j}{a_i + a_j}. \quad (9)$$

wl

a

ca

T

T

i

i

R

where A is the Hamaker constant, x is the separation distance of the two particles, a_i and a_j are the particle radii of particles i and j , respectively. The Hamaker constant can be calculated from dielectric constant by Bleier's method [20]

$$A_i = 113.7 \frac{(\epsilon_i - 1)^2}{(\epsilon_i + 1)^{3/2} (\epsilon_i + 2)^{1/2}} \quad (10)$$

The total interaction energy is

$$V_T = V_R + V_A \quad (11)$$

The attractive force, V_A , dominates at small separations. A primary minimum in the interaction energy curve results at particle/particle contact. As particle separation increases, double-layer repulsion dominates. The total interaction energy curve shows a peak. This is the energy barrier of particle coagulation [11]. A secondary shallow minimum develops at large distances, the attractive energy again dominates. Figure 5 is a schematic of the interaction energy as a function of separation between two particles in suspension [11].

If particles approach close to the primary minimum, they form hard agglomerates. The secondary minimum also can result in coagulation, which forms soft agglomerates [11].

1.1.3 Stability Ratio

The stability ratio, W , measures the effectiveness of the potential barrier in preventing the particles from coagulating:

$$W = \frac{\text{Number of collisions between particles}}{\text{Number of collisions that result in coagulation}} \quad (12)$$

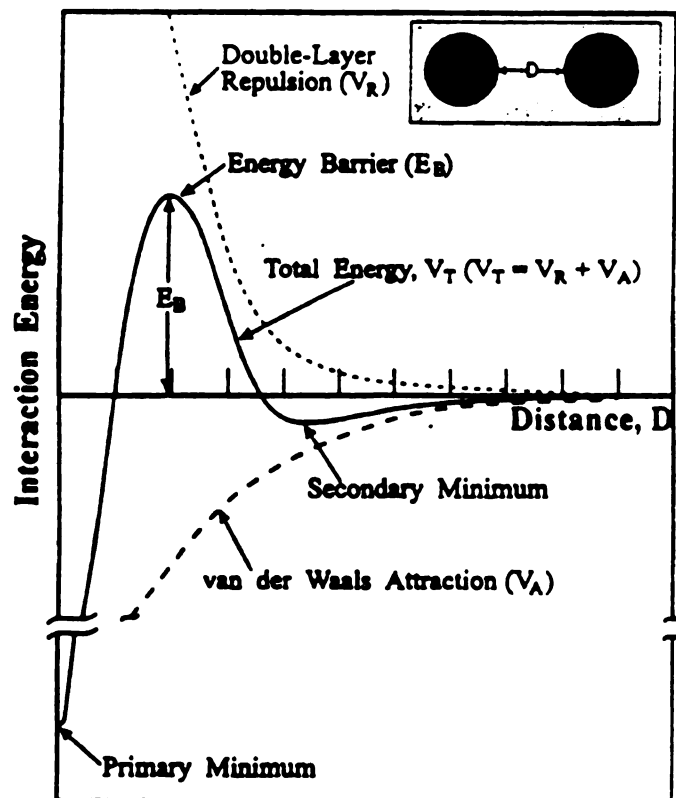


Figure 5 Schematic of the interaction energy as a function of separation between two particles in suspension [11].

For two nonidentical particles of radii a_i and a_j and a distance of separation x , the W_{ij} (stability ratio for stability between particle i and j) is [21]:

$$W_{ij} = (a_i + a_j) \int_{(a_i + a_j)}^{\infty} \exp\left(\frac{V_T}{kT}\right) \left(\frac{dx}{x^2}\right) \quad (13)$$

where $V_T = V_A + V_R$.

Hogg, Healy and Fuerstenau [22] developed a variable W_T (total stability ratio) to describe the total stability of the system:

$$W_T = \left(\frac{n^2}{W_{11}} + \frac{(1-n)^2}{W_{22}} + \frac{2n(1-n)}{W_{12}} \right)^{-1} \quad (14)$$

where n is the proportion of the type 1 particles, and $(1-n)$ is the proportion of the type 2 particles.

1.1.4 Refinements of DLVO Theory

The general equation describing the interparticle forces consists of attractive and repulsive terms [23]:

$$V_T = V_A(\text{van der Waals}) + V_R(\text{electrostatic}) + V_S(\text{steric}) + V_S(\text{solvation}) \quad (15)$$

Surfactants with high molecular weight promote steric stabilization. The solvation forces are short range hydration and hydrophobic forces. The solvation and steric forces can be attractive or repulsive in nature. Polyelectrolytes are added to suspensions to promote steric stabilization. In this case, the particle surface potential, Ψ_o , is replaced by the zeta potential ζ [25]. Figure 6 shows the shift in the shear plane after absorbing polyelectrolyte on the particle surface. A parameter β measures how the presence of the polyelectrolyte affects the free energy of the ions. The additional free energy is

incorporated into the Boltzmann equation.

The relative ζ -potential (Z) is expressed as $Z = \frac{\zeta_{\beta}}{\zeta_o}$, where ζ_{β} is the ζ -potential in the presence of polyelectrolyte and ζ_o is the ζ -potential without the presence of a polyelectrolyte.

Using the appropriate boundary conditions, the relative ζ -potential is calculated as [24]:

$$Z = \exp\left(\frac{\beta}{2}\right) . \quad (16)$$

In most cases, it was found that $Z > 1$ [24]. The experiments showed [24] that polymer adsorption can lead to large increases in the absolute value of the ζ -potential of biological (red blood cell), organic (polystyrene latex) and inorganic (SiO_2) surfaces. Brooks [25] shows that even if the adsorption of the polymer leaves the surface charge and the shear plane unaffected, an increase in $|\zeta|$ is predicted due to the change in the ion distribution in the diffuse double layer. The change is produced chiefly by the influence of the excluded volume of the polymer on the free energy of the double-layer ions. The overall effect, if the surface charge is kept constant, is to increase the extension of the double layer and hence to increase the surface potential of the underlying particle (see Figure 6, which incorporates the possibility that the shear plane may be shifted away from the particle surface by the adsorbed polymer without causing a decrease in $|\zeta|$ [24]).

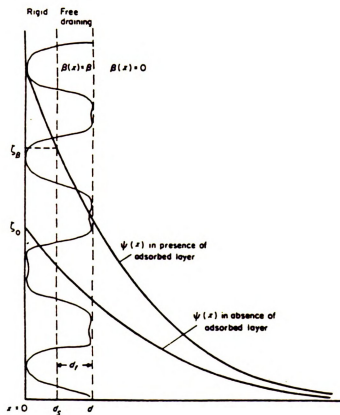


Figure 6 Model for treating the effect of adsorbed polymer on zeta-potential. The model allows for the possibility of a shift in the shear plane as well as a modified ion distribution in the diffuse layer [24].

1.2 Processing Techniques of Ceramic Matrix Composites

Colloidal processing involves the manipulation of interparticle forces. The only possible way of avoiding coagulation is by developing repulsive forces between particles, either V_r (electrostatic) or V_r (steric). This can be done by pH control and changing the electrolyte or its concentration in the first case and by using macromolecules (polyelectrolytes) which may be adsorbed onto the particle surface in the second. Colloidal methods are used to break apart weakly bonded agglomerates, eliminate strongly bonded agglomerates, eliminate inorganic and organic inclusions greater than a given size, homogeneously mix two or more powders, and consolidate powders to high bulk densities.

In the electrostatic approach, ions or charged molecules are attracted to, or dissociated from the particle surfaces to produce a system of similarly charged particles. When the repulsive double-layer electrostatic forces between the particles are greater than the attractive van der Waals forces, the particles repel each other to produce a dispersed system. The net interparticle force (in aqueous solutions) can be altered by changing the type and concentration of the ionic species, the pH and by addition of specific adsorbing organic or inorganic compounds or polyelectrolytes [26]. When the particle charge approaches zero, the particles flocculate. The zeta potential provides a convenient experimental measure of such forces. ESA (Electrokinetic Sonic Amplitude) is the pressure amplitude generated by the colloid particle per electric field strength. O'Brien's theory [27,28] for electro-acoustic effects in a dilute suspension of spherical particles is used to calculate the suspension zeta potential from the measured ESA.

By understanding the zeta potential to pH relationship, the suspension properties of

individual ceramic suspensions may be manipulated to give stable, multi-component composite suspensions. Figure 7 is an example of how electrophoresis data can be used to indicate suspension dispersion characteristics for single component materials [29]. The graph shows how the zeta potential varies with pH and also illustrates the regions in which the suspension undergoes flocculation (unstable, $|\zeta| < 25\text{mv}$) and dispersion (stable, $|\zeta| > 25\text{mv}$). The state of agglomeration of the primary particles in the liquid will depend on the stability of the dispersion against coagulation.

The critical coagulation concentration is the concentration of the indifferent electrolyte at which the potential energy barrier opposing coagulation is zero. Therefore, electrolyte concentrations less than the critical coagulation concentration should be used.

With the steric approach, bifunctional macromolecules attach themselves to the particles. The macromolecular additives are usually completely soluble in the dispersing fluid, but are designed with certain functional groups to bind them to the particles. The particles then repel one another once their separation distance is less than the radius of gyration of the macromolecule.

Polyelectrolytes are multi-charged macromolecules that may adsorb on or anchor to surfaces of ceramic particles in a polar (often aqueous) medium. Observations suggest that certain polyelectrolytes can be most efficient in dispersing a wide range of ceramic powders. It is known that they can produce an electrostatic double layer surface charge, thereby opposing the attractive van der Waals forces in addition to offering the possibility of steric interaction. J. Cesarano III and I. A. Aksay [30] concluded that once enough polyelectrolyte has been adsorbed, there is a stabilization effect due solely to the polyelectrolyte, even in the absence of appreciable repulsion due to electrostatics.

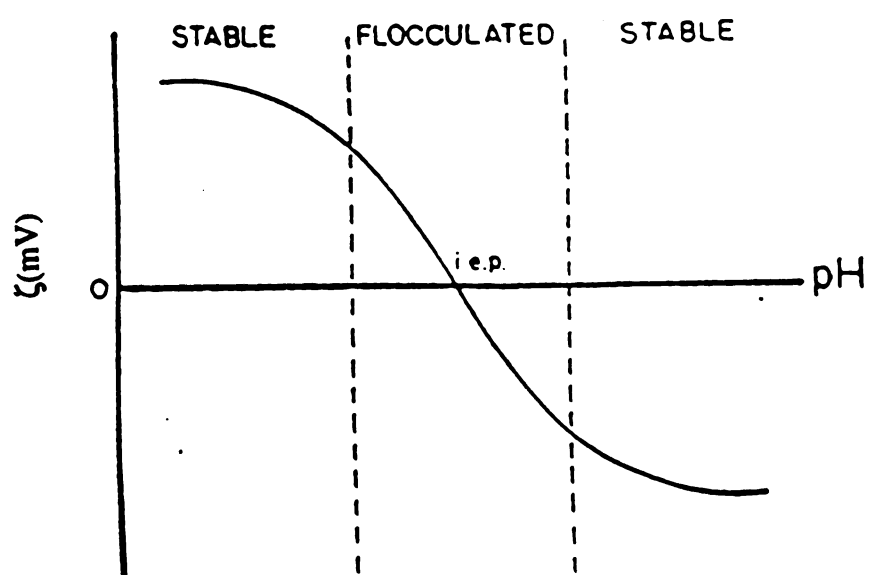


Figure 7 Plot of ζ versus pH showing the location of the iso-electric point (i.e.p.) and the regions of stability [29].

The interparticle forces produced by polyelectrolytes may be controlled by altering pH, ionic strength, temperature, molecular weight and concentration.

Most processing of whisker composites has been made by hot pressing [1-2, 31-34], see Table 1. Skeletal networks of SiC whiskers prevent the development of full densification. The methods of using high pressure have achieved high densities [32]. Progress has also been made in the area of pressureless sintering. Tiegs and Becher [3] (Table 1) have shown that Al_2O_3 and 16 vol% SiC_w can be sintered to 95% of theoretical density at 1700-1850°C, using 0.5 wt% MgO and 2 wt% Y_2O_3 (for liquid phase sintering) to give reasonable mechanical properties. However, higher loadings of whiskers limited achievable densities in pressureless sintering.

The mechanical properties of Al_2O_3 -SiC whisker composites by pressureless sintering were not as good as those for hot pressing specimens because the densification is inhibited as a result of whisker interference with particle rearrangement and composite shrinkage.

Slurries were milled to reduce the aspect ratio of SiC whisker. The aspect ratio was reduced to improve the density by improving the particle/whisker packing for increased green density and enhanced the ability of the whiskers to rearrange themselves during sintering. Increasing the amount of liquid phase present during sintering also improves densification by aiding whisker rearrangement. However, as the amount of liquid phase reaches about 30%, no further improvement in densification is observed because of decomposition of the liquid phases [3].

Porter, Lange and Chokshi [32] fabricated $\text{Al}_2\text{O}_3/\text{SiC}_w$ composites by slip casting and pressureless sintering. Pressureless sintering was discontinued because slip cast

Table1 Composite processing and mechanical properties.

Materials	Fabrication methods and conditions	Green density (% of theoretical density)	Final density (% of theoretical density)	Fracture toughness K_{IC} (MPa·m ^{1/2})	Flexure strength (MPa)	Reference
Al ₂ O ₃ +20-30vol% SiC _w	HP 1850-1900°C, 40-60Pa, vacuum.	*	95%	9	800	Becher and Wei [1-2]
Al ₂ O ₃ +10-20vol% SiC _w +MgO+Y ₂ O ₃	CP 140MPa IP420MPa sinter 1700-1850°C Ar	57-59%	10vol%SiC _w 7 91-96% 20vol%SiC _w 66-89%		330	Tiegs, Becher and Dillard [3,35]
Al ₂ O ₃ +30vol% SiC _w	HP 31.2MPa 1800-1950°C, Ar	*	97-100%	6.8-9.5	350-650	Homeny, Vaughn and Ferber [31]
Al ₂ O ₃ +5-15vol% SiC _w	pressure filtration HP 24MPa 1500°C	59-65%	99.5%	3.6-4.6	391-652	Porter, Lange and Chokshi [32]
Al ₂ O ₃ +0-30vol% SiC _w	HP 22MPa 1827°C, Ar	*	>99%	3.8-10	500-620	Smith, Singh and Scattergood [33]
Al ₂ O ₃ +0-30vol% SiC _w	CIP 250MPa sintering of coated powder at 1800°C, He	40-42%	1680°C: Al ₂ O ₃ : 98% 1800°C: 10-20vol% SiC _w : 98% 30vol%SiC _w 86%	*	*	Hu and Rahaman [36]

Table 1 (cont'd).

Materials	Fabrication methods and conditions	Green density (% of theoretical density)	Final density (% of theoretical density)	Fracture toughness K_{IC} (MPa·m ^{1/2})	Flexure strength (MPa)	Reference
Al ₂ O ₃ + 5-30vol% SiC _w	slip casting, centrifugal casting, sintering at 1600°C, N ₂	67%	5vol%SiC _w : 92% 15vol%SiC _w 88% 30vol%SiC _w 84%	*	*	Sacks, Lee and Rojas [37]
Al ₂ O ₃ + 9.1vol% SiC _w	CIP, sinter	*	97%	5.5	414	ACMC [34]
Al ₂ O ₃ + 29.3vol% SiC _w	sinter+ HIP	*	100%	6.7	641	ACMC [34]
Al ₂ O ₃	air cast, suspension stabilized with PMAA, sinter at 1350- 1400°C	65.8%	99%	*	*	Cesarano III and Aksay [30]

Note: HP: hot press, CP: cold press, IP: isopress, CIP: cold isostatic press,
HIP: hot isostatic press, ACMC: Advanced Composite Materials Corporation
* No data available.

components with a 15 wt% whisker loading sintered at 1550°C in vacuum for 30 min with no applied pressure, failed to densify.

Smith [33] at Argonne National Laboratory reported that well mixed and nearly fully dense $\text{SiC}_w/\text{Al}_2\text{O}_3$ composites were fabricated by wet blending the constituents and uniaxially hot-pressing the resulting powder.

Hu and Rahaman [36] at the University of Missouri made $\text{Al}_2\text{O}_3/\text{SiC}$ whisker composites by free sintering of coated powder. SiC whiskers were coated with a thick cladding of fine-grained Al_2O_3 powder by controlled heterogeneous precipitation in a concentrated suspension of whiskers. After calcination, a loose powder consisting of SiC whiskers coated with Al_2O_3 was obtained. The sinterability of the composites formed from the coated whiskers was significantly higher than that for similar composites formed from mechanically mixed powders. Increasing the whisker aspect ratio produced a decrease in the sinterability of the composites formed from the coated powders. Doping with 250ppm Mg to control the grain growth of the Al_2O_3 matrix led to an increase in the sinterability of the composites.

Sacks, Lee and Rojas [37] at the University of Florida produced homogeneous $\text{Al}_2\text{O}_3/\text{SiC}_w$ composites by suspension processing. By optimizing the conditions for particle/whisker codispersion, castable suspensions could be prepared at total solids concentration of 50 vol%. Green bodies with a high relative density (~66% TD) were obtained with SiC whisker contents in the range of 5 to 30 vol%. Although densification was severely inhibited by the SiC whiskers, significantly higher sintered densities were obtained by suspension processing as compared to dry processing.

Cesarano III and Aksay [30] studied the processing of highly concentrated

(65-

und

adisc

for

con

den

red

tech

hon

Dif

abc

wh

mi

fat

de

(65-70 vol%) aqueous α -Al₂O₃ suspensions stabilized with polyelectrolytes. By understanding the chemistries of the polyelectrolyte and particle surface, polyelectrolyte adsorption behavior and polyelectrolyte rheological effects, the viscosity and rheology for all solids levels may be controlled. Their results show that processing from highly concentration polyelectrolyte-stabilized suspensions leads to higher consolidated densities (100% of theoretical density) and these benefits carry over in the form of reduced sintering temperatures.

Cesarano III and Aksay's studies [30] show the potential for colloidal processing techniques. The sintering temperature for composites decreased by achieving homogeneous microstructure in consolidated states compared to conventional processes. Different ways of fabricating the Al₂O₃/SiC_w composites have been tried. Besides the above-mentioned methods, microwave sintering, freeze-drying, sol-gel [38], and whiskers coated by amorphous silica [39] have been used to improve processing.

Figure 8 indicates that the properties of ceramic products are dependent on product microstructure and ceramic processing [40]. Advances [41,42] from two extremes of the fabricating process (powder, right at the beginning, and sintering, the last operation) have demonstrated the central importance of the green compact [43] (Figure 9).

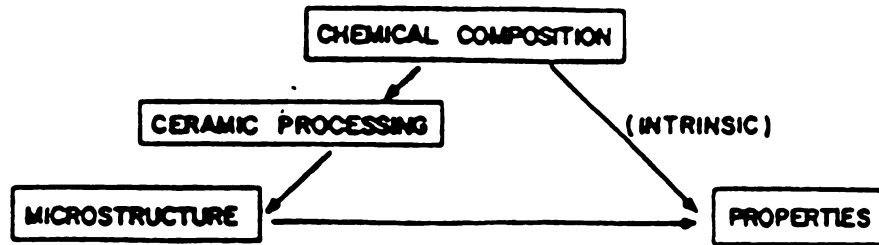


Figure 8 The properties of ceramic product [40].

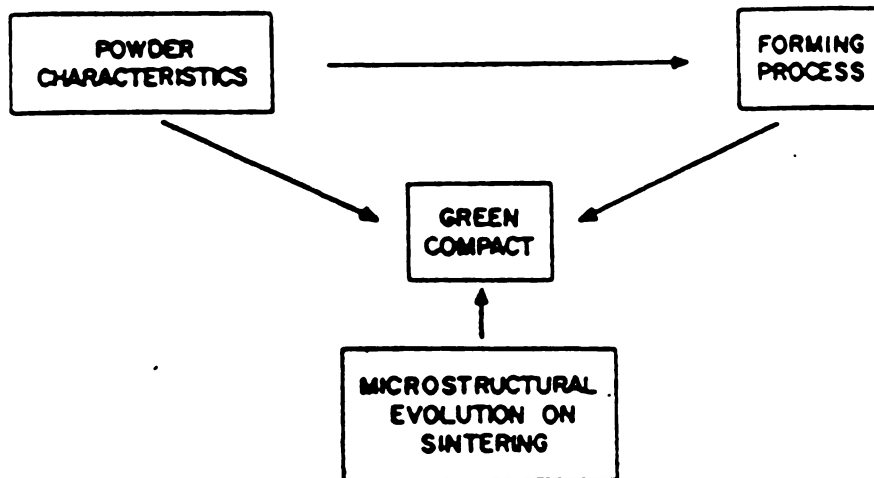


Figure 9 Relationship between different parts of the ceramic process [43].

CHAPTER 2 EXPERIMENTAL PROCEDURES

A flow chart of experimental procedures is summarized in Figure 10.

2.1 Materials

The materials used in this study were α - Al_2O_3 powder (Sumitomo, AKP-30 and AKP-50) and β -SiC whisker (Tokai, TWS-100). Major characteristics of Tokai TWS-100 SiC whisker, Sumitomo AKP-30 and AKP-50 alumina powder and Y_2O_3 powder as supplied by the manufacturers [44] are listed in Table 2. For SiC whiskers, the length and diameter are 5-15 μm and 0.3-0.6 μm , respectively, giving an aspect ratio of 10 to 40. The AKP-30 and AKP-50 Al_2O_3 powder diameters are 0.3-0.5 μm and 0.1-0.3 μm , respectively. Y_2O_3 powder (Rhone-Poulenc Basic Chemicals Company) and MgO powder (Rhone-Poulenc Basic Chemicals Company) are used as sintering aids. The purity of MgO as labeled by manufacturer is 99.9 wt%.

2.2 Zeta Potential Measurement

Matec Applied Sciences ESA-8000 System was used to measure the ESA potential of particle suspensions where the solids loading of each suspension was 0.5 vol%. Each type of powder was suspended in 220ml deionized water of varying electrolyte concentration (0.001-0.1N KNO_3), polyelectrolyte (0.03-0.5 vol% ammonium salt of polymeric carboxylic acid), or varying ethanol/electrolyte ratios. The pH was varied for this system by titration of 1N HNO_3 and 1N KOH. Suspensions were dispersed using an ultrasonic probe.

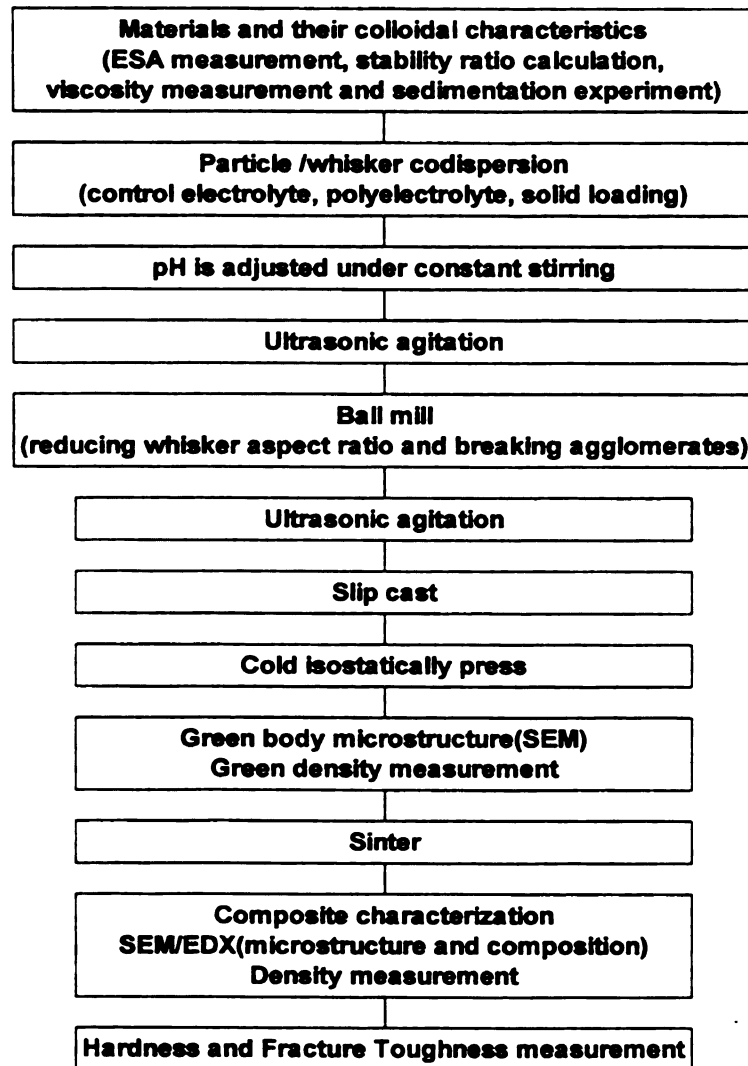


Figure 10 A flow chart of experimental procedures.

Table 2 Major characteristics of Tokai TWS-100 SiC whisker, Sumitomo AKP-30, AKP-50 alumina powder and Y₂O₃ powder [44]

Grade	TWS-100	AKP-30	AKP-50	Y ₂ O ₃
Crystal Form	β	α	α	–
Diameter (μm)	0.3-0.6	0.3-0.5	0.1-0.3	1-3
Length (μm)	5-15	-	-	-
Aspect Ratio	10-40	-	-	-
Density (g/cm ³)	3.20	3.98	3.98	5.01
Loose Bulk Density (g/cm ³)	0.06-0.12	0.7-1.0	0.6-1.1	-
Pack Bulk Density (g/cm ³)	-	1.1-1.5	0.9-1.3	-
Specific Surface Area (m ² /g)	2-4	6-10	9-15	-
Purity (wt%)	99	>99.99	>99.995	99.99
Particulate Content (wt%)	<1	-	-	-
Coefficient of Thermal Expansion from RT to 1400°C (x10 ⁻⁶ /°C)	5.0	-	-	-
Impurities(wt%)				
SiO ₂	0.5	-	-	-
Si	-	0.004	0.0025	<0.005
Na	-	0.001	0.001	-
Ca	0.05	-	-	<0.005
Mg	0.02	0.001	0.001	<0.005
Fe	0.05	0.002	0.002	<0.005
Cr	0.05	-	-	-
Co	0.05	-	-	-
Al	0.08	-	-	<0.005
Cu	-	0.001	0.001	-

2.3 Viscosity Measurement

Viscosity measurements of particle suspensions were made as a function of pH using a Brookfield Digital Viscometer, Model DV-II. The #3 spindle, 100rpm, and 0.001N KNO₃ electrolyte solution were used for all the viscosity measurements. The accuracy of the measurements is within 5%. Measurements were then repeated for suspensions of varying ethanol/electrolyte ratios.

2.4 Sedimentation Experiment

Sedimentation densities for pure Al₂O₃ and pure SiC_w were determined for 5-10 vol% solids content suspensions in 0.001N KNO₃ electrolyte. The suspensions were ultrasonically dispersed and the pH adjusted by addition of either acid (HNO₃) or base (KOH). The test tubes were then covered and the suspension allowed to settle until the sedimentation height reached stable value. The sedimentation volumes were calculated from the sediment height and used to determine the sedimentation densities.

2.5 Stability Ratio Calculation

From the zeta potential data as a function of pH, the stability ratios for homo- and heterocoagulation, $W_{SiC-SiC}$ (and $W_{Al_2O_3-Al_2O_3}$) and $W_{SiC-Al_2O_3}$, respectively, were calculated using Stable Suspension (c)[16,45]. The relative volume fraction of components was 0.5, the electrolyte concentration was 0.001N KNO₃, and the Hamaker constant was calculated from the dielectric constant using a method developed by Bleier [20].

2.6 Dispersion and Slip Casting

From ESA results and stability ratio calculations, different pH regions were chosen to process the suspensions. Trial experiments demonstrated that the unstable slurry had the consistency of ice cream and failed to cast. Suspensions prepared at pH 4 are stable because the stability ratio (W) is greater than 10^{25} for all the possible interactions of $\text{Al}_2\text{O}_3/\text{Al}_2\text{O}_3$, $\text{Al}_2\text{O}_3/\text{SiC}_w$ and $\text{SiC}_w/\text{SiC}_w$. pH 11 was also chosen for processing composites with sintering aids because Y_2O_3 dissolves at $\text{pH} < 7$. Therefore, pH 4 and pH 11 were used for processing composites.

Individual suspensions were slowly mixed using a magnetic stirrer. After the solids content adjustment to 35-50 vol%, the composite suspension was homogenized by ultrasonic agitation (Branson Sonifier 250). The 120W output and 20kHz ultrasonic waves were applied to suspensions for 20 minutes. An ultrasonic probe was embedded directly in the slurry. To prevent overheating, the suspension containers were cooled in a cold water bath.

Al_2O_3 , sintering aids (Y_2O_3 and MgO) and SiC whisker were dispersed and mixed in electrolyte or a mixture of ethanol and electrolyte. Some suspensions had varying concentrations of a polyelectrolyte (0.03-0.5 vol% ammonium salt of polymeric carboxylic acid). The pH was adjusted by additions of HNO_3 or KOH .

By using a combination of pH adjustment, electrolyte, polyelectrolyte, and ultrasonic agitation, Al_2O_3 particles, SiC whiskers and sintering aids (Y_2O_3 and MgO) were codispersed at a relatively high overall solids concentration (50 vol%) while maintaining the relatively low viscosities desired for casting.

Slurries were ball-milled using Al_2O_3 grinding cylinders, which were 12mm in

diameter

lined pol

10 minur

liquid w

the mold

Por

Compan

mixed p

25-30 m

plaster n

removed

and cut i

ceramic

held in p

Dur

formed.

green bo

samples

heated to

moisture

electroni

weight a

density d

diameter and 15mm in height. The grinding cylinders and slurries were filled in rubber-lined polyethylene jars. After 25-50 hours, the ball milled slurries were ultrasonicated for 20 minutes before slip casting. Slips were poured into porous plaster molds where the liquid was absorbed by capillary action into the mold leaving a layer of ceramic against the mold wall.

Porous molds were made from No. 1 Plaster powder from the American Gypsum Company. Plaster and water were mixed in a ratio of 100g plaster/75ml water. The mixed plaster slurry was poured into a plastic weighing boat and allowed to thicken for 25-30 minutes. A negative mold was inserted into the thickened plaster slurry. The plaster mold was air-dried for 24 hours. After the plaster mold dried, the plastic boat was removed and the negative mold was pulled out. Plaster molds were then put in clamps and cut into two halves by a hand saw. The split molds facilitate easier release of the ceramic green specimen. Before slip casting, the two halves of the plaster mold were held in place by elastic bands.

During slip casting, slurry was periodically added until the desired wall thickness formed. Solid casting was applied by leaving sufficient slurry in the mold to get solid green body. The green body was left in the mold for 36 hours. After further air drying, samples were ground on 400 grit abrasive paper to smooth the surfaces. Samples were heated to 100°C and held at this temperature for two hours to remove any residual moisture. The weight and the dimensions of the green bodies were then measured by electronic balance and calipers, respectively. The green density was obtained from the weight and dimensions of the samples. Five specimens were measured for each green density data point. The green compacts were subsequently vacuum-sealed into double

tered soft

2.7 Sint

A high

ng Inc.) u

composites

The temper

5°C minute

temperatur

for 30 min

to room tem

2.8 Mic

Green

Electron M

structure a

were gold

Electron M

Environme

15kV. Enc

detector in

mapping te

layered soft rubber bags and cold isostatically pressed at 310MPa (Iso-Spectrum, Inc.).

2.7 Sintering

A high temperature graphite-element furnace (Model 1000-4560, Thermal Technology Inc.) under flowing nitrogen at 1600-1700°C was used for pressureless sintering the composites. The samples were covered with Al_2O_3 powder in a closed graphite crucible. The temperature was increased at 10°C/minute from room temperature to 1000°C, then 5°C/minute and 2°C/minute from 1000 to 1450°C and 1450°C to the final sintering temperature, respectively. The samples were then held at the final sintering temperature for 30 minutes. Samples were cooled inside the furnace at a cooling rate of 20°C/minute to room temperature.

2.8 Microstructure and Composition

Green compacts and sintered composites were characterized using Scanning Electron Microscopy and Energy dispersive X-ray spectroscopy to examine their structure and composition. Fracture surfaces of green compacts and sintered composites were gold coated for three minutes and examined in the Hitachi S-2500C Scanning Electron Microscope (SEM) at an accelerating voltage of 15-20kV and in an Environmental Scanning Electron Microscope (ESEM) at an accelerating voltage of 10-15kV. Energy dispersive X-ray spectroscopy analysis was performed using an X-ray detector in the ESEM to measure the composition of the samples. An elemental dot-mapping technique was used to distinguish the whisker composition (at%) distribution.

2.9 De

Bulk

displace

were deter

were no d

componen

Samp

present at

shared d

2.10 H

Vicke

ique of p

appropriat

the approp

diamond v

her polisi

made on a

the length

using the t

The V

2.9 Density Measurement

Bulk densities and apparent porosities were measured by the Archimedes displacement method using deionized water as the immersion medium. Relative densities were determined by dividing the bulk density by the theoretical densities. Because there were no data for the glassy phase, the theoretical density were calculated from each component's density and its wt% by a superposition method.

Samples were boiled in deionized water for one hour to release any air bubbles present at the sample surface and open pores. Three specimens were measured for each sintered density data point.

2.10 Hardness and Fracture Toughness Measurement

Vickers hardness and fracture toughness determinations used the indentation technique of polished specimens at a load of 5kg. Different loads were tried to find the most appropriate load. 1kg was not enough to make a penny-like crack. 5kg turned out to be the appropriate load. Sintered samples were cut using an Accutom-5 high speed diamond wheel cutting machine, ground using SiC grinding papers (400 and 600 grit) and then polished using diamond pastes (10, 6, and 1 μm). Indentation measurements were made on a Vickers Hardness Tester. Five impressions were made on each specimen and the lengths of the diagonals and the radial cracks produced by indentation were measured using the built-in optical microscope.

The Vickers hardness was calculated using the applied load and the length of the

half diagonal of the indentation with the following formula [46, 47]:

$$H=0.47P/a^2 \quad (17)$$

where H is Vickers hardness, P is the applied load and a is the length of the half-diagonal indentation.

A dimensional analysis of indentation fracture has shown that the indentation crack length, c, should be related to the impression radius a by [48]:

$$K_{IC}(\Phi/H)a^{\frac{1}{2}} = F_1(c/a)F_2(\nu, \mu, (R_p/a)) \quad (18)$$

where K_{IC} is fracture toughness, H is hardness, Φ the constraint factor (about 3), ν Poisson's ratio, μ the friction coefficient between the indenter and the material, R_p the plastic zone radius, and F_1 and F_2 indicated that c/a depends strongly on $K_{IC} \Phi/Ha^{1/2}$, but is approximately independent of F_2 [48]. From Evans and Charles's simplified results [48,49] based on theoretical assumptions and material characteristics Singh et al. [50] assessed fracture toughness of whisker reinforced Si_3N_4 composites by simplifying equation (18) using the following relation:

$$K_{IC} = 0.057Ha^{\frac{1}{2}}\left(\frac{E}{H}\right)^{\frac{2}{5}}\left(\frac{c}{a}\right)^{\frac{3}{2}} \quad (19)$$

where c is one-half the median crack length and E the elastic modulus. Equation (19) was chosen to calculate fracture toughness in this study because this equation is specifically derived from the whisker reinforced composites. The value of E was taken from the reference [51].

3.1 Summary

The results

chemical pro

chemical che

of SiC-Al₂O₃

performance

Figure

composites.

rolled. The

existing app

suspension

SiC-Al₂O₃

and to brea

imposed by

and 4) a po

mixed SiC

four proces

elieviate w

high densit

Detail

special add

CHAPTER 3 RESULTS AND DISCUSSION

3.1 Summary and Overview of Research Approaches

The research of this dissertation has two goals. The first is an in depth study of the colloidal properties and suspension parameters of the $\text{SiC}_w/\text{Al}_2\text{O}_3$ system. Based on the colloidal chemistry, fundamental theories, and recent developments, the colloidal system of $\text{SiC}_w/\text{Al}_2\text{O}_3$ is fully examined and discussed. The second is to obtain high performance ceramic matrix composites through improved processing approaches.

Figure 11 illustrates a processing approach to produce high performance ceramic composites. In a step by step method, it was established how the processing must be controlled. There are four aspects to the concept of colloidal processing and improved processing approaches: 1) colloidal processing was used to control surface chemistry and suspension stability after a systematic investigation of colloidal interactions of the $\text{SiC}_w/\text{Al}_2\text{O}_3$ system; 2) ball milling served to control the aspect ratio of the SiC whiskers and to break down agglomerates; 3) sintering aids were added to relax the back stresses imposed by the SiC whisker networks to enhance the densification of these composites; and 4) a polyelectrolyte was used to control the surface chemistry and to stabilize the mixed $\text{SiC}_w/\text{Al}_2\text{O}_3$ suspension and sintering aids, Y_2O_3 and MgO . By manipulating these four processing steps it was possible to tailor-make composite microstructure and alleviate whisker network effects on sintering to achieve high performance which means high density, fracture toughness and hardness.

Details of the mechanisms of non-aqueous suspensions or aqueous suspensions with special addition of polyelectrolyte are less known than those for general aqueous

suspension

electrolyte

The second

combined

also lowered

whisker ne

SiC, densi

boundary l

particular i

polyelectro

point of ce

suspension

Al₂O₃ susp

lined in th

chemistry.

control ov

whisker re

conditions

polyelectr

pressurele

suspensions. Consequently, the first effort was to explore Al_2O_3 and SiC_w in mixtures of electrolyte and ethanol and the aqueous system with the addition of a polyelectrolyte. The second step has been the development of $\text{SiC}_w/\text{Al}_2\text{O}_3$ where colloidal processing is combined with ball milling to form uniform deagglomerated green bodies. Ball milling also lowered the aspect ratio of the SiC whiskers, which serves to decrease the number of whisker networks. To eliminate or minimize the impact of defects or problems related to SiC_w densification, sintering aids were added to the system. Sintering aids create grain boundary liquid phases and relax the back stress from the SiC whisker networks. Of particular importance in forming ceramic matrix composites (CMCs) involves polyelectrolyte additives that are able to reverse the zeta potential or shift the iso-electric point of ceramic powders. Polyelectrolyte creates a steric barrier that restabilizes the suspension even after the addition of Y_2O_3 , disrupting stable interactions in the $\text{SiC}_w/\text{Al}_2\text{O}_3$ suspension system. Four different methods were being explored and were combined in this research. This processing research combines the use of colloidal surface chemistry, mechanical methods, sintering aids and polyelectrolyte additives to achieve control over compaction, consolidation, forming and densification of CMCs. SiC whisker reinforced Al_2O_3 suspensions were slip cast using numerous processing conditions (SiC whisker volume fraction, solids loading, ball milling, sintering aids, polyelectrolyte and pH). Green specimens were cold isostatically pressed and pressureless sintered in a flowing nitrogen atmosphere.

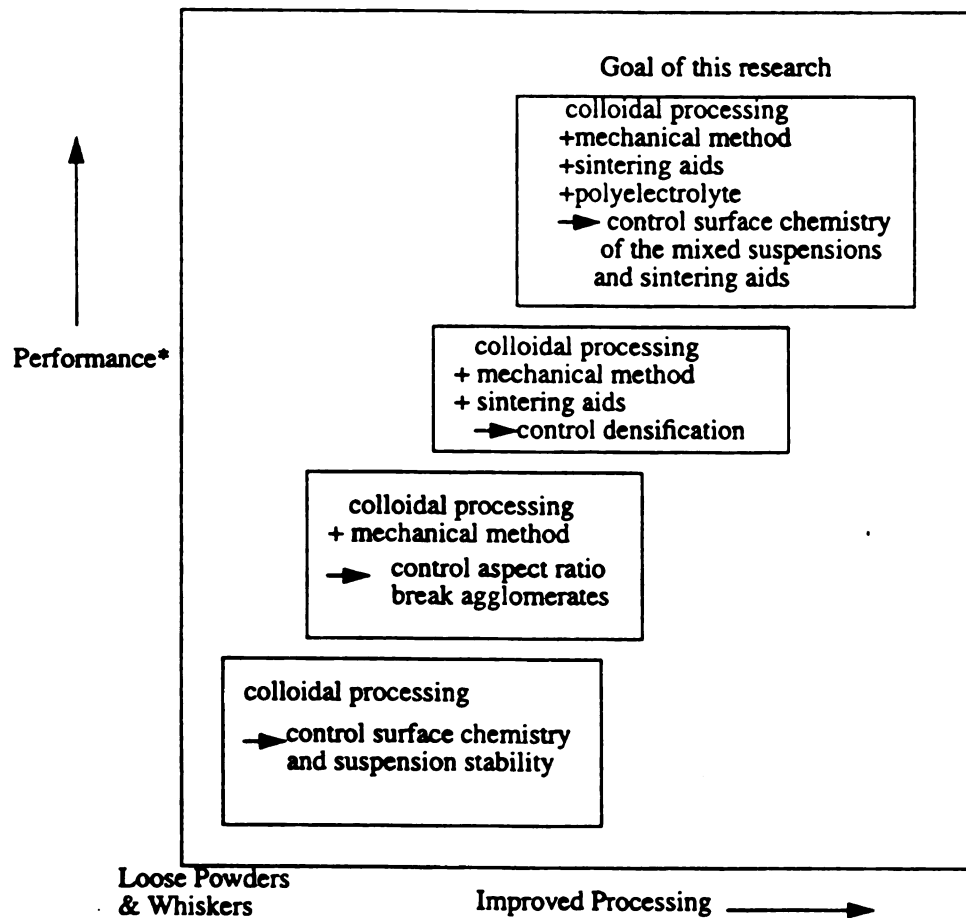


Figure11 The processing approach of high performance ceramic composites. Improved performance is achieved through controlled processing approaches. *Density, Fracture Toughness, Hardness

3.2 C
at

By

different

changing

of single

ion (ele

stability

the parti

discusse

3.2.1

Ele

critical

the susp

coagula

coagula

of Al_2O_3

and SiC

Fig

at 0.007

was sel

Ne

was me

3.2 Colloidal Stability and Suspension Parameters of SiC_w/Al₂O₃ in Aqueous and Nonaqueous Systems

By manipulating the interparticle forces of ceramic colloidal systems, suspensions of different dispersing abilities were obtained. The net interparticle force was altered by changing the concentration of the ionic species, pH, and the solution. The zeta potentials of single component suspensions of varying concentration of ionic species, pH and solution (electrolyte, ethanol, or a ratio of electrolyte and ethanol) were measured. The stability ratio W , which measures the effectiveness of the potential barrier in preventing the particles from coagulation, and the interaction between the components were discussed.

3.2.1 Zeta Potential

Electrolyte was added to a suspension to control the particle double layer. The critical coagulation concentration (c.c.c.) is the concentration of the electrolyte at which the suspension is stable. If the electrolyte concentration is higher than the critical coagulation concentration, the particle's double layer is compressed, causing rapid coagulation. By using the sedimentation technique, the critical coagulation concentration of Al₂O₃ occurs at 0.001N KNO₃. Figures 12 and 13 show the zeta potential of Al₂O₃ and SiC_w versus pH for various electrolyte strengths, respectively.

Figures 12 and 13 showed that the zeta potential for both Al₂O₃ and SiC_w is greater at 0.001N KNO₃ than at other electrolyte concentrations. Therefore, the 0.001N KNO₃ was selected for all the suspensions in this research.

Next the zeta potential for Al₂O₃ and SiC_w in a mixture of electrolyte and ethanol was measured. The zeta potentials of SiC versus pH, for varying ratios of

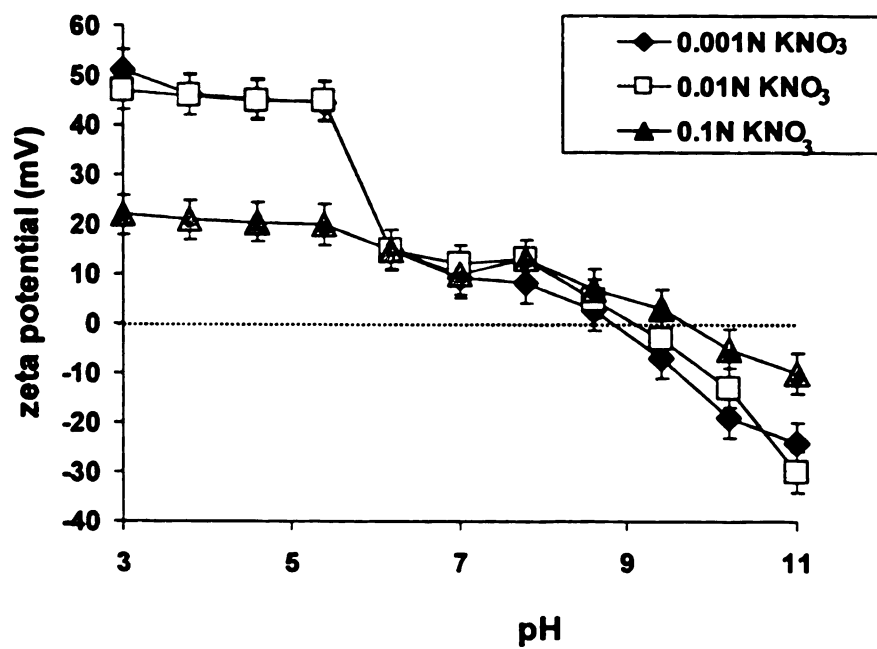


Figure 12 Zeta potential of Al_2O_3 versus pH at different electrolyte strengths.

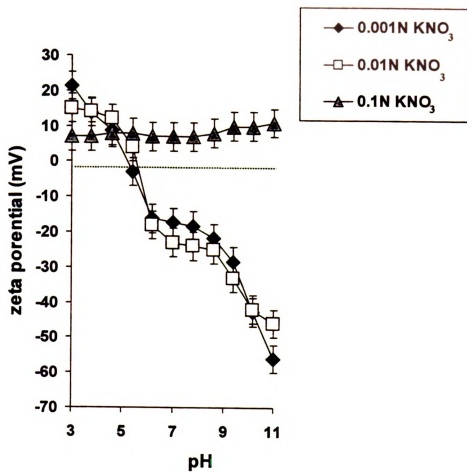


Figure 13 Zeta potential of SiC_w versus pH at different electrolyte strengths.

and electrolyte

the surface [52]

of the zeta

electric point

electrolyte suspen-

and pH plots.

The zeta po-

tion in Figure

has in 100%

ethanol is ac-

The absol-

at 15. decreas-

stant (D) of

increases, the

zeta potential. T

increasing eth

$$\frac{1}{\kappa} = \left(\frac{8\pi}{\epsilon} \right)$$

Equation (20)

ethanol/electrolyte, are plotted in Figure 14. SiC, which has been shown to have an acidic surface [52]. Thus, in 100% electrolyte, the iso-electric point is in the acidic region of the zeta potential plot (pH=5.2±0.5). After increasing the ethanol content, the iso-electric point moves towards higher pH values (pH=7). In 99% ethanol and 1% electrolyte suspensions, there are no more iso-electric point showing in the zeta potential versus pH plots, which show positive zeta potential values for all pHs tested.

The zeta potential versus pH for Al₂O₃, at varying ratios of ethanol/electrolyte, is shown in Figure 15. Al₂O₃ has been shown to have a basic surface characteristic [52]. Thus, in 100% electrolyte, the iso-electric point is in the basic pH region (pH=8.8±0.5). As ethanol is added, the iso-electric point decreases to a more acidic pH (pH=7.3).

The absolute value of the zeta-potential for SiC_w and Al₂O₃, as shown in Figures 14 and 15, decreases as the ratio of ethanol to electrolyte increases. Since the dielectric constant (D) of ethanol is approximately 1/3 that of water, as the ethanol content increases, the suspension dielectric constant decreases assuming a rule of mixtures calculation. Therefore, the thickness of the double layer (1/κ) will decrease with increasing ethanol content. The dependence of (1/κ) on dielectric constant can be seen in

$$\frac{1}{\kappa} = \left(\frac{DkT}{8\pi m_o Z^2 e^2} \right)^{\frac{1}{2}} \quad (20)$$

Equation (20).

ζ (mV)

Figure

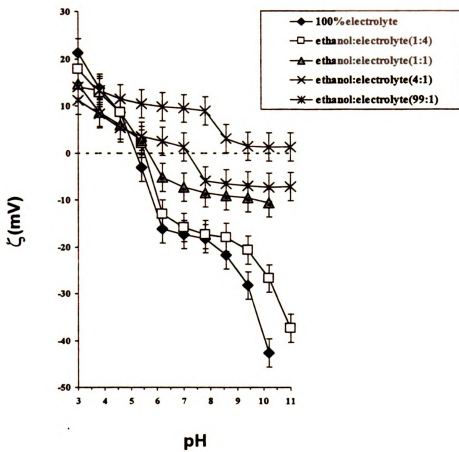


Figure 14 Zeta potential versus pH for SiC_w at varying ratios of ethanol to electrolyte under 0.001N KNO_3 and 0.5 vol% solids content.

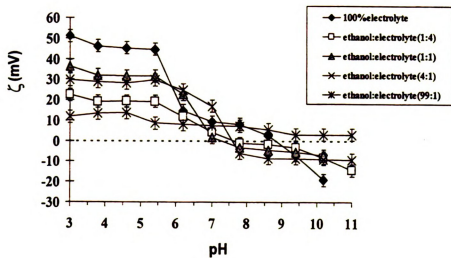


Figure 15 Zeta potential versus pH for Al_2O_3 at varying ratios of ethanol to electrolyte under 0.001N KNO_3 and 0.5 vol% solids content.

2020

Evolution.

2. From 7

02-2100

322 Stat

Figures:

anolyte (

News the

and ele

was hon

more ele

100029

23: ele

000000

کتابخانه

Ar.

 ΔH°

File No.

107

between

REPORT

 H_2O

DLVO theory predicts that the particle double layers provide a repulsive force against flocculation. Therefore, the zeta potential decreases due to compression of the double layer. From zeta potential measurements, SiC_w and Al_2O_3 suspensions become unstable as the ratio of ethanol to electrolyte increases, in agreement with DLVO predictions.

3.2.2 Stability Ratio

Figures 16 to 20 give the stability ratios as a function of pH under constant electrolyte (0.001N KNO_3) concentration and varying ethanol to electrolyte ratios. Table 3 shows the stable pH ranges, as indicated by $\log W > 10$ [23], for each of the ethanol/electrolyte ratios. From Figures 16-20 and Table 3, it is seen that the stability against homocoagulation between $\text{SiC}_w/\text{SiC}_w$ shifts from pH 3 to 5 and from pH 6 to 11, in pure electrolyte, to pH 3 to 8 for 99% ethanol and 1% electrolyte. Stability against homocoagulation between $\text{Al}_2\text{O}_3/\text{Al}_2\text{O}_3$ shifts from pH 3 to 5 and from pH 10 to 11 for 100% electrolyte to pH 3 to 5 for 99% ethanol and 1% electrolyte. Stability against heterocoagulation between $\text{SiC}_w/\text{Al}_2\text{O}_3$ is in regions of pH 3 to 6 and pH 9 to 11 for aqueous suspensions and from pH 3 to 5 for 99% ethanol and 1% electrolyte suspensions.

Analysis shows that the stability generally decreases as ethanol content increases. At pH > 8 range the stability decreases to zero as ethanol content increases to 99%. The stable range for interactions between SiC_w and Al_2O_3 , and Al_2O_3 and Al_2O_3 , at 99% ethanol and 1% electrolyte, remains at pH < 5. However, the stable range for interactions between SiC_w and SiC_w expands to pH 8 in the 99% ethanol and 1% electrolyte suspensions. Therefore, at pH < 5, interactions for SiC_w to SiC_w , SiC_w to Al_2O_3 , and Al_2O_3 to Al_2O_3 are stable in 99% ethanol and 1% electrolyte.

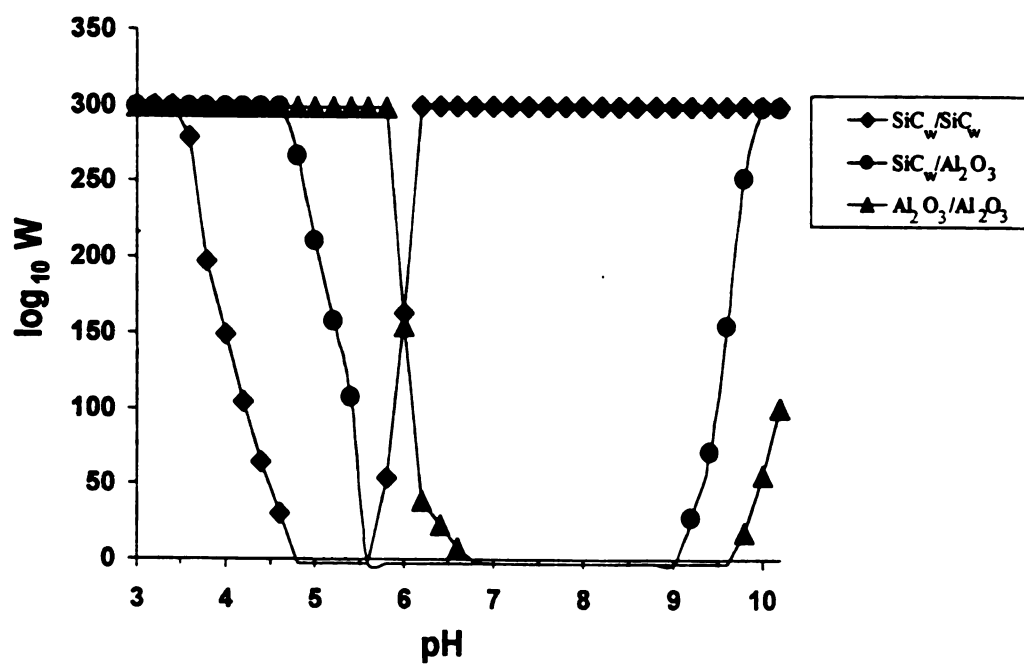


Figure 16 Stability ratio versus pH for $\text{SiC}_w/\text{Al}_2\text{O}_3$ in 0.001N KNO_3 and ethanol:electrolyte (0:1).

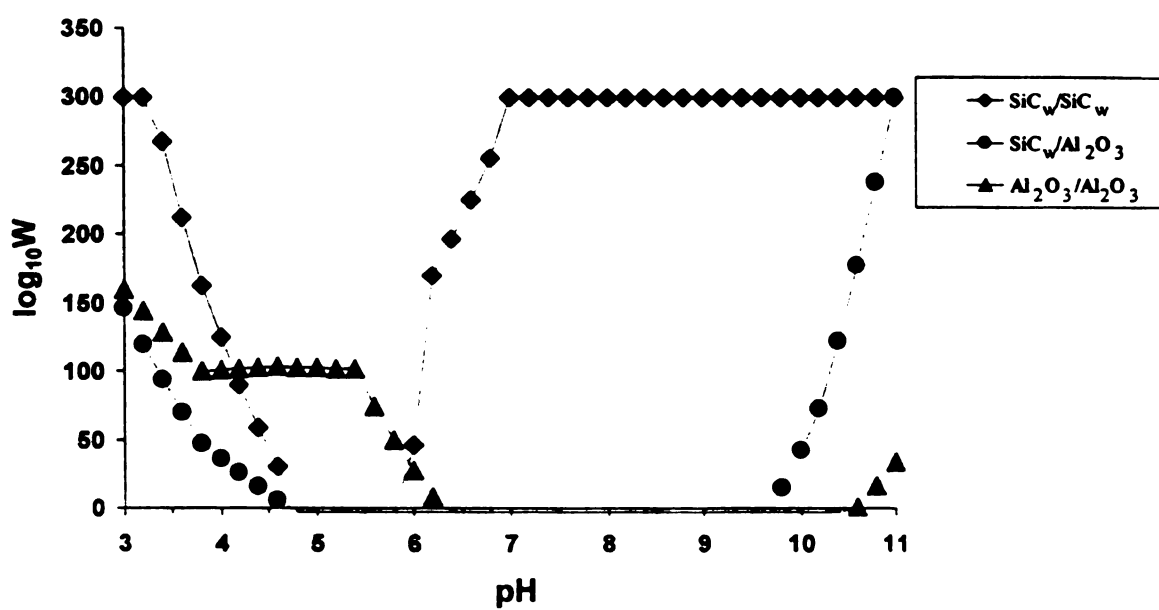


Figure 17 Stability ratio versus pH for SiC_w/Al₂O₃ in 0.001N KNO₃ and ethanol:electrolyte (1:4).

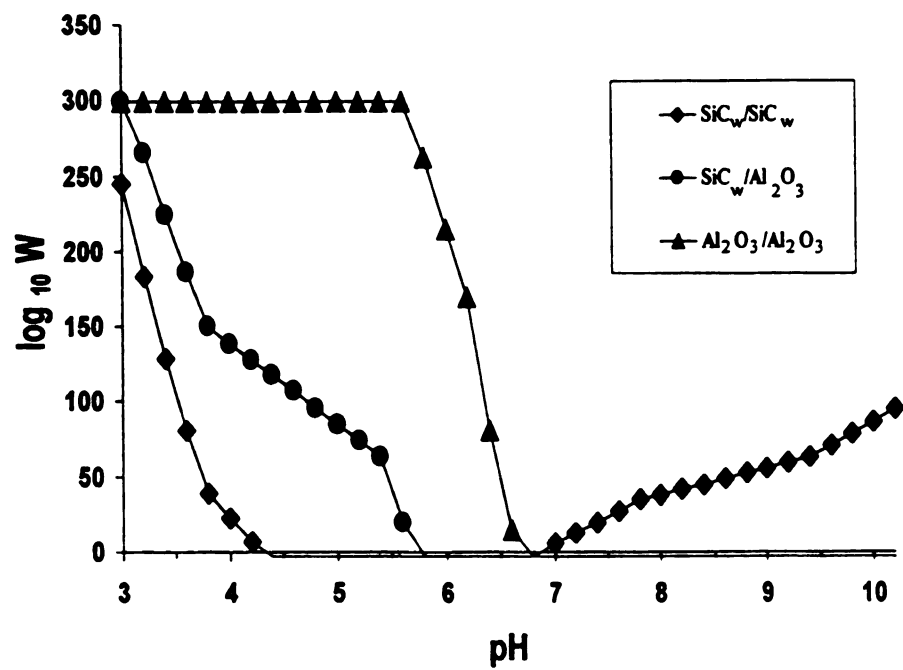


Figure 18 Stability ratio versus pH for $\text{SiC}_w/\text{Al}_2\text{O}_3$ in 0.001N KNO_3 and ethanol:electrolyte (1:1).

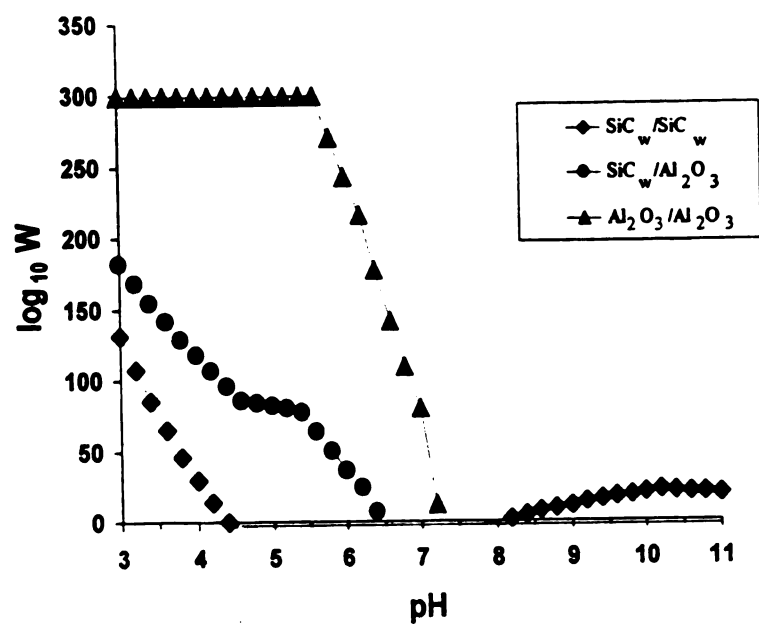


Figure 19 Stability ratio versus pH for SiC_w/Al₂O₃ in 0.001N KNO₃ and ethanol:electrolyte (4:1).

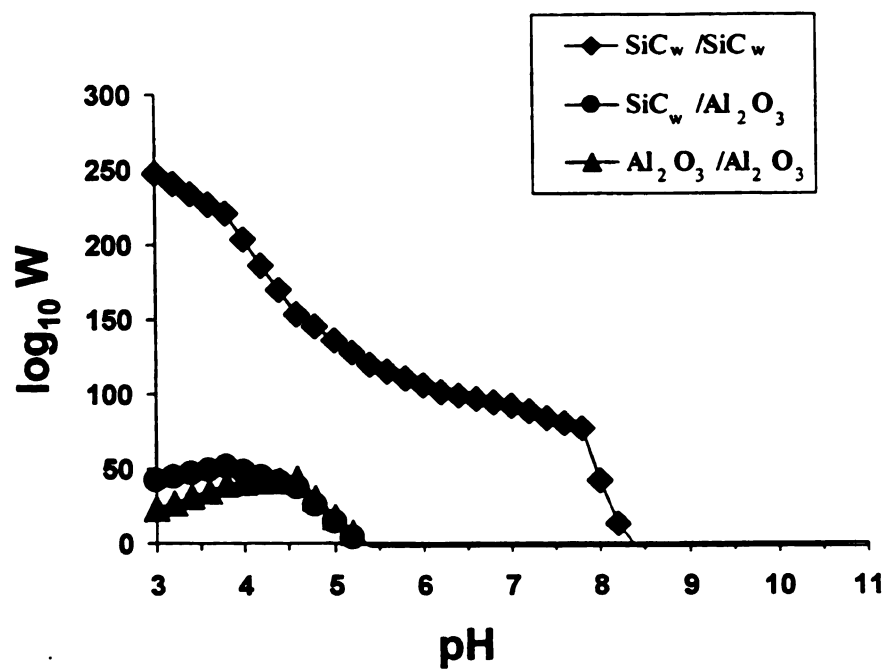


Figure 20 Stability ratio versus pH for $\text{SiC}_w/\text{Al}_2\text{O}_3$ in 0.001N KNO_3 and ethanol:electrolyte (99:1).

The st

anol and

between Si

berry acc

ergy and

V

As sta

increased c

V_2 is subst

generally b

predicted t

has shown

increase in

between Si

Table 3 S

100% ele

ethanol:

(1:4)

ethanol:

(1:1)

ethanol:

(4:1)

ethanol:

(99:1)

The stable range for interactions between $\text{SiC}_w/\text{Al}_2\text{O}_3$, and $\text{Al}_2\text{O}_3/\text{Al}_2\text{O}_3$ in 99% ethanol and 1% electrolyte become smaller. However, the stable range for interactions between SiC_w and SiC_w in 99% ethanol and 1% electrolyte expands to pH 8. DLVO theory accounts for the total energy of interaction between the repulsive interaction energy and van der Waal's attractive energy as:

$$V_T = V_A + V_R \quad (11)$$

As stated previously, the repulsive energy, V_R , decreases as the ethanol content is increased due to the compression of the double layer. It is believed that the decrease in V_R is substantially great and results in an overall decrease in V_T . Thus, suspensions generally become increasingly unstable as the ethanol content is increased. Bleier [20] predicted the stability of SiC in ethanol and water respectively by calculation of V_A , and has shown that V_A is higher in ethanol compared to V_A in water. It is believed that the increase in V_A for SiC in ethanol results in the stability improvement for the interactions between SiC_w and SiC_w in 99% ethanol and 1% electrolyte at $\text{pH} < 8$.

Table 3 Stable pH range in various media

	$\text{SiC}_w/\text{SiC}_w$	$\text{SiC}_w/\text{Al}_2\text{O}_3$	$\text{Al}_2\text{O}_3/\text{Al}_2\text{O}_3$
100% electrolyte	3-5, 6-11	3-6, 9-11	3-7, 10-11
ethanol:electrolyte (1:4)	3-5, 6-11	3-5, 10-11	3-6, 11
ethanol:electrolyte (1:1)	3-4, 7-11	3-6	3-7
ethanol:electrolyte (4:1)	3-4, 9-11	3-6	3-7
ethanol:electrolyte (99:1)	3-8	3-5	3-5

3.2.3 Viscosity

Figure 21 shows the viscosity of 10 vol% $\text{SiC}_w/\text{Al}_2\text{O}_3$ suspensions with 40 wt% solids loading at varying ratios of ethanol/electrolyte. For 100% electrolyte, the suspension viscosity is low at $\text{pHs} < 8$ and $\text{pHs} > 11$ and high from pH 9 to 10. When the ethanol content increases, the viscosity increases dramatically at high pHs. But at $\text{pHs} < 4$, even in 99% ethanol and 1% electrolyte, the 10 vol% $\text{SiC}_w/\text{Al}_2\text{O}_3$ suspensions have low viscosities. These measurements verify the stability predictions, where high stability coincides with lower viscosities and low stability coincides with higher viscosities.

3.2.4 Sedimentation Bulk Density

Figure 22 shows plots of sedimentation bulk density as a function of pH for Al_2O_3 and SiC_w in 100% electrolyte and a mixture of 99% ethanol and 1% electrolyte suspensions. A comparison of SiC_w and Al_2O_3 sedimentation densities in 100% electrolyte and in a mixture of 99% ethanol and 1% electrolyte shows that the sedimentation density in the electrolyte at high pHs is higher than that in a mixture of 99% ethanol and 1% electrolyte. The stable suspensions at low pHs from stability prediction have high sedimentation densities and unstable suspensions at high pHs have low sedimentation densities. The low sedimentation densities are believed to be due to the loose packing of agglomerates.

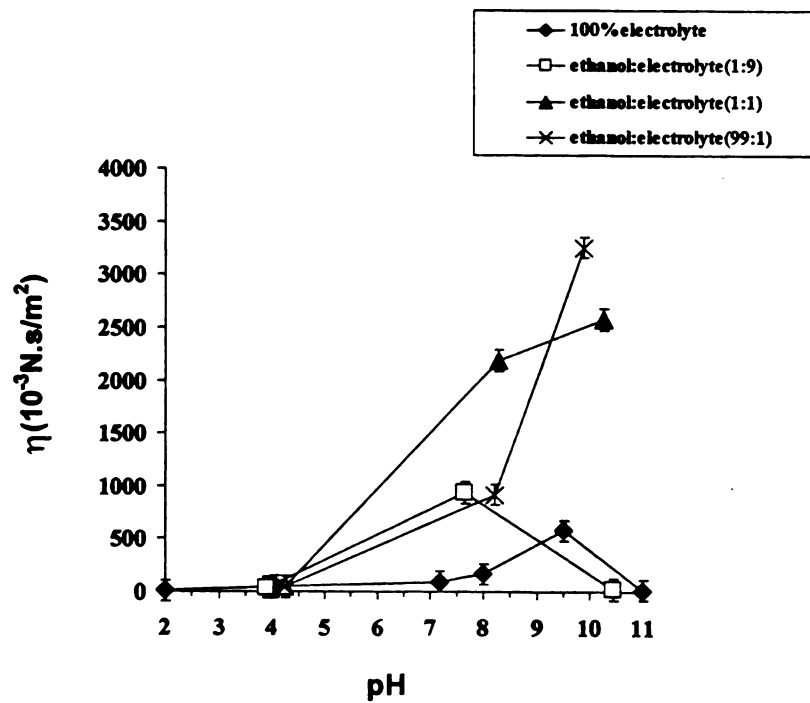


Figure 21 Viscosity of 10 vol% $\text{SiC}_w/\text{Al}_2\text{O}_3$ with 40 wt% solids content at varying ratios of ethanol to electrolyte.

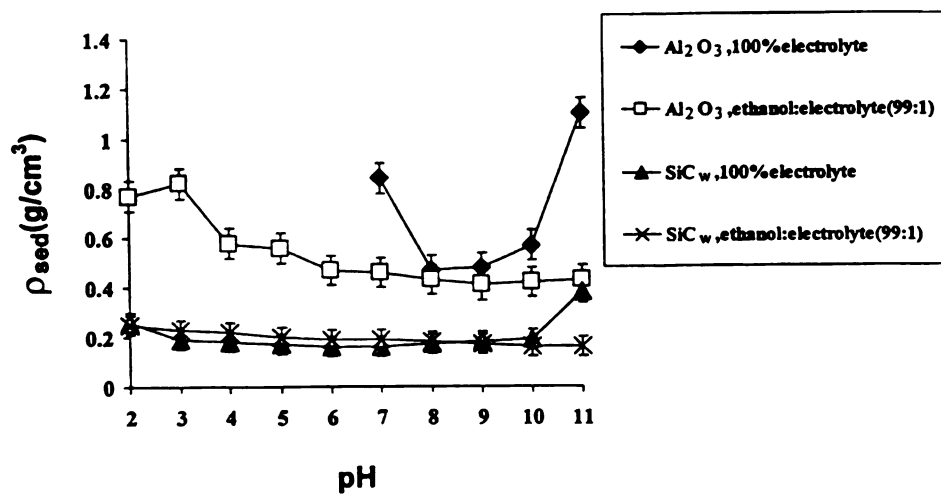


Figure 22 Sedimentation bulk density versus pH for Al_2O_3 and SiC_w in electrolyte and ethanol, respectively (0.001N KNO_3).

3.2.5 Microstructure

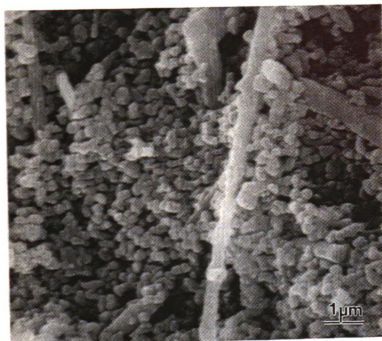
The green body microstructures (Figure 23) show the SiC_w to be evenly distributed and unagglomerated in electrolyte, a mixture of ethanol and electrolyte (1:1), and a mixture of 99% ethanol and 1% electrolyte. There is no obvious heterocoagulation between SiC_w and Al₂O₃ and only slight homocoagulation between Al₂O₃ particles at 99% ethanol and 1% electrolyte, consistent with the stability predictions.

In Figure 24, the microstructures of partially sintered (1650-1700°C, 2h) 10 vol% SiC_w/Al₂O₃ samples show that SiC_w is well distributed within the partially sintered Al₂O₃ matrix. The SiC_w and Al₂O₃ are uniformly distributed throughout suspensions in 100% electrolyte and ethanol:electrolyte (1:1).

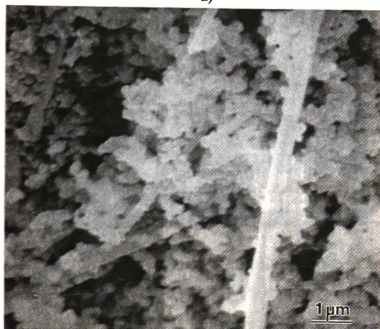
3.2.6 Conclusions

As the ethanol content increases, the absolute values of the zeta potential for both SiC_w and Al₂O₃ decrease. The iso-electric point likewise shifts for SiC_w to more basic pHs and for Al₂O₃ to more acidic pHs. This leads to a decrease in stability for both materials, as verified by sedimentation experiments. A comparison of SiC_w and Al₂O₃ sedimentation densities in 100% electrolyte and in a mixture of 99% ethanol and 1% electrolyte shows that the sedimentation density in the electrolyte at high pHs is higher than that in a mixture of 99% ethanol and 1% electrolyte. The stable suspensions at low pHs from stability prediction have high sedimentation densities and unstable suspensions at high pHs have low sedimentation densities.

Ethanol and a mixture of ethanol to electrolyte reduce the dielectric constant of both

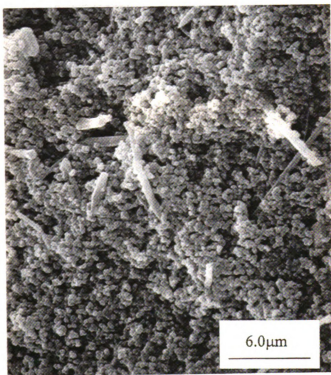


a)



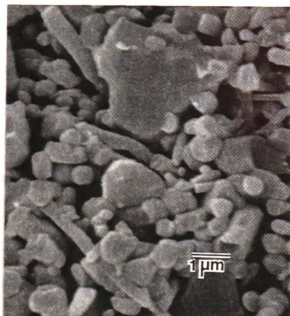
b)

Figure 23 SEM photomicrographs of 10 vol% $\text{SiC}_w/\text{Al}_2\text{O}_3$ green body in a) electrolyte, b) ethanol:electrolyte (1:1), and c) ethanol:electrolyte (99:1) (0.001N KNO_3 , non-ball-milled, pH 4, no polyelectrolyte and sintering aids).

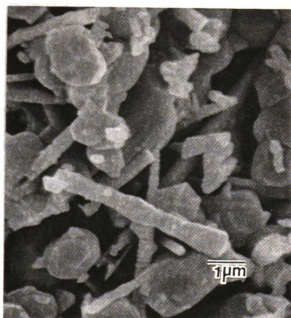


c)

Figure 23 (cont'd)



a)



b)

Figure 24 SEM photomicrographs of 10 vol% $\text{SiC}_w/\text{Al}_2\text{O}_3$ partially sintered samples: a) electrolyte, b) ethanol:electrolyte (1:1) (0.001N KNO_3 , non-ball-milled, pH 4, no polyelectrolyte and sintering aids, sintered at 1650°C for 1h, nitrogen atmosphere).

suspensions. The zeta potential decreases due to compression of the double layer. The stability ratio shows that the stability generally decreases as the ethanol content increases. But at pH<8 the interactions between SiC/SiC are more stable as the ethanol content increases. Green body microstructure shows the SiC_w and Al₂O₃ to be well dispersed both in electrolyte and in ethanol:electrolyte (1:1). However, there is a slight homo-coagulation of Al₂O₃ in ethanol:electrolyte (1:1). The partially sintered microstructure again shows good dispersion of SiC_w.

3.3 Colloidal Processing of SiC_w/Al₂O₃ Composites

Figure 25 showed colloidal processing approaches in the beginning of this research. Successful processing in practice required trial and error to determine the proper conditions. The theoretical results were used as a guide in the searching of the proper processing.

3.3.1 Monolithic Alumina

It is recognized that inhomogeneities (i.e., local variations of chemical composition, grain size or density) within the green compact can limit the extent of densification attained. It is important to eliminate inhomogeneities from monolithic powder compacts in the form of packing differences, grain size differences or composition differences [53]. Colloidal processing was used to achieve homogeneous green bodies. A green density of 64% of the theoretical density was obtained by slip casting. Colloidal processing yielded higher densities at lower sintering temperatures and shorter times. A 99% of the theoretical density was obtained at 1400°C (one hour) for AKP-30 alumina powder with 0.3-0.5µm particle size at pH 4 and 0.001N KNO₃ electrolyte.

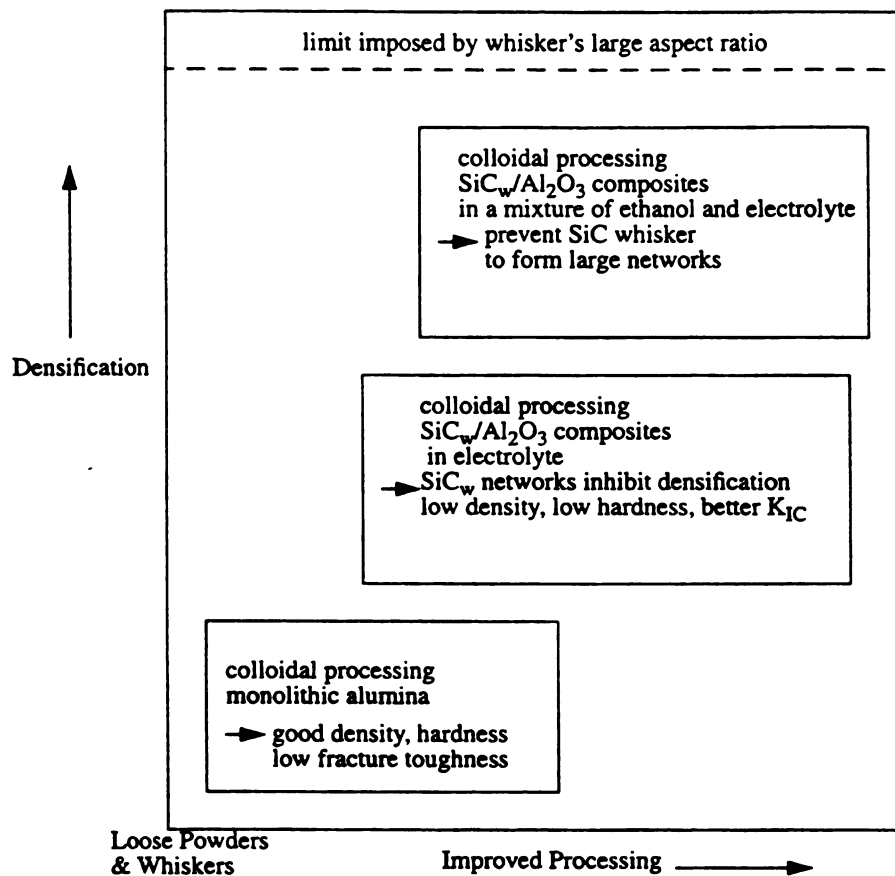
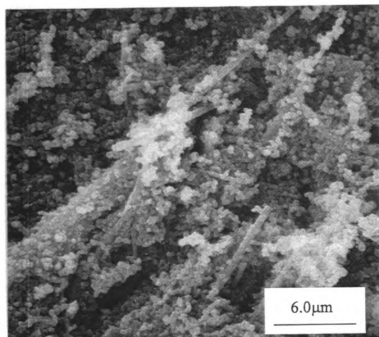


Figure 25 Colloidal processing approaches.

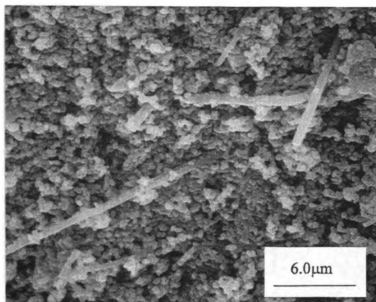
3.3.2 Processing of SiC_w/Al₂O₃ Composites in Aqueous Systems

Figure 26 shows SEM photomicrographs of green microstructures of 10 vol% SiC_w/Al₂O₃ composite processed from suspensions of different pH. Homogeneous SiC_w/Al₂O₃ green bodies with densities of 2.55 g/cm³ (~65% TD) were obtained. A comparison of the SEM photomicrographs (Figure 26) shows that uniform green microstructures were obtained at pH 3, 4 and 11; agglomerated microstructures were obtained at pH 2, 8 and 10. These green microstructure results are in good agreement with the stability predictions for suspensions at different pHs. Figure 27 shows SEM photomicrographs of sintered microstructures of 5 and 10 vol% SiC_w/Al₂O₃ composites sintered at 1650°C for one hour. Densification was inhibited by the SiC whiskers. The sintered densities of 5 and 10 vol% SiC_w/Al₂O₃ were only 3.15 g/cm³ (~80% TD) and 2.84 g/cm³ (~73% TD), respectively, slightly better than the density values obtained by researchers at MIT for the same composite (60-70% TD) [54]. From stability predictions and slip casting experiments, pH 4 was the optimum processing condition. Figure 28 shows green density changes at different whisker loadings. The green density decreases as the whisker loading increases. This can be explained by the whisker network effect. The higher the whisker loading, the more the whisker network forms. The loose packed whisker networks cause a decrease in the green density.

The stress induced by the presence of the whisker networks stopped further sintering of the composites. Improvements in the sintering of the composites will only then occur if the whisker network can be removed or reduced. Additions of certain alcohols to the whiskers were found to prevent the formation of large flocs [55]. Stability predictions indicate that SiC whiskers in a mixture of ethanol and electrolyte should be stable at

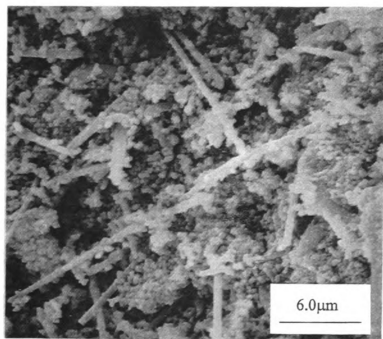


a)

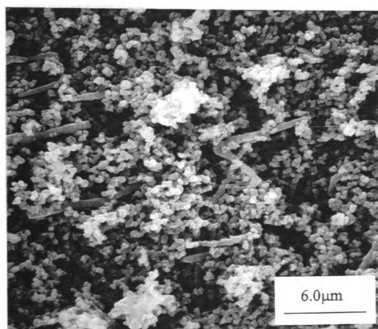


b)

Figure 26 SEM photomicrographs of green microstructures of 10 vol% SiC_w/Al₂O₃ composite processed from different pHs: a) pH 2, b) pH 3, c) pH 4, d) pH 8, e) pH 10, and f) pH 11 (0.001N KNO₃, non-ball-milled, no polyelectrolyte and sintering aids).

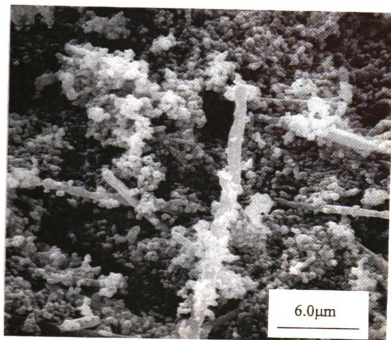


c)

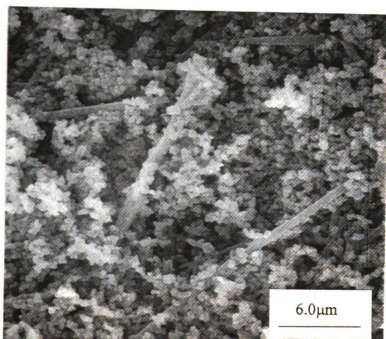


d)

Figure 26 (cont'd).

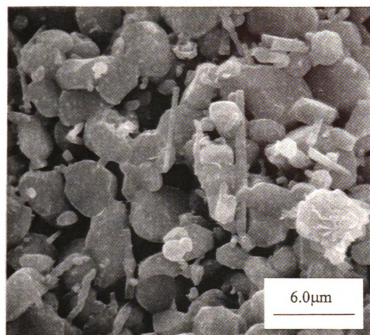


e)

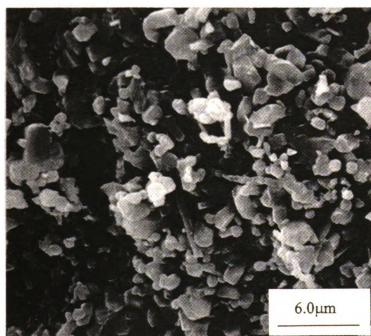


f)

Figure 26 (cont'd).



a)



b)

Figure 27 SEM photomicrographs of sintered microstructures: a) 5 vol% $\text{SiC}_w/\text{Al}_2\text{O}_3$ and b) 10 vol% $\text{SiC}_w/\text{Al}_2\text{O}_3$. Sintered at 1650°C for 1h, nitrogen atmosphere (0.001N KNO_3 , non-ball-milled, pH 4, no polyelectrolyte and sintering aids).

Figure

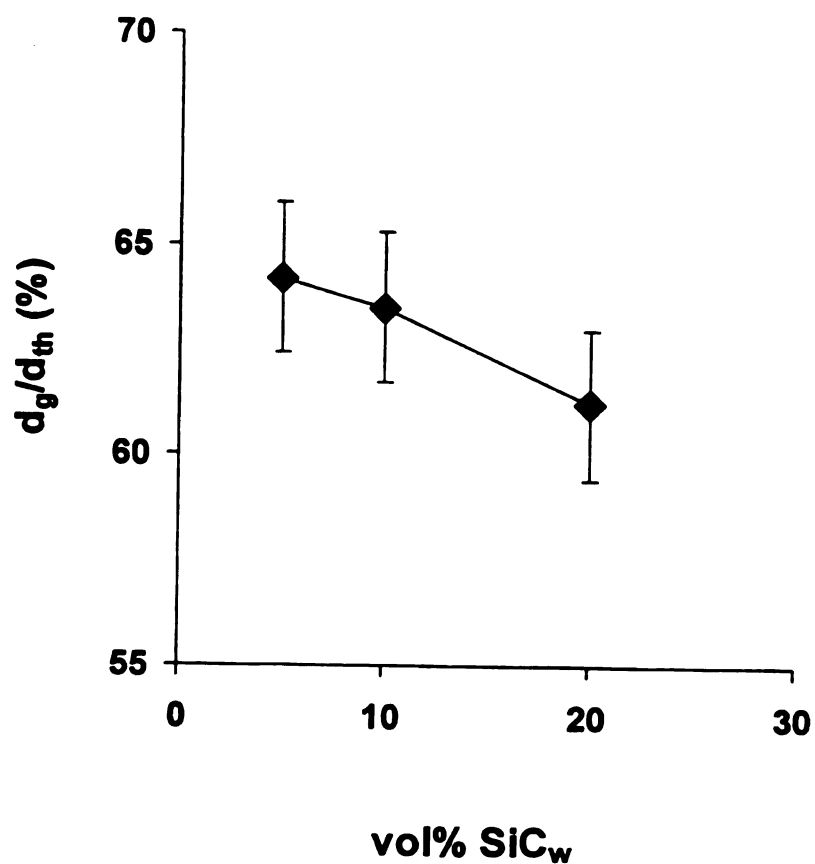


Figure 28 Green density versus whisker loading (0.001N KNO_3 , non-ball-milled, pH 4, no polyelectrolyte and sintering aids).

pH < 6. The

the comp

section.

3.3.3

To

thought t

Stability

electrolyt

processin

vol% SiC

ethanol e

g cm^{-3} (~6

microstru

mixture o

processed

from only

composite

Sinte

ethanol an

effect. Fro

composite.

increased s

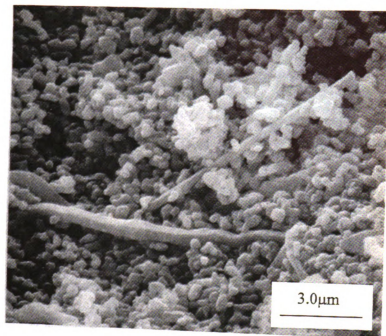
indicated th

pH<6. The results of efforts to weaken the SiC_w network, through effective processing of the composite in a mixture of ethanol and electrolyte, are discussed in the following section.

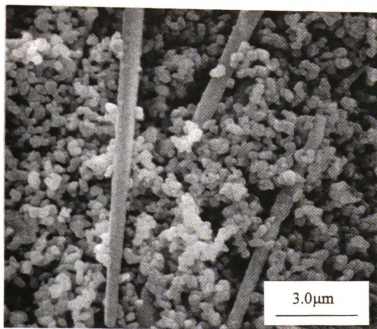
3.3.3 Processing of SiC_w/Al₂O₃ Composites in Nonaqueous System

To prevent the formation of large flocs, ethanol was added to the whiskers. It was thought that this might alleviate the stress effect of the whisker network on densification. Stability calculations predicted that SiC whiskers should be stable in 99% ethanol and 1% electrolyte at pH<6. Therefore, a mixture of ethanol and electrolyte was used during processing. Figure 29 shows SEM photomicrographs of green microstructures of 10 vol% SiC_w/Al₂O₃ composites cast from a mixture of ethanol and electrolyte with different ethanol/electrolyte ratios. Homogeneous SiC_w/Al₂O₃ green bodies with densities of 2.55 g/cm³ (~65% TD) were obtained. Figure 30 shows SEM photomicrographs of sintered microstructures of 10 vol% SiC_w/Al₂O₃ composites cast from a) electrolyte and b) a mixture of ethanol and electrolyte. From Figure 30 it was seen that the composite processed from a mixture of ethanol and electrolyte (1:1) is better densified than the one from only electrolyte. Figure 31 shows that the green density of 10 vol% SiC_w/Al₂O₃ composites varies at different ethanol/electrolyte ratios.

Sintered densities of 10 vol% SiC_w/Al₂O₃ composites slip cast from a mixture of ethanol and electrolyte were only 2.92 g/cm³ (~75% TD) due to the whisker network effect. From Figure 30 it is seen that whisker networks inhibited the sintering in this composite. Comparing with the results from the aqueous system, the sintered density increased slightly 2.84±0.08 g/cm³ (~73% TD) to 2.92±0.08 g/cm³ (~75% TD), which indicated that ethanol was not able to sufficiently alleviate the whisker network.

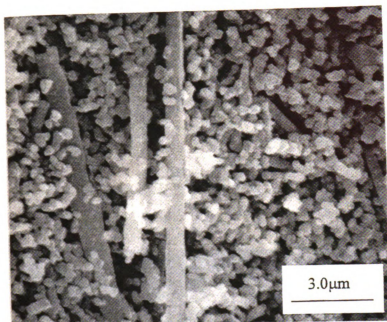


a)

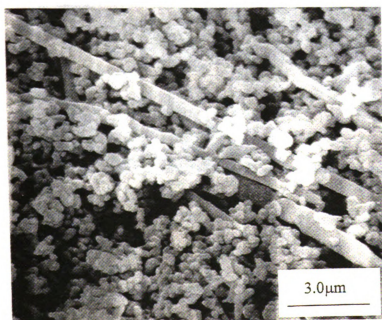


b)

Figure 29 SEM photomicrographs showing the green microstructures of 10 vol% $\text{SiC}_w/\text{Al}_2\text{O}_3$ composites: a) 100% electrolyte, b) ethanol:electrolyte (1:4), c) ethanol:electrolyte (1:1), d) ethanol:electrolyte (4:1) and e) ethanol:electrolyte (99:1) (0.001N KNO_3 , non-ball-milled, pH 4, no polyelectrolyte and sintering aids).

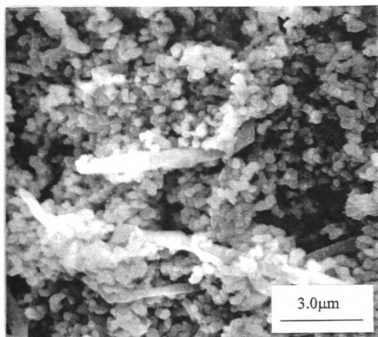


c)



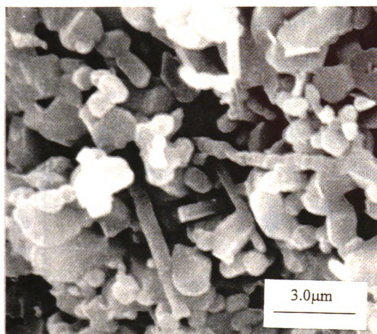
d)

Figure 29 (cont'd).

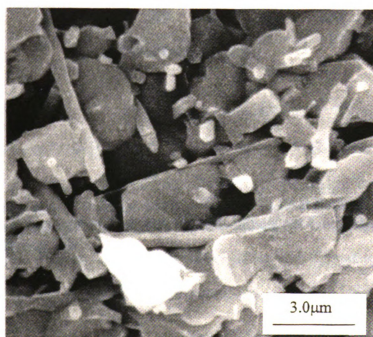


e)

Figure 29 (cont'd).



a)



b)

Figure 30 SEM photomicrographs of sintered microstructures of 10 vol% $\text{SiC}_w/\text{Al}_2\text{O}_3$, a) electrolyte and b) ethanol:electrolyte (1:1) (0.001N KNO_3 , non-ball-milled, pH 4, no polyelectrolyte and sintering aids, sintered at 1650°C for 1h, N_2).

Figure

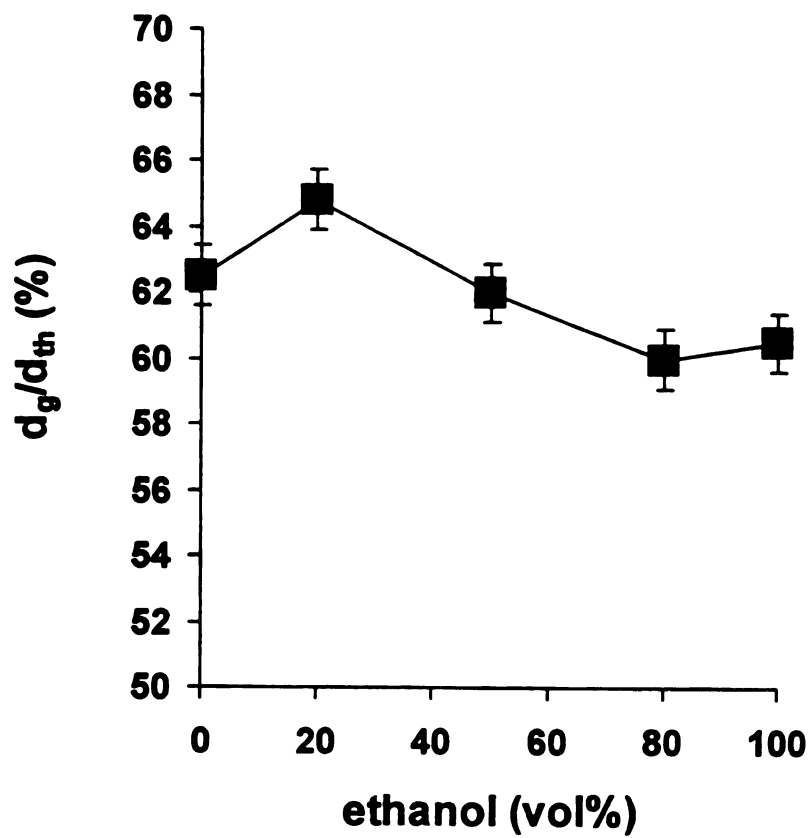


Figure 31 Green density variation of 10 vol% SiC_w/Al₂O₃ at different ratios of ethanol to electrolyte (0.001N KNO₃, non-ball-milled, pH 4, no polyelectrolyte and sintering aids).

A

electrol

inhibite

1400°C

compos

Although

whisker

pressure

stress on

form a ne

causes no

[57]. Ev

densifica

Alte

First, whi

network.

relaxed th

were adde

that becom

suspension

3.3.4 Discussion and New Approaches

Although the composite suspension is stable and codispersion of SiC_w and Al_2O_3 in electrolyte and a mixture of ethanol and electrolyte is good, densification was inhibited by the SiC whisker network effect. Monolithic alumina can be sintered at 1400°C to near full densification. However, the sintered density of 10 vol% $\text{SiC}_w/\text{Al}_2\text{O}_3$ composites in electrolyte or a mixture of ethanol and electrolyte were only 73-75%. Although ethanol may prevent formation of large whisker flocs, the problem related to whisker networks stops further sintering of the composites. Complete densification by pressureless sintering is often impossible to achieve [55]. The whiskers exert a back stress on the sintering matrix, which acts to impede densification [53,56]. The whiskers form a network with unequal distances between pairs of neighboring whiskers. This causes nonuniform local shrinkage that produces stresses, which impede densification [57]. Eventually, a continuous network of contacting whiskers can form, stopping further densification [57,58].

Alternative approaches that were explored are discussed in the following chapter. First, whiskers were ball milled to reduce the aspect ratio and to physically reduce the network. Second, sintering aids were added to create a grain boundary liquid phase that relaxed the back stresses that resulted from the network effect. Third, polyelectrolytes were added. It was thought that polyelectrolytes might assist in forming a surface coating that becomes an interphase region between whiskers and particles to stabilize the mixed suspensions.

3.4 D
A

3.4.1

The

composi

phase an

and Evan

suggest t

greater th

various se

cracks and

the same

initial aspe

manufactu

testing. Th

After bal

Figure:

milling time

identification

returning bac

While th

loadings were

of the slip dur

3.4 Densification of SiC_w/Al₂O₃ Composites through Improved Processing Approaches

3.4.1 Colloidal Processing Combined with Mechanical Methods

The aspect ratio of the whiskers has a strong influence on the sinterability of the composites because the problems associated with heterogeneous packing of the matrix phase and interactions between the whiskers increase as the aspect ratio increases. Faber and Evans [59] studied the toughening effect by using toughening models. Their results suggest that little additional toughening be obtained from whiskers with aspect ratios greater than 10-15. They calculated the toughness increment of composites containing various second phases and considered the existence of crack deflection reactions between cracks and second phases. The contribution of second phases to the toughening is almost the same in the region after the aspect ratio becomes greater than 12. The whisker's initial aspect ratio in this research is from 10 to 40, which is provided by the manufacturer. Therefore, the suspensions were ball milled for 25-50 hours before slip casting. The microstructure of the composites showed a range of aspect ratios from 6 to 20 after ball milling.

Figures 32 and 33 show that green density and sintered density increase as the ball-milling time increases. The physical reduction of the whisker networks enhanced the densification of the composites by allowing better packing of shorter whiskers and reducing back stress.

While the aspect ratio was reduced to prevent whisker networks, higher solids loadings were used to avoid segregation of powders and whiskers by differential settling of the slip during slip casting. The risk of differential sedimentation of the components in

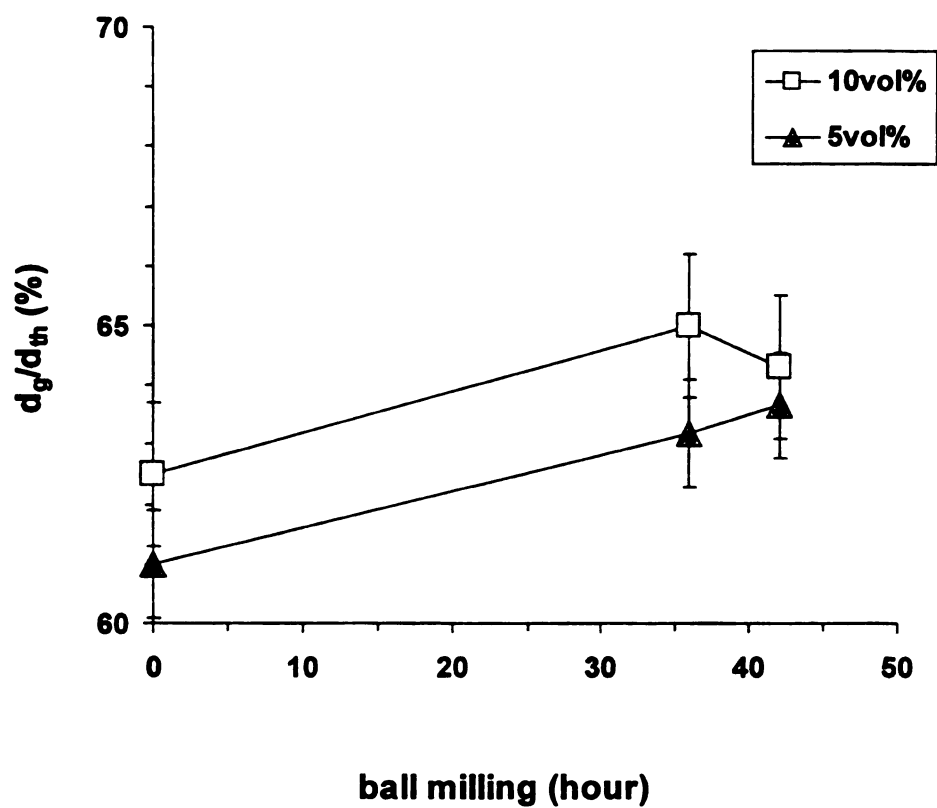


Figure 32 Green density of 5 and 10 vol% $\text{SiC}_w/\text{Al}_2\text{O}_3$ as a function of ball milling time (0.001N KNO_3 , ball-milled, pH 4, no polyelectrolyte and sintering aids).

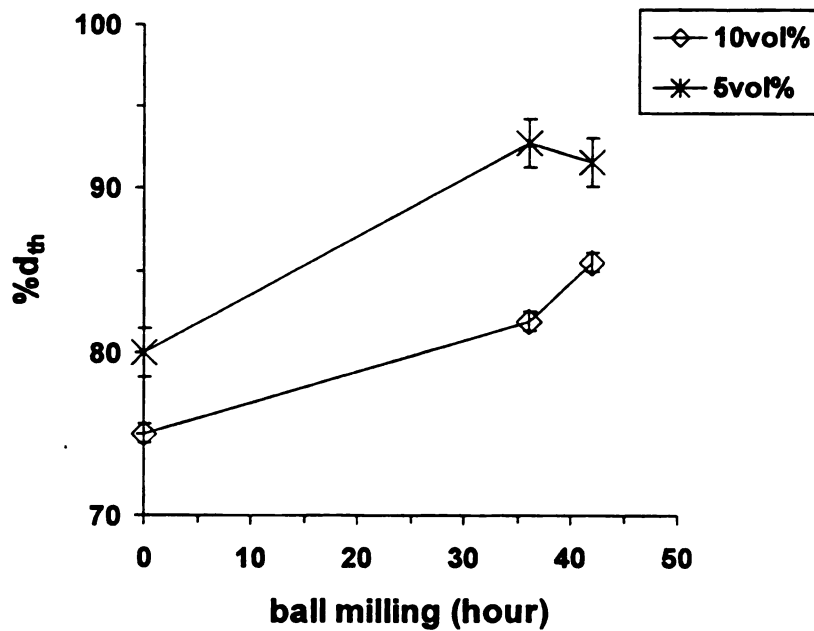


Figure 33 Sintered density of 5 and 10 vol% SiC_w/Al₂O₃ as a function of ball milling hour (0.001N KNO₃, ball-milled, pH 4, no polyelectrolyte and sintering aids, sintered at 1600°C for 1h, nitrogen atmosphere).

the liquid processing of ceramic composites is reduced if the suspensions are dense [60]. Processing of ceramic composites from dense liquid suspensions, containing up to 50 vol% solids, can reduce the settling rates of the components and avoid the risk of differential sedimentation of whiskers and matrix powders during processing. Figures 34 and 35 show that the green density and sintered density of 5-10 vol% SiC_w/Al₂O₃ at pH 4 changes at different solids loadings. Increasing the solids loading from 34 vol% to 50 vol% increased the green density due to less segregation and better packing. However, the sintered density did not show a significant difference as the solids loading changed. The whisker aspect ratio reduction had a more dramatic effect in achieving dense composites in 20 vol% SiC whisker composites in comparison to 5 or 10 vol% SiC whisker composites. High densities with 10 vol% SiC whisker and sintering aids were attainable without an aspect ratio reduction (see Figure 43 in Chapter 3.4.3).

Ball milling the aqueous suspension to control the whisker aspect ratio and break agglomerates resulted in better densification. However, densification was still inhibited by the presence of the whisker networks. The presence of a boundary liquid phase was predicted to reduce the whisker's network effect during sintering [53]. Therefore, the next step was to promote liquid phase sintering by using sintering aids.

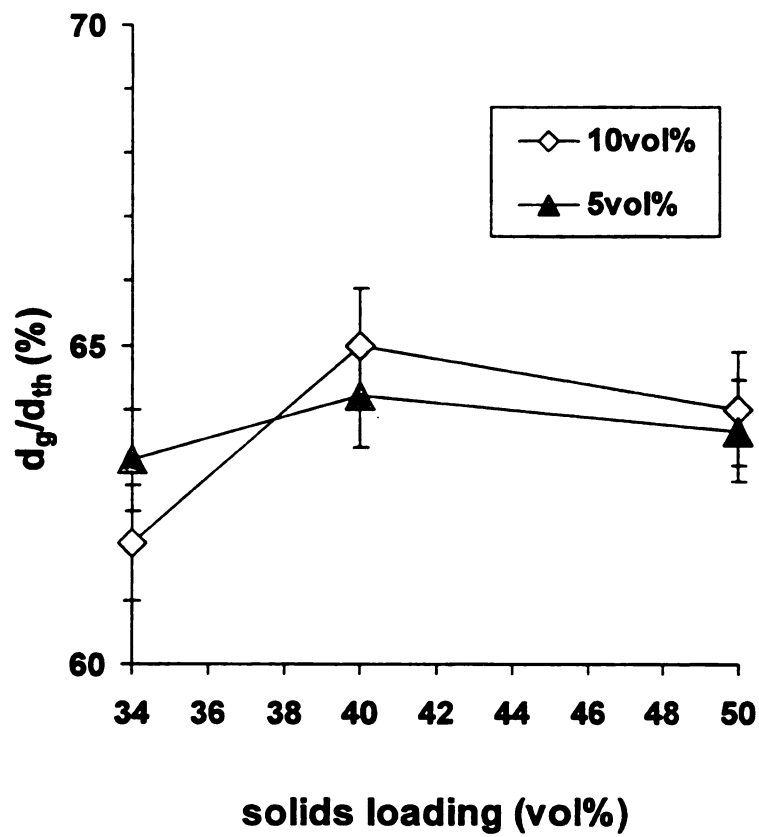


Figure 34 Green density of 5 and 10 vol% $\text{SiC}_w/\text{Al}_2\text{O}_3$ as a function of solids loading (0.001N KNO_3 , non-ball-milled, pH 4, no polyelectrolyte and sintering aids).

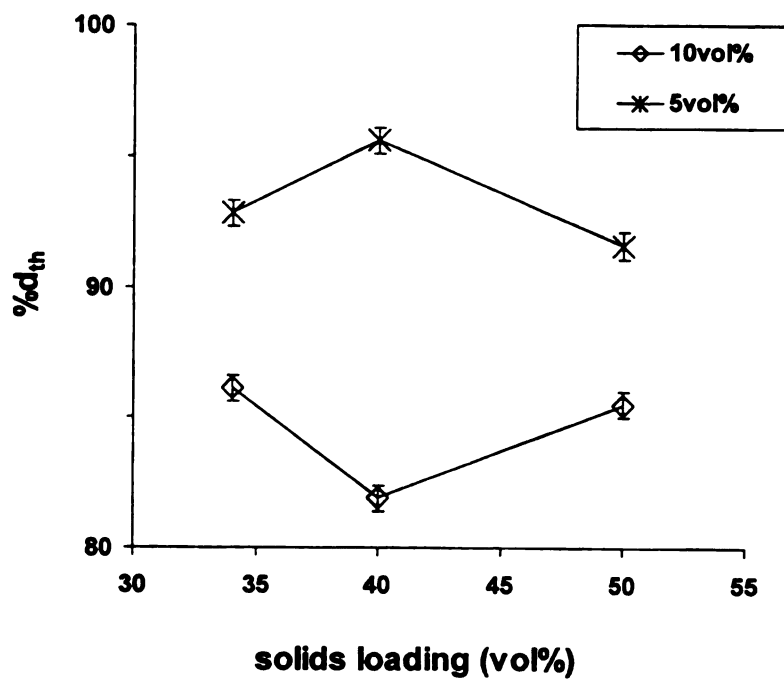


Figure 35 Sintered density of 5 and 10 vol% SiC_w/Al₂O₃ as a function of solids loading (0.001N KNO₃, non-ball-milled, pH 4, no polyelectrolyte and sintering aids, sintered at 1600°C for 1h, nitrogen atmosphere).

3.4.2 Sintering Aids

Theoretical calculations indicate that the presence of a liquid boundary phase will increase the stress relaxation rate and increase densification [53]. Studies by O. Sudre and coworkers [61,62] have demonstrated that the factors controlling the sintering of ceramic particulate composites involve the packing of the matrix phase and interactions between the inclusions, which lead to a constraining network. Sintering aids may therefore reduce these factors and increase sinterability.

Figure 36 shows an Al_2O_3 - Y_2O_3 - SiO_2 phase diagram [63]. At above 1600°C , liquid forms in the Si-rich area such as the SiC whisker surface with Al_2O_3 and Y_2O_3 particles [63]. Tokai whiskers have a high surface oxygen content where the oxide resembled SiO_2 [64]. The bulk oxygen is 0.23 wt% from fusion analysis whereas the surface oxygen is 12.1 at% as measured by x-ray photoelectron spectroscopy [64]. Therefore, additions of Y_2O_3 will react with the SiO_2 and Al_2O_3 powders to form a glass grain boundary phase that improves sinterability.

Figure 37 shows plots of green density of 5 and 10 vol% $\text{SiC}_w/\text{Al}_2\text{O}_3$ versus Y_2O_3 content. Green density stays relatively constant after the addition of 2-4 wt% Y_2O_3 although the green density decreased at the addition of 0.1-0.5 wt% Y_2O_3 . Figure 38 shows plots of sintering density of 5 and 10 vol% $\text{SiC}_w/\text{Al}_2\text{O}_3$ versus Y_2O_3 content. Sintered densities increased after introducing Y_2O_3 content. For 5 and 10 vol% $\text{SiC}_w/\text{Al}_2\text{O}_3$, respectively, the sintered densities remained almost constant at Y_2O_3 additions greater than 0.5 and 2 wt%, respectively. Sintering aids improved the sintering of the composites, however, the suspensions were slightly agglomerated and experienced some degree of difficulty in slip casting. The following section describes attempts to

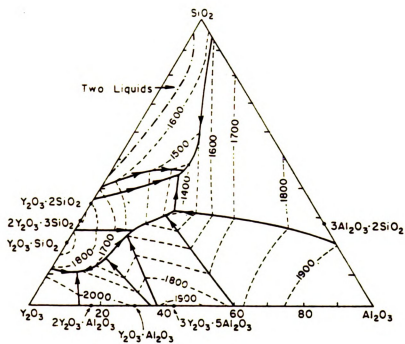


Figure 36 The Al_2O_3 - Y_2O_3 - SiO_2 phase diagram [63].

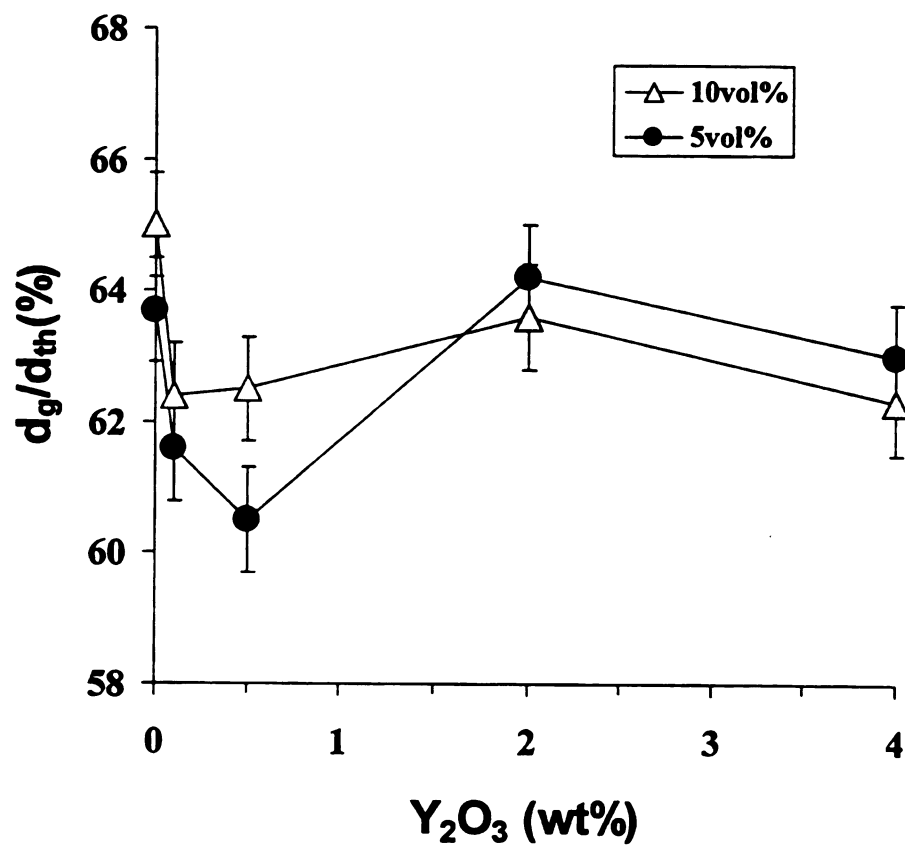


Figure 37 Green density of 5 and 10 vol% SiC_w/Al₂O₃ as a function of Y₂O₃ content (0.001N KNO₃, ball-milled, pH 11, 2.5 vol% polyelectrolyte).

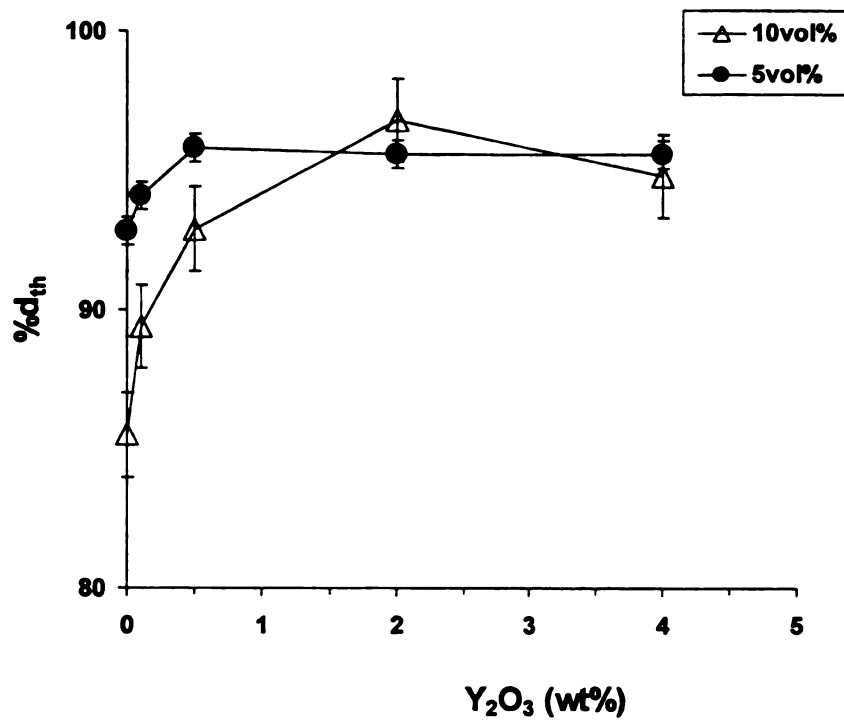


Figure 38 Sintered density of 5 and 10 vol% SiC_w/Al₂O₃ as a function of Y₂O₃ content (0.001N KNO₃, ball-milled, pH 11, 2.5 vol% polyelectrolyte, sintered at 1600°C for 1h, nitrogen atmosphere).

further stabilize the composite suspensions in the presence of sintering aids by adding a polyelectrolyte to make stable homogeneous microstructures to finally achieve good densification and mechanical properties.

3.4.3 Polyelectrolyte

A polyelectrolyte stabilizes suspensions to promote a uniform spatial distribution of the multiphases. A phase between the matrix and inclusion phases may be required to control the strength of the bond between the two phases [55]. A variety of coating and inclusion combinations have been demonstrated using dispersants to control the surface potential of the materials [55]. Polyelectrolytes are powerful additives that are able to reverse the zeta potential or to shift the iso-electric point of ceramic powders. Charge reversal mechanisms include ion change, surface complexing, ion-solvent interaction, adsorption of different species and steric stability of dispersant using polymeric carboxylic salts. It is important to select dispersants that are compatible in mixed systems [54]. The selected polyelectrolyte for this research is an ammonium salt of a polymeric carboxylic acid. It was reported that CA, tricarboxylic acid, might be the interface coating to stabilize the suspensions and also interact with particles electrostatically [26]. An ammonium salt of a polymeric carboxylic acid was also used successfully in stabilizing the suspensions [65].

Tables 4 and 5 list stable pH ranges for different components in aqueous media and in ethanol and allow a compatibility range to be identified. In aqueous media, the compatible processing range is pH 10-11.

Table 4. Compatibility of stable pH ranges for different components in aqueous media

Components	Stable pH range
Al ₂ O ₃ in electrolyte	3-7, 10-11
SiC _w in electrolyte	3-5, 6-11
Interaction between SiC _w and Al ₂ O ₃ in electrolyte	3-6, 9-11
Polyelectrolyte [66]	10-11
Y ₂ O ₃ [67]	8-12
Compatible processing range	11

Table 5 Compatibility of stable pH ranges for different components in 99% ethanol and 1% electrolyte

Components	Stable pH range
Al ₂ O ₃ in 99% ethanol and 1% electrolyte	3-5
SiC _w in 99% ethanol and 1% electrolyte	3-8
Interaction between SiC _w and Al ₂ O ₃ in 99% ethanol and 1% electrolyte	3-5
Polyelectrolyte[66]	10-11
Y ₂ O ₃ [67]	8-12
Compatible processing range	none

Polyelectrolyte dispersants can alter the Al_2O_3 surface charge. Figure 39 shows the zeta potential of Al_2O_3 versus pH for varying concentrations of polyelectrolyte. Figure 39 shows that the zeta potential at pH 4 changes from positive to negative after adding the polyelectrolyte, consistent with Cesarano III and Aksay's results [30]. In Figure 39, the increase in polyelectrolyte concentration caused the iso-electric point shifting from pH 8.8 to 3.2. The iso-electric point at pH 3.2 did not decrease further with additional increases in polyelectrolyte above 0.23 vol%. The absolute value of the zeta potential decreased at polyelectrolyte concentrations greater than 0.23 vol%. This is consistent with depletion flocculation at excess polyelectrolyte [30]. Table 6 lists the iso-electric point for Al_2O_3 at different polyelectrolyte concentrations. Table 7 shows the comparison of the iso-electric point for Al_2O_3 determined in this research and that published. The iso-electric point values of Al_2O_3 for suspensions with addition of different polyelectrolytes: citric acid, PMMA and ammonia salt of polymeric carboxylic acid, respectively, are within 0.5 pH. It is believed that the addition of these three different polyelectrolytes results in the formation of a negative charge on the alumina particles. As a result, the iso-electric point of an alumina suspension shifts towards pH 3. Additions of excess polyelectrolyte impact hardly any further change on the electrokinetic properties of the particles [71]. The saturation of the surface that is evident from the ESA measurements (Figure 39) is in very good agreement with the results of other researchers (Table 7).

Polyelectrolyte adsorbs onto the surface of Al_2O_3 , leading to a change in the surface charge as well as the magnitude of the zeta potential of the particles. It is possible to control the interaction potential between the powder particles by varying the polyelectrolyte

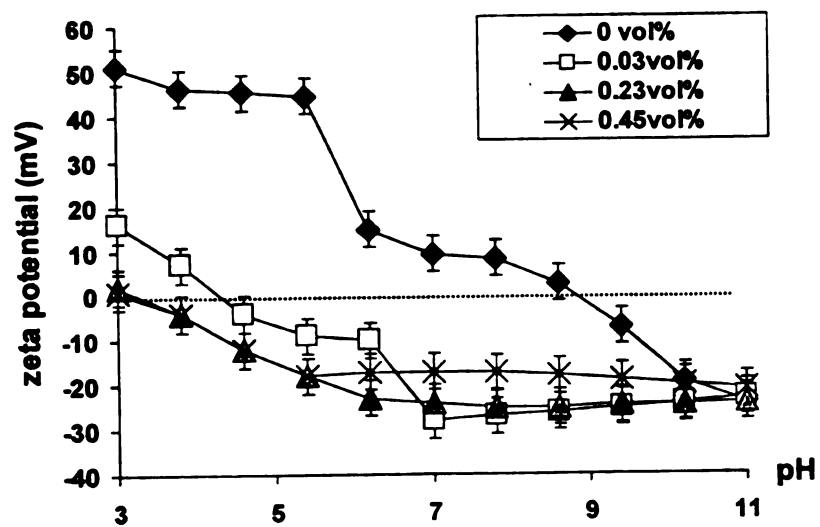


Figure 39 Zeta potential for Al_2O_3 versus pH at different polyelectrolyte concentrations (0.001N KNO_3).

Table 6 Comparison of polyelectrolyte addition to iep and ζ -potential for Al_2O_3

Polyelectrolyte	iso-electric point of Al_2O_3	Zeta potential versus pH plots
0	8.8	Original
0.03 vol%	4.2	Shifted
0.23 vol%	3.2	Saturated
0.45 vol%	3.2	Saturated

Table 7 Comparison of iso-electric point of Al_2O_3 between this research and published data [26,30]

Authors	iso-electric point in electrolyte	iso-electric point in electrolyte with polyelectrolyte addition
Hidber, Graule and Gauckler [26]	9.2	0.4 wt% CA: 3.2
Cesarano III and Aksay [30]	8.7	enough PMAA: 3.4
This research	8.8	0.23 vol% NH_4PCA : 3.2

Note: CA= tricarboxylic acid PMAA= polymethacrylic acid
 NH_4PCA = ammonia salt of polymeric carboxylic acid

concentration, thus enabling the isoelectric point (iso-electric point) of the Al_2O_3 as well as the viscosity of the suspension to be adjusted to the specific requirements of a given process [65,68].

Addition of 2.5 vol% polyelectrolyte stabilized the 10 and 20 vol% $\text{SiC}_w/\text{Al}_2\text{O}_3$ suspension in increasing the composite densities. However, further additions of polyelectrolyte past the adsorption saturation limit left excess polyelectrolyte in suspension. This excess polyelectrolyte lowered the densities of the composites due to depletion

flocculation in which the excess polyelectrolyte remaining in the solution leads to an increase of the ionic strength [71]. The presence of a large amount of unadsorbed polyelectrolyte in the solution results in a decrease of Debye length and, subsequently, an increase of the flocculation. Figures 40 and 41 show plots of green and sintered densities of the composites versus polyelectrolyte concentration. The sintered density increased as the polyelectrolyte was introduced. Without polyelectrolyte addition the suspension contained hard agglomerates and experienced some degree of difficulty in slip casting. Polyelectrolytes had a powerful effect in stabilizing the mixed suspensions. The optimum addition was found at a polyelectrolyte concentration of 2.5 vol%. Increasing the concentration beyond 2.5 vol% caused a slight decrease in the sintered density.

The addition of a polyelectrolyte (polymeric carboxylic salt as a dispersant-ammonium salt of a polymeric carboxylic acid) in controlling the dispersion and stability of $\text{SiC}_w/\text{Al}_2\text{O}_3$ in the presence of sintering aids in aqueous suspension proved successful. The carboxylic salt molecules absorbed on the surface not only influenced the surface charge of the alumina particles but also created a steric barrier that acted to inhibit the mutual approach of the individual particles [10].

Figures 42 and 43 are plots of the green and sintered densities of 10 and 20 vol% $\text{SiC}_w/\text{Al}_2\text{O}_3$ with sintering aids and polyelectrolyte at pH 11 as a function of changes in ball milling time. Because sintering aids relax the back stress of whisker networks and polyelectrolytes stabilize the suspensions, the whisker network effect due to a high aspect ratio is reduced. Ball milling had no apparent effect on green density (Figure 42). Sintered density improved slightly only at high whisker loadings (Figure 43). By controlling the surface chemistry to eliminate inhomogeneities and choosing suitable

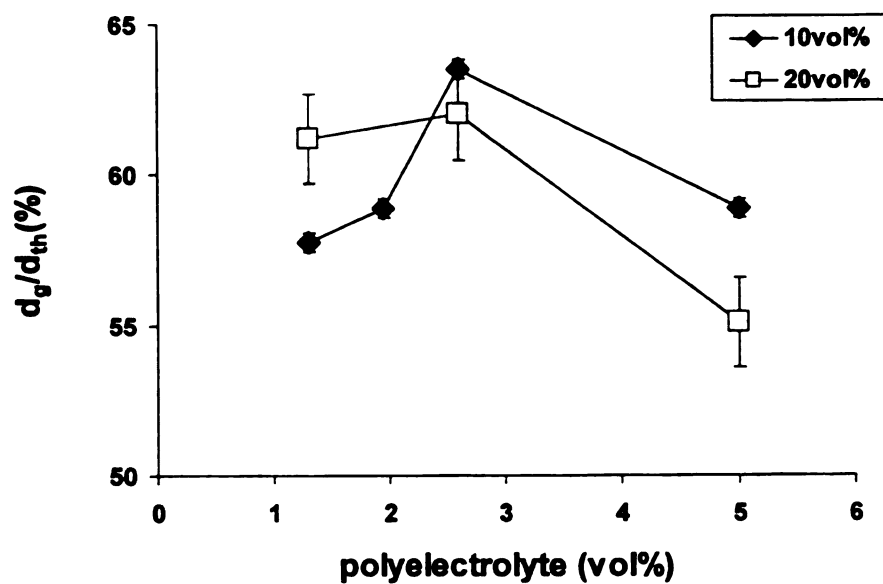


Figure 40 Green density of 10 and 20 vol% SiC_w/Al₂O₃ as a function of polyelectrolyte concentration (0.001N KNO₃, ball-milled, pH 11, 0.5 wt% MgO and 2 wt% Y₂O₃).

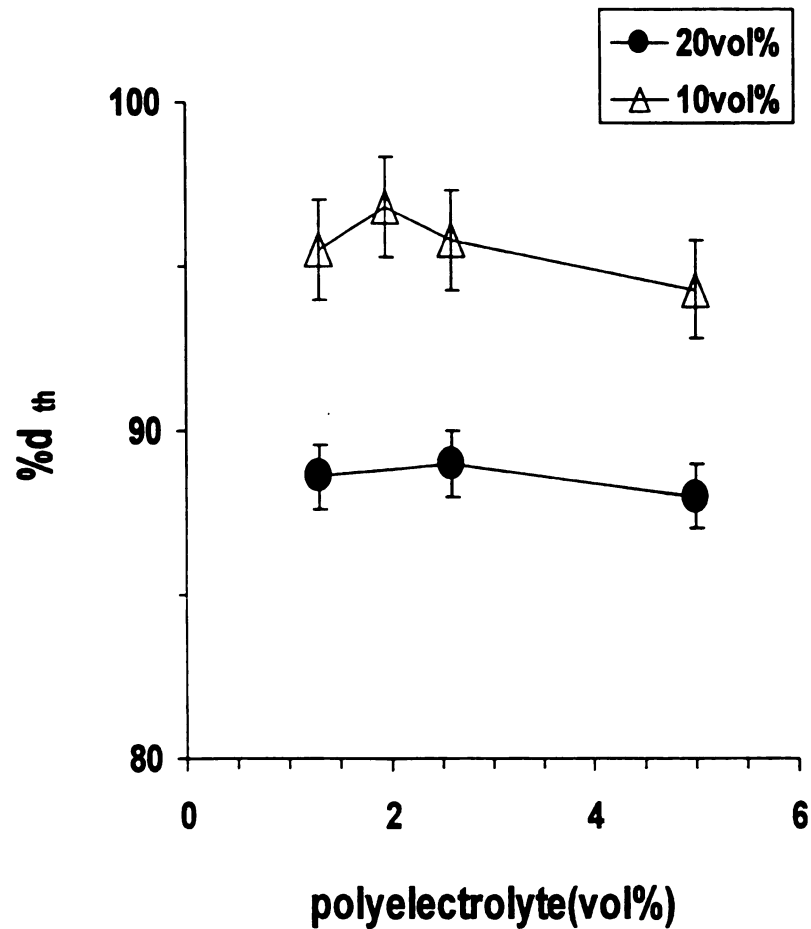


Figure 41 Sintered density of 10 and 20 vol% SiC_w/Al₂O₃ as a function of polyelectrolyte concentration (0.001N KNO₃, ball-milled, pH 11, 0.5 wt% MgO and 2 wt% Y₂O₃, sintered at 1600°C for 1h, nitrogen atmosphere).

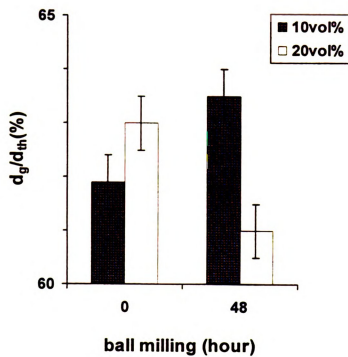


Figure 42 Green density of 10 and 20 vol% SiC_w/Al₂O₃ as a function of ball milling hour (0.001N KNO₃, ball-milled, pH 11, 2.5 vol% polyelectrolyte, 0.5 wt% MgO and 2 wt% Y₂O₃).

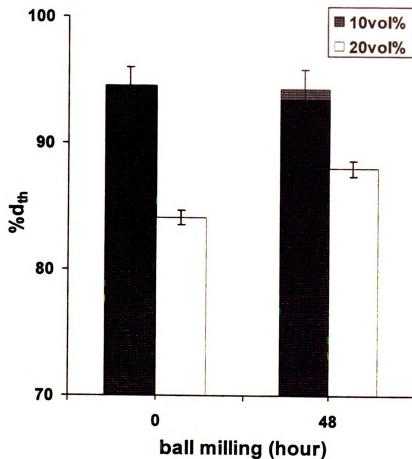


Figure 43 Sintered density of 10 and 20 vol% SiC_w/Al₂O₃ as a function of ball milling hour (0.001N KNO₃, ball-milled, pH 11, 2.5 vol% polyelectrolyte, 0.5 wt% MgO and 2 wt% Y₂O₃, sintered at 1600°C for 1h, nitrogen atmosphere).

sintering aids to alleviate the back stress of whisker networks, densification of 10 vol% SiC_w/Al₂O₃ with high aspect ratio whiskers can be achieved.

3.4.4 Discussion

The combined use of different approaches has been successful in producing dense SiC_w/Al₂O₃ composites in aqueous suspensions. pH 11 was determined to be the optimum processing pH value for SiC_w/Al₂O₃ composites with 2 wt% Y₂O₃, 0.5 wt% MgO and 2.5 vol% polyelectrolyte (ammonia salt of polymeric carboxylic acid).

The stable pH range for composites with sintering aids and polyelectrolyte and the stable pH range for the composite suspension in a mixture of ethanol and electrolyte are not compatible (see Table 5). From stability predictions the stable pH ranges for Al₂O₃, SiC_w and the interaction between Al₂O₃ and SiC_w in 99% ethanol and 1% electrolyte are pH 3-5, pH 3-8 and pH 3-5, respectively. However, the stable pH range for the polyelectrolyte as reported by the manufacturer is pH 10-11, and since Y₂O₃ dissolves only in acid, it can only be used at pH>7. Thus, there is no compatible processing pH range for Al₂O₃ particles, SiC_w whiskers Y₂O₃ and polyelectrolyte in 99% ethanol and 1% electrolyte. Therefore, the composites which were slip cast from a mixture of ethanol and electrolyte were devoid of Y₂O₃ as a sintering aid and the ammonium salt of a polymeric carboxylic acid as a stabilizing polyelectrolyte to improve densification.

The effect of non-aqueous media in ceramic colloidal suspensions has not been clearly identified. For nonaqueous suspensions, it is a challenge to find suitable sintering aids and appropriate polyelectrolytes to match the SiC_w/Al₂O₃ suspension systems. The current processing effort focused on aqueous suspensions. For nonaqueous suspensions,

further research should be directed to creating compatible processing ranges by choosing suitable sintering aids and an appropriate polyelectrolyte to match the stable pH range of Al_2O_3 and SiC_w in the non-aqueous suspension.

3.5 Improved properties of $\text{SiC}_w/\text{Al}_2\text{O}_3$ Composites

3.5.1 Sintered density

A bulk density of 3.79 g/cm^3 (97% TD) for 10 vol% $\text{SiC}_w/\text{Al}_2\text{O}_3$ was achieved at a sintering temperature of 1600°C under nitrogen flow for one hour. Densification was inhibited by the presence of the SiC whiskers. Bulk densities of 3.80 g/cm^3 (96% TD), 3.79 g/cm^3 (97% TD), and 3.40 g/cm^3 (89% TD) were obtained at 1600°C for composite samples containing 5, 10 and 20 vol% SiC whiskers, respectively. Figure 44 depicts the green and sintered densities for different pH values. Bulk densities for the 10 vol% $\text{SiC}_w/\text{Al}_2\text{O}_3$ composites were 3.79 g/cm^3 at pH 11 and 3.66 g/cm^3 at pH 4, respectively. At pH 7, the “creamy” slip failed to cast. Figure 45 is a comparison of the sintered density for $\text{SiC}_w/\text{Al}_2\text{O}_3$ composites for this study and other published results from Tiegs and Becher [3] at Oak Ridge National Laboratory, Sacks, Lee and Rojas [73] at the University of Florida and Barclay, Fox and Bowen [54] at Massachusetts Institute of Technology. The bulk sintered densities achieved in this study on average were higher at lower sintering temperatures and sintering time shorter by an average of 60 min. Tiegs and Becher [3] ball milled the whiskers, used sintering aids and sintered at $1700\text{--}1800^\circ\text{C}$. HIP at 1600°C and 170MPa in an argon atmosphere were also used along with the pressureless sintering. Sacks, Lee and Rojas [73] used suspension processing, polyelectrolytes, slip casting, and sintering at 1600°C for 4 hours in a flowing nitrogen atmosphere. Barclay, Fox and

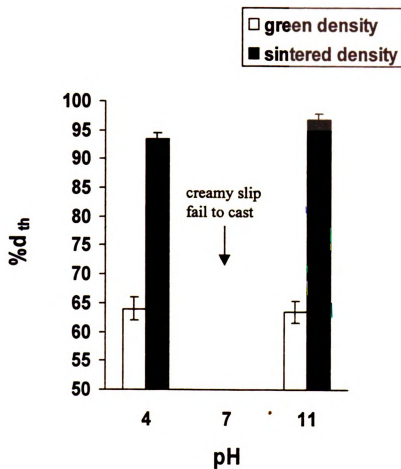


Figure 44 Green and sintered density of 10 vol% SiC_w/Al₂O₃ as a function of pH (0.001N KNO₃, ball-milled, 2.5 vol% polyelectrolyte, 0.5 wt% MgO and 2 wt% Y₂O₃, sintered at 1600°C for 1h, nitrogen atmosphere).

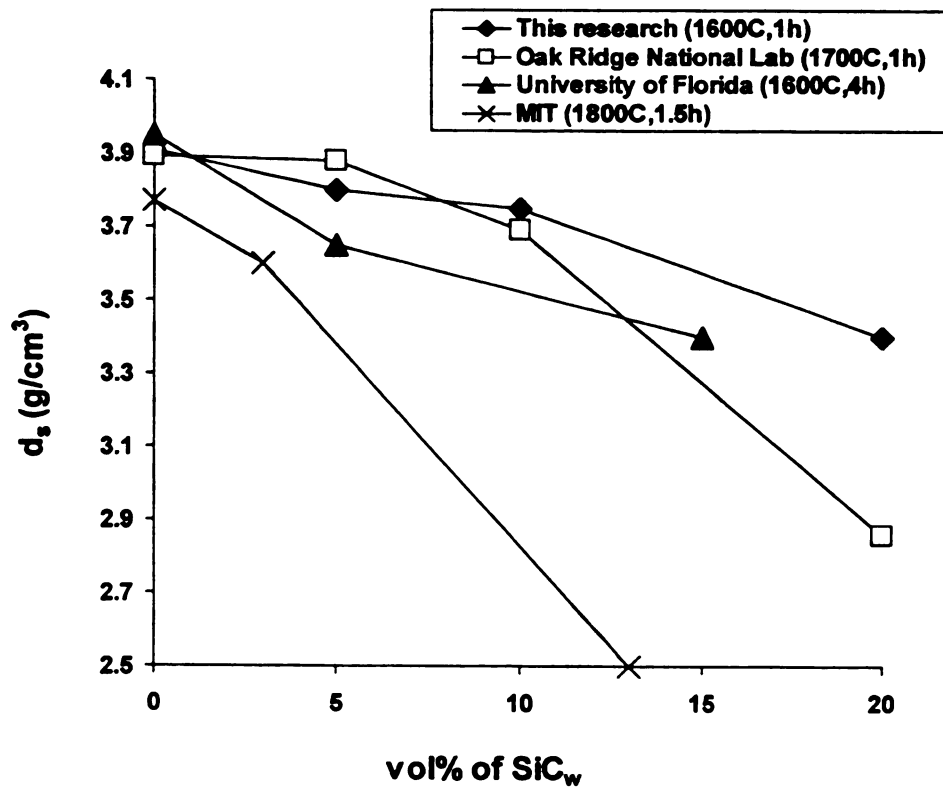


Figure 45 Comparison of sintered density of $\text{SiC}_w/\text{Al}_2\text{O}_3$ composites between this research and other published results [3,54,73].

Bowen [54] used yttrium isopropoxide as a sintering aid, polymeric dispersants and pressureless sintering at 1800°C for one and a half hours in a flowing argon atmosphere. The composites of this research used polyelectrolyte, sintering aids, ball milling and pressureless sintering at 1600°C for one hour under nitrogen flow. By combining different methods together this research achieved high densification. Compared with hot pressing, the pressureless sintering is less expensive, is able to produce complicated shapes and is isotropic in mechanical properties. However, the mechanical properties are not as good as those for hot pressing specimens because the densification of Al_2O_3 -SiC whisker composites by pressureless sintering is inhibited as a result of whisker interference with particle rearrangement and composite shrinkage.

Figure 46 shows the relationship between the sintered density and the green density. The higher green density tends to have the higher sintered density. Better packed green body has less inhibition in densification.

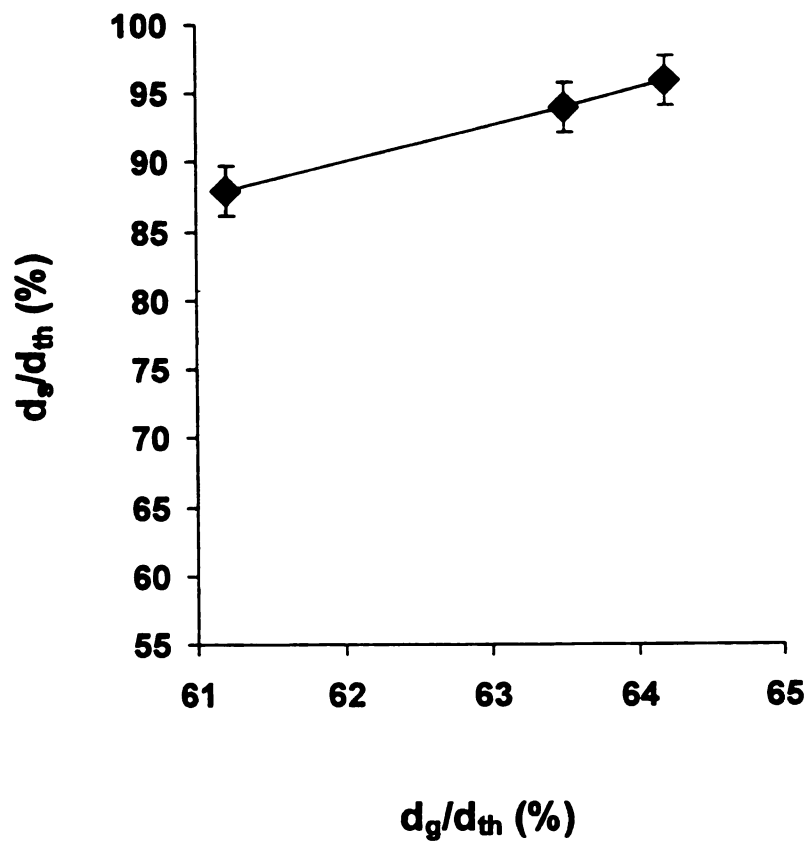


Figure 46 The sinterd density versus the green density (5-20 vol% SiC_w/Al₂O₃, 0.001N KNO₃, ball-milled, pH11, 2.5 vol% polyelectrolyte, 0.5 wt% MgO and 2 wt% Y₂O₃, sintered at 1600°C for 1h, nitrogen atmosphere).

3.5.2 Microstructure and EDX analysis

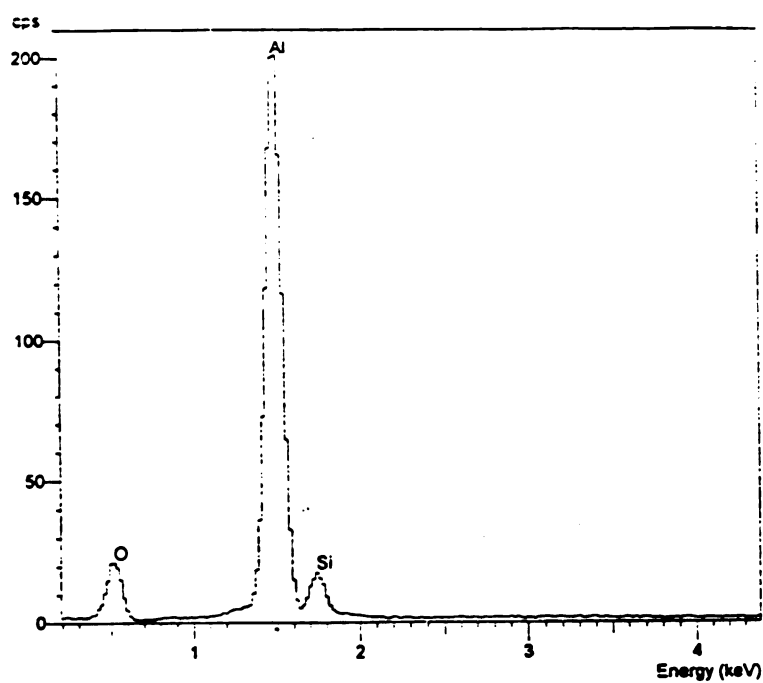
The final microstructure of 10 vol% SiC_w/Al₂O₃ composites revealed homogeneous near fully densified composites as evidenced by the whiskers being completely surrounded by the alumina matrix without space between them. Compositions of the composites were characterized by EDX. Figure 47 shows the Energy Dispersive X-ray Spectra of 10 and 20 vol% SiC_w/Al₂O₃ composites, respectively. Table 8 lists the EDX composition of 10 and 20 vol% SiC_w/Al₂O₃ composites (at%).

Table 8 EDX composition of 10 and 20 vol% SiC_w/Al₂O₃ composites

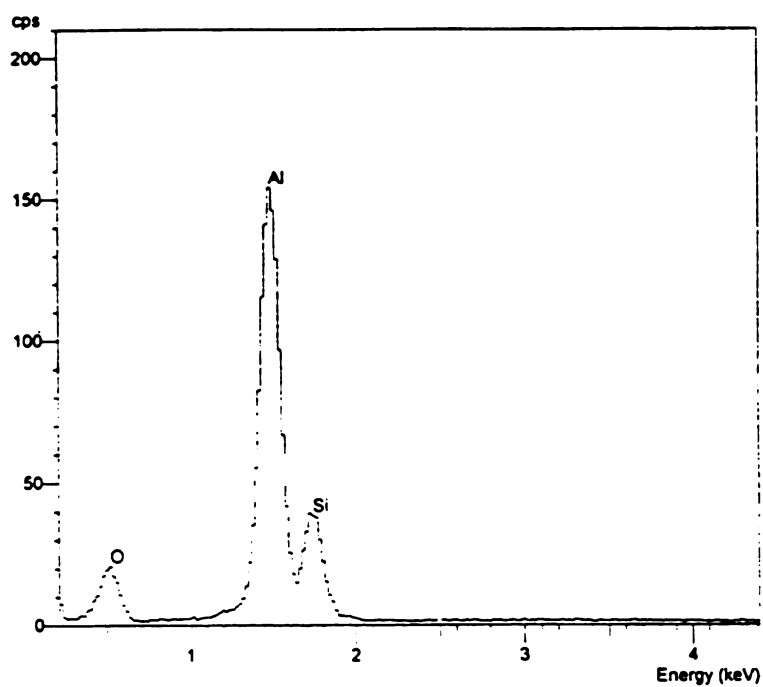
Element	10vol%	20vol%
Al (at%)	89.8	72.0
Si (at%)	10.2	28.0

The Si at% may be in error because of some nearby peaks of yttrium, aluminum and some impurities. The energy of the silicon peak is at 1.8keV, that of yttrium is at 1.95keV. The energy of the aluminum peak is at 1.5~1.6keV. The peaks of yttrium and aluminum are close to that of silicon. The yttrium peak is too small to be identified. Furthermore, since all the peaks have a width as big as 0.3keV, some overlaps between those of aluminum, yttrium and silicon are expected, and probably cause the measured silicon composition to be somewhat higher than the actual composition.

Figures 48 to 50 are SEM photomicrographs of the fracture surfaces of 5, 10, 20 vol% SiC_w/Al₂O₃ ball-milled composites. The fracture surfaces were taken in the Hitachi S-2500C SEM at an accelerating voltage of 15kV from broken chips made by a hammer.



a)



b)

Figure 47 EDX composition spectra: a) 10 vol% SiC_w/Al₂O₃, b) 20 vol% SiC_w/Al₂O₃ (0.001N KNO₃, ball-milled, pH 11, 2.5 vol% polyelectrolyte, 0.5 wt% MgO and 2 wt% Y₂O₃, sintered at 1600°C for 1h, nitrogen atmosphere).

Figure 48 shows cleavage fracture and transgranular fracture in the composite containing 5 vol% SiC_w whiskers. The photomicrograph of Figure 49 shows only transgranular fracture and whisker pullout in the composite containing 10 vol% SiC_w whiskers. The composite is very densified around SiC whiskers. Figure 50 shows transgranular fracture and pores. Figure 51 is a SEM photomicrograph of the fracture surface of 20 vol% SiC_w/Al₂O₃ composites that were not ball-milled. Figure 51 shows the mixed transgranular, intergranular, cleavage fractures for composite that were not ball-milled. The thermal expansion coefficient of the SiC whisker is only one half that of alumina. This thermal mismatch causes a tensile stress in the alumina matrix when the composites are cooled after sintering is complete. Baek and Kim [69] believe that this stress weakens the alumina matrix. They reported that dislocations were observed in the alumina matrix around the SiC whiskers in composites. The dislocations weakened the alumina matrix. Therefore, the appearance of transgranular fracture is an indication that dislocations around the SiC whiskers have weakened the alumina matrix.

Table 9 lists the different grain sizes for the 5 and 20 vol% SiC_w loadings. The grain sizes were measured on the SEM photomicrographs by the intercept method [72]. A straight line of a known length L was drawn on a photomicrograph of magnification M. The number of grains, g, which were intersected by the straight line, was counted. The following equation was then used to compute the grain size:

$$G.S = L/(g.M) \quad (21)$$

This method was repeated three times and an average value for the grain size was then computed.

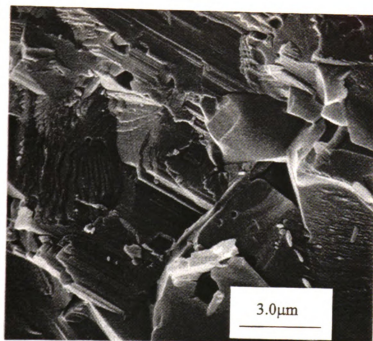


Figure 48 SEM photomicrograph of the fracture surface of 5 vol% SiC_w/Al₂O₃ (0.001N KNO₃, non-ball-milled, pH 4, no polyelectrolyte and sintering aids, sintered at 1600°C for 1h, nitrogen atmosphere).

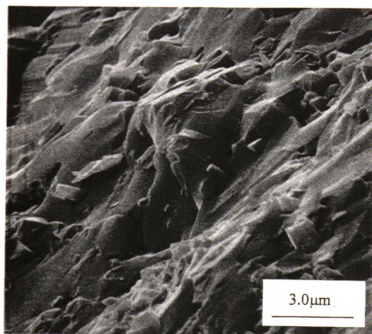


Figure 49 SEM photomicrograph of fracture surface of 10 vol% SiC_w/Al₂O₃ (0.001N KNO₃, ball-milled, pH 11, 2.5 vol% polyelectrolyte, 0.5 wt% MgO and 2 wt% Y₂O₃, sintered at 1600°C for 2h, nitrogen atmosphere).

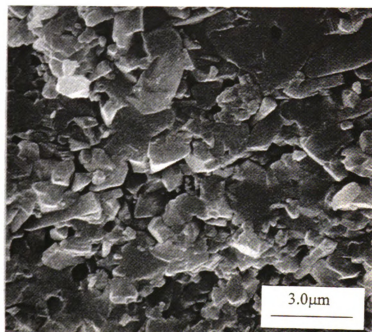


Figure 50 SEM photomicrograph of fracture surface of 20 vol% $\text{SiC}_w/\text{Al}_2\text{O}_3$ (0.001N KNO_3 , ball-milled, pH 11, 2.5 vol% polyelectrolyte, 0.5 wt% MgO and 2 wt% Y_2O_3 , sintered at 1600°C for 4h, nitrogen flow).

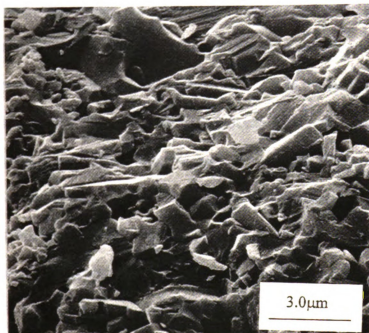


Figure 51 SEM photomicrograph of fracture surface of 20 vol% SiC_w/Al₂O₃ (0.001N KNO₃, non-ball-milled, pH 11, 2.5 vol% polyelectrolyte, 0.5 wt% MgO and 2 wt% Y₂O₃, sintered at 1600°C for 4h, nitrogen atmosphere).

Table 9 Different grain sizes for the 5 and 20 vol% SiC_w loading.

SiC _w loading (vol%)	5 (ball milled)	20 (ball milled)	20 (without ball milling)
Grain size(μm)	2.7	0.8	0.6

Figures 52 and 53 show SEM photomicrographs of fracture surfaces of 5 and 20 vol% SiC_w/Al₂O₃, respectively, sintered at 1600°C for 4 hours under nitrogen flow. A comparison of Figures 52 and 53 shows that the grain size has decreased as the whisker loading increased. The grain size decreases from 2.7μm to 0.8μm as the whisker loading increases from 5 to 20 vol%. Smith, Singh and Scattergood [70] believe that grain boundary pinning is responsible for the decrease in grain size at higher whisker loadings.

Figures 54 and 55 show SEM photomicrographs of the fracture surfaces of 20 vol% SiC_w/Al₂O₃ with and without ball milling, respectively. 0.8 μm and 0.6 μm grains were measured using the intercept method. A comparison of Figures 54 and 55 shows that ball milling the SiC whiskers serves to increase the size of grains slightly.

Another feature that is shown in the photomicrographs of the composites is the ragged fracture appearance. Baek and Kim [69] believe that the ragged fracture surfaces result from a crack deflection mechanism.

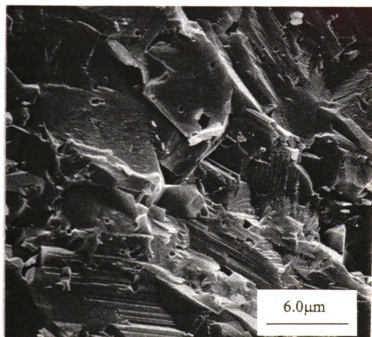


Figure 52 SEM photomicrograph of the fracture surface of 5 vol% SiC_w/Al₂O₃ (0.001N KNO₃, non-ball-milled, pH 4, no polyelectrolyte and sintering aids, sintered at 1600°C for 1h, nitrogen atmosphere).

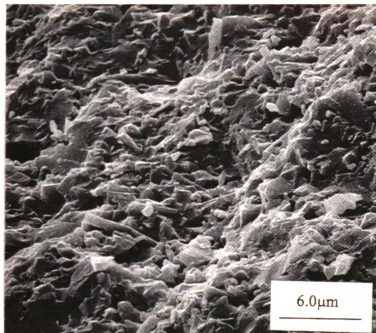


Figure 53 SEM photomicrograph of the fracture surface of 20 vol% SiC_w/Al₂O₃ (0.001N KNO₃, ball-milled, pH 11, 2.5 vol% polyelectrolyte, 0.5 wt% MgO and 2 wt% Y₂O₃, sintered at 1600°C for 4h, nitrogen atmosphere).

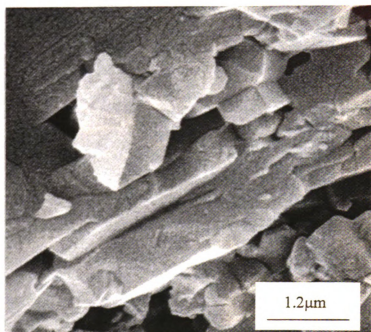


Figure 54 SEM photomicrograph of the fracture surface of 20 vol% SiC_w/Al₂O₃ (0.001N KNO₃, ball-milled, pH 11, 2.5 vol% polyelectrolyte, 0.5 wt% MgO and 2 wt% Y₂O₃, sintered at 1600°C for 4h, nitrogen flow).

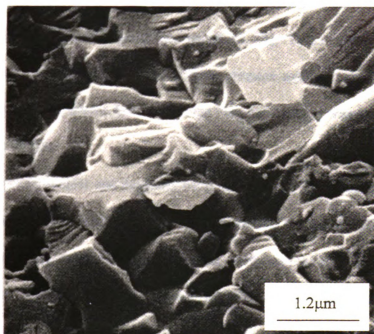


Figure 55 SEM photomicrograph of the fracture surface of 20 vol% SiC_w/Al₂O₃ (0.001N KNO₃, non-ball-milled, pH 11, 2.5 vol% polyelectrolyte, 0.5 wt% MgO and 2 wt% Y₂O₃, sintered at 1600°C for 4h, nitrogen atmosphere).

3.5.3 Hardness and Fracture Toughness

The critical value of the stress intensity factor required to initiate fracture, K_{IC} is a measure of the resistance of a material to fracture, i.e., of its toughness. Figures 56 and 57 show the fracture toughness and hardness for the composites as a function of ball milled whisker loadings with 2.5 vol% polyelectrolyte at pH 11 and sintered at 1600°C, one hour under nitrogen flow. Figure 56 shows a comparison of fracture toughness between this research and other published results [3, 74]. This research achieved good fracture toughness at lower temperature without pressure assisted consolidation. The high fracture toughness results from Oak ridge National Lab [3] were obtained by high pressure consolidation.

The fracture toughness and hardness were measured by the indentation technique [49]. The equations for calculating both the hardness and fracture toughness are discussed in the Experimental Procedure section. Although the hardness decreased as the whisker loading increased due to the whisker's ability to inhibit densification, the fracture toughness increased as whisker loading increased from $3.8 \pm 0.2 \text{ MPa}\cdot\text{m}^{1/2}$ to $6.3 \pm 0.2 \text{ MPa}\cdot\text{m}^{1/2}$ after adding 20 vol% ball milled SiC whiskers.

Figures 58 and 59 are comparisons of fracture toughness and hardness of $\text{SiC}_w/\text{Al}_2\text{O}_3$ composites with and without ball milling, respectively. Figure 58 shows that the fracture toughness decreased from $7.3 \pm 0.2 \text{ MPa}\cdot\text{m}^{1/2}$ to $6.3 \pm 0.2 \text{ MPa}\cdot\text{m}^{1/2}$ after ball milling 48 hours. This is due to the whisker pullout toughening mechanism in which the longer whisker length contributes to higher fracture toughness.

The fracture toughness of Al_2O_3 improved with increasing whisker content. The fracture toughness of the 20 vol% $\text{SiC}_w/\text{Al}_2\text{O}_3$ composite was twice that of the

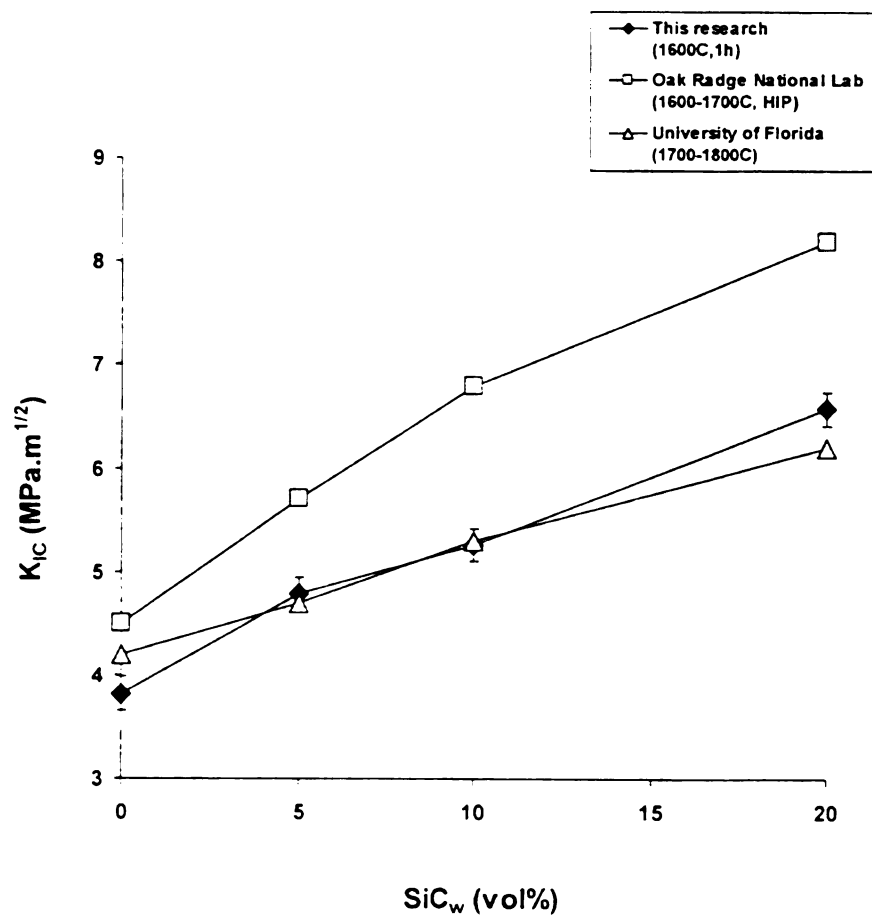


Figure 56 K_{IC} of composites versus whisker loading showing the comparison between this research and other published results [3, 74].

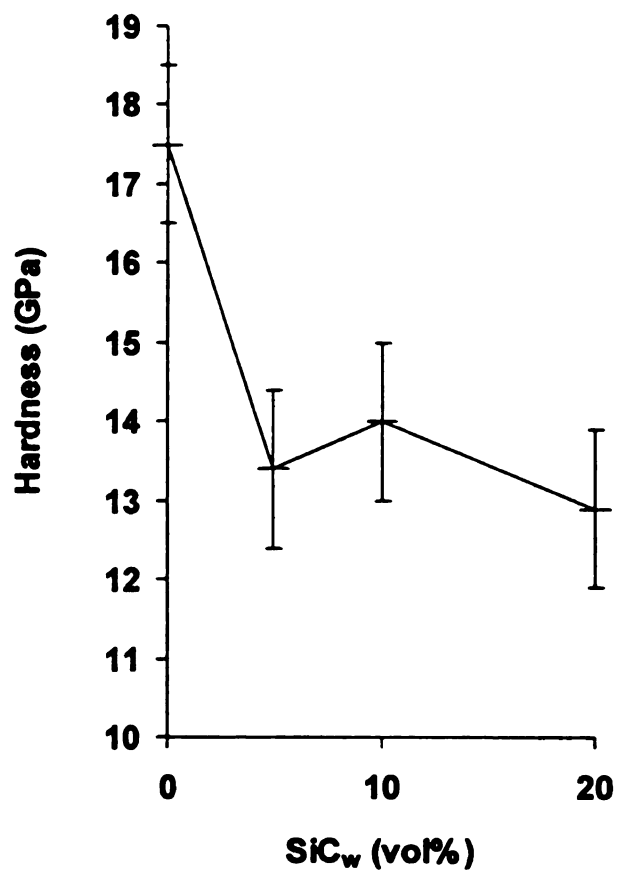


Figure 57 Hardness of composites versus whisker loading (0.001N KNO₃, ball-milled, pH 11, 2.5 vol% polyelectrolyte, 0.5 wt% MgO and 2 wt% Y₂O₃, sintered at 1600°C for 1h, nitrogen atmosphere).

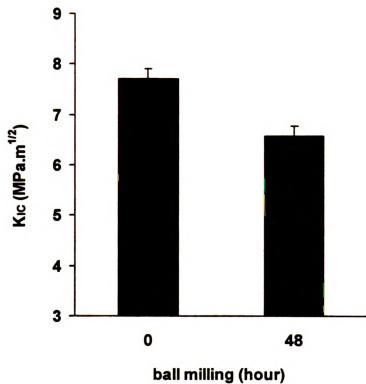


Figure 58 Comparison of K_{IC} of 20 vol% SiC_w composites with ball milling and without ball milling (0.001N KNO_3 , pH 11, 2.5 vol% polyelectrolyte, 0.5 wt% MgO and 2 wt% Y_2O_3 , sintered at 1600°C for 1h, nitrogen atmosphere).

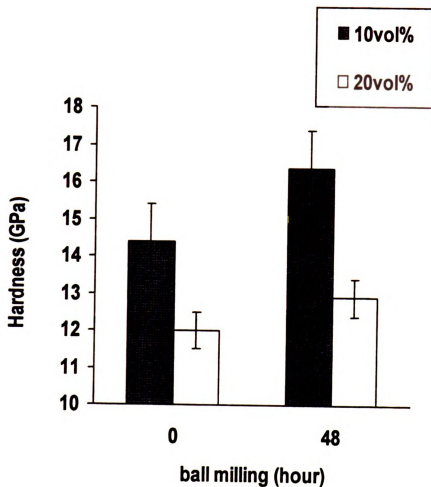
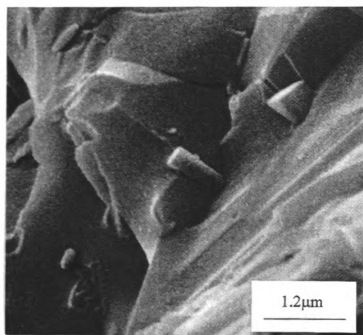


Figure 59 Comparison of Hardness of 10 and 20 vol% SiC_w composites with ball milling and without ball milling (0.001N KNO₃, pH 11, 2.5 vol% polyelectrolyte, 0.5 wt% MgO and 2 wt% Y₂O₃, sintered at 1600°C for 1h, nitrogen atmosphere).

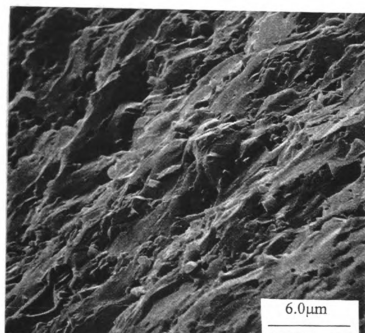
Al_2O_3 matrix. Baek and Kim [69] reported that the whisker length influenced the whisker protruding length of the fracture surface. Figure 58 shows that the composite without ball milling where the whisker lengths (5-15 μm) are longer has a higher fracture toughness in comparison to the composite having 20 vol% SiC whiskers (5-10 μm) which were ball milled. Figure 60 shows SEM photomicrographs of the fracture surface for the 10 vol% SiC_w/Al₂O₃ showing long whisker protruding length (a) and deep whisker pull-out holes (b).

The experimental data with theoretical prediction by Smith, Singh and Scattergood [70] showed that whisker pullout, whisker bridging, and crack deflection each contributed to the toughening increase. The present results agree with the conclusion of Smith, Singh and Scattergood as evidenced in the SEM photomicrographs of the fracture surfaces that show evidence of whisker pullout and crack deflection.

Figure 61 is a graph of hardness of the 10 vol% SiC_w/Al₂O₃ as a function of pH. At pH 11, the better densified composite has a higher hardness when compared to the composite processed at pH 4. Figure 62 is a plot of the hardness of 10 vol% SiC_w/Al₂O₃ at pH 11 as a function of Y₂O₃ content (sintered at 1600°C for one hour) which shows that the hardness increases as Y₂O₃ content increases. Hardness increases linearly at Y₂O₃ content less than 2 wt%, probably because the density of composites increases as Y₂O₃ content increases. However, when the Y₂O₃ content is increased over 2 wt%, the hardness value decreases slightly. Figure 63 is a plot of hardness of 10 vol% SiC_w/Al₂O₃ as a function of density (sintered at 1600°C for one hour). Figure 64 is a plot of hardness of 10 vol% SiC_w/Al₂O₃ at pH 4 as a function of ball milling time (sintered at 1600°C for one hour). Hardness also increases as the ball milling time increases. Figure 65 is a plot of



a)



b)

Figure 60 SEM photomicrographs of the fracture surface of 10 vol% SiC_w/Al₂O₃ showing (a) long whisker protruding length and (b) deep whisker pullout holes (0.001N KNO₃, ball-milled, pH 11, 2.5 vol% polyelectrolyte, 0.5 wt% MgO and 2 wt% Y₂O₃, sintered at 1600°C for 1h, nitrogen atmosphere).

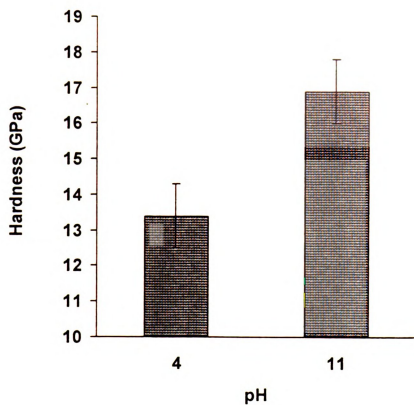


Figure 61 Hardness of 10 vol% SiC_w/Al₂O₃ as a function of pH (0.001N KNO₃, ball-milled, no polyelectrolyte and sintering aids at pH 4 and 2.5 vol% polyelectrolyte and 2 wt% Y₂O₃ at pH 11, sintered at 1600°C for 1h, nitrogen atmosphere).

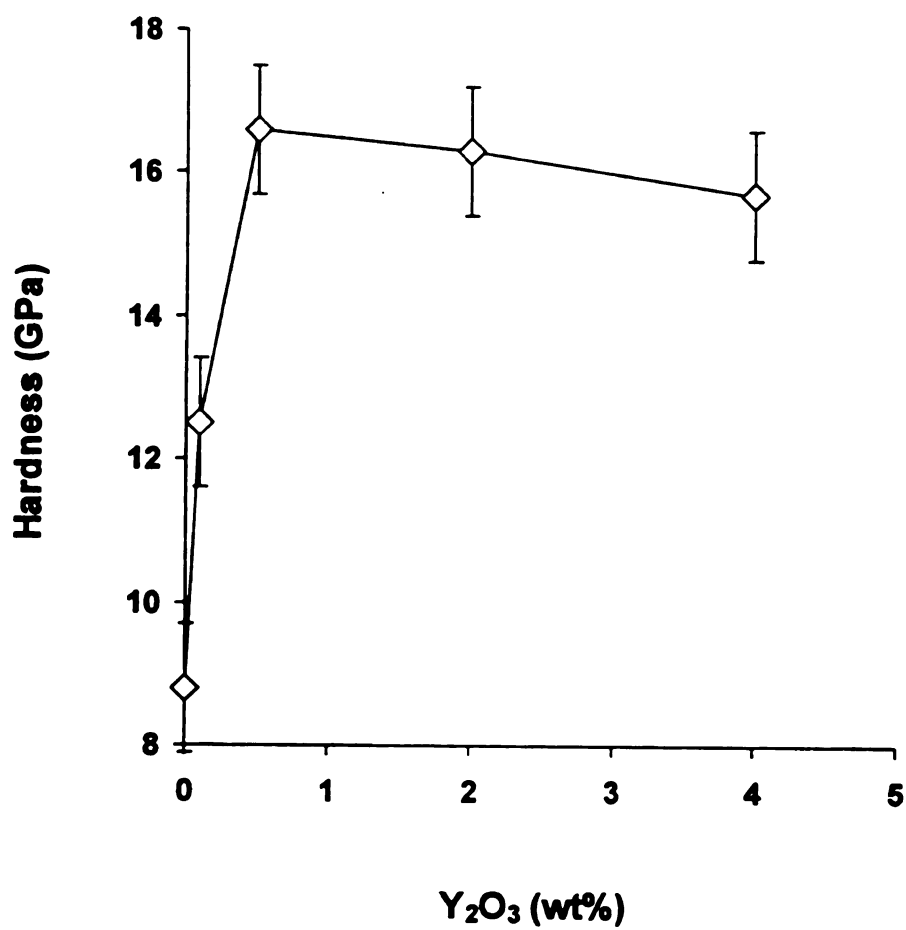


Figure 62 Hardness of 10 vol% SiC_w/Al_2O_3 as a function of Y_2O_3 content (0.001N KNO_3 , ball-milled, pH 11, 2.5 vol% polyelectrolyte, sintered at 1600°C for 1h, nitrogen atmosphere).

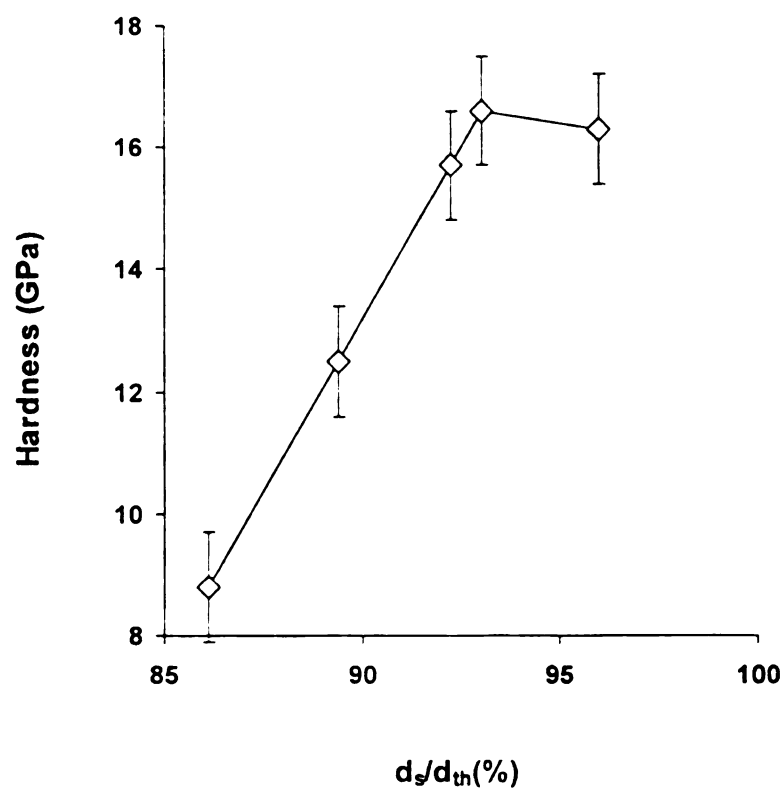


Figure 63 Hardness of 10 vol% SiC_w/Al₂O₃ as a function of density (0.001N KNO₃, ball-milled, pH 11, 2.5 vol% polyelectrolyte, 0.5 wt% MgO and 2 wt% Y₂O₃, sintered at 1600°C for 1h, nitrogen atmosphere).

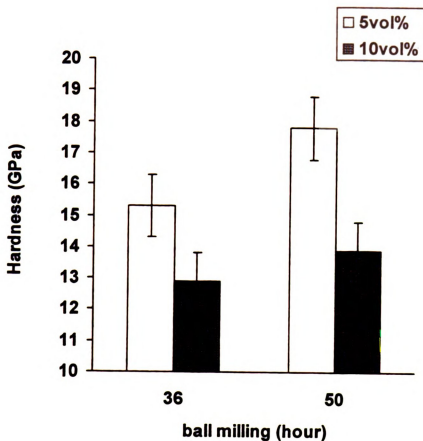


Figure 64 Hardness of 10 vol% SiC_w/Al₂O₃ as a function of ball milling time (0.001N KNO₃, ball-milled, pH 4, no polyelectrolyte and sintering aids, sintered at 1600°C for 1h, nitrogen atmosphere).

hardness of 10 vol% SiC_w/Al₂O₃ at pH 11 as a function of polyelectrolyte concentration (sintered at 1600°C for one hour). Hardness increases from 14.9±1.0 GPa to 16.3±1.0 GPa as the polyelectrolyte concentration increases from 1.2 to 2.5 vol%. Further increasing the polyelectrolyte concentration to 5 vol% causes a decrease in hardness from 16.3±1.0 GPa to 14.5±1.0 GPa. Figure 66 is a plot of hardness of 10 vol% SiC_w/Al₂O₃ at pH 4 as a function of solids loading (sintered at 1600°C for one hour). Hardness increases as the solids loading increases. Higher solids loading prevents the alumina and SiC whiskers from differential settling during slip casting and the resulting homogeneous distribution of powders and whiskers results in a higher hardness value.

In general, the hardness of composites changes closely as density changes. The higher density results in a higher hardness value. The processing which produces the best densification of composites also produces the highest hardness. However, there is no apparent relation between the fracture toughness and the density of the composites. The fracture toughness only depends on the volume percent and the length of the SiC whiskers and their interaction with the alumina matrix. The fracture toughness values are higher when the composites have higher non-ball-milled whisker loadings.

Figure 67 shows plots of K_{IC} and hardness of sintered composites versus the green density of their green bodies, respectively. The higher green density results in better densification that contributes to the higher hardness value. However, the higher green density is not a factor to achieve a higher fracture toughness value.

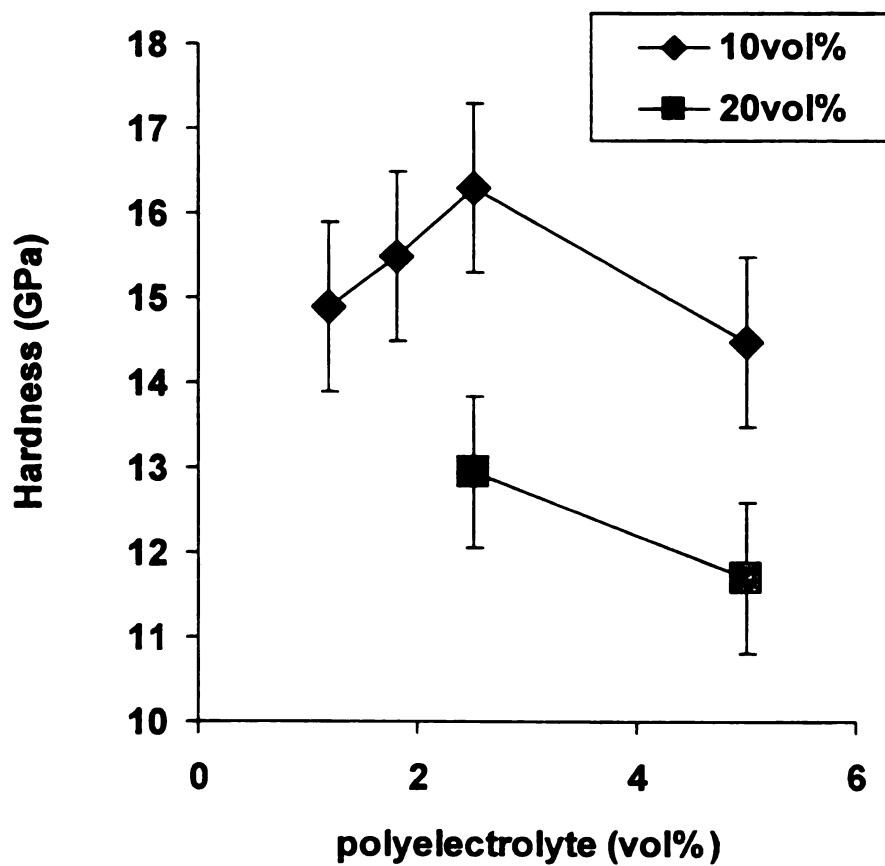


Figure 65 Hardness of 10 vol% SiC_w/Al₂O₃ as a function of polyelectrolyte concentration (0.001N KNO₃, ball-milled, pH 11, 0.5 wt% MgO and 2 wt% Y₂O₃, sintered at 1600°C for 1h, nitrogen atmosphere).

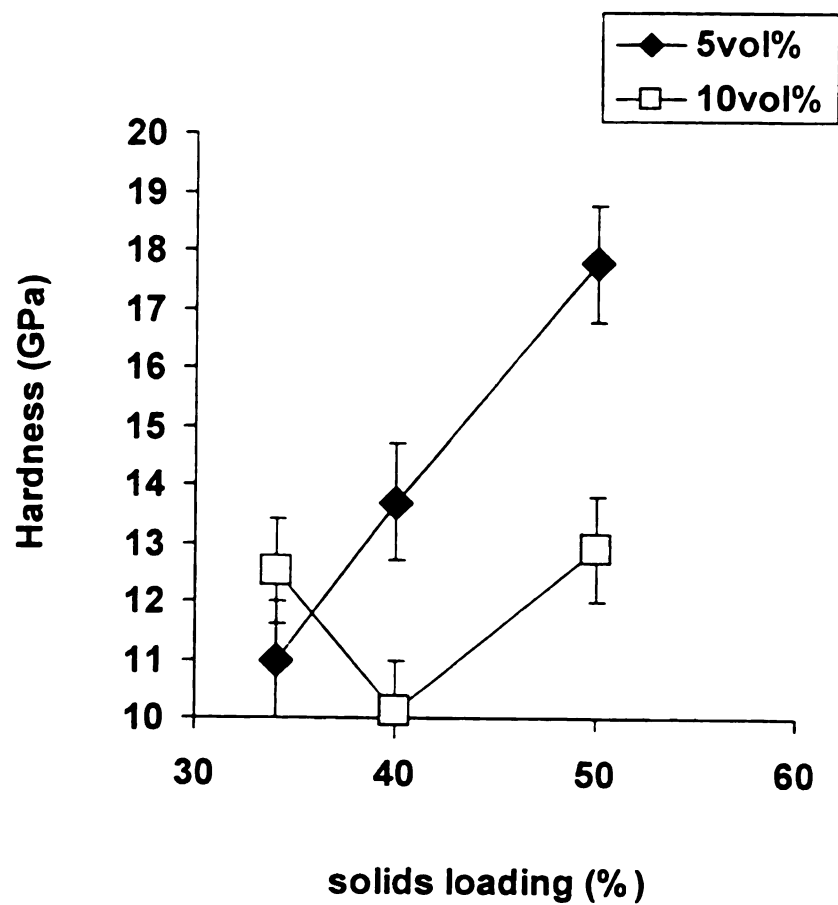


Figure 66 Hardness of 10 vol% SiC_w/Al₂O₃ as a function of solids loading (0.001N KNO₃, non-ball-milled, pH 4, no polyelectrolyte and sintering aids, sintered at 1600°C for 1h, nitrogen atmosphere).

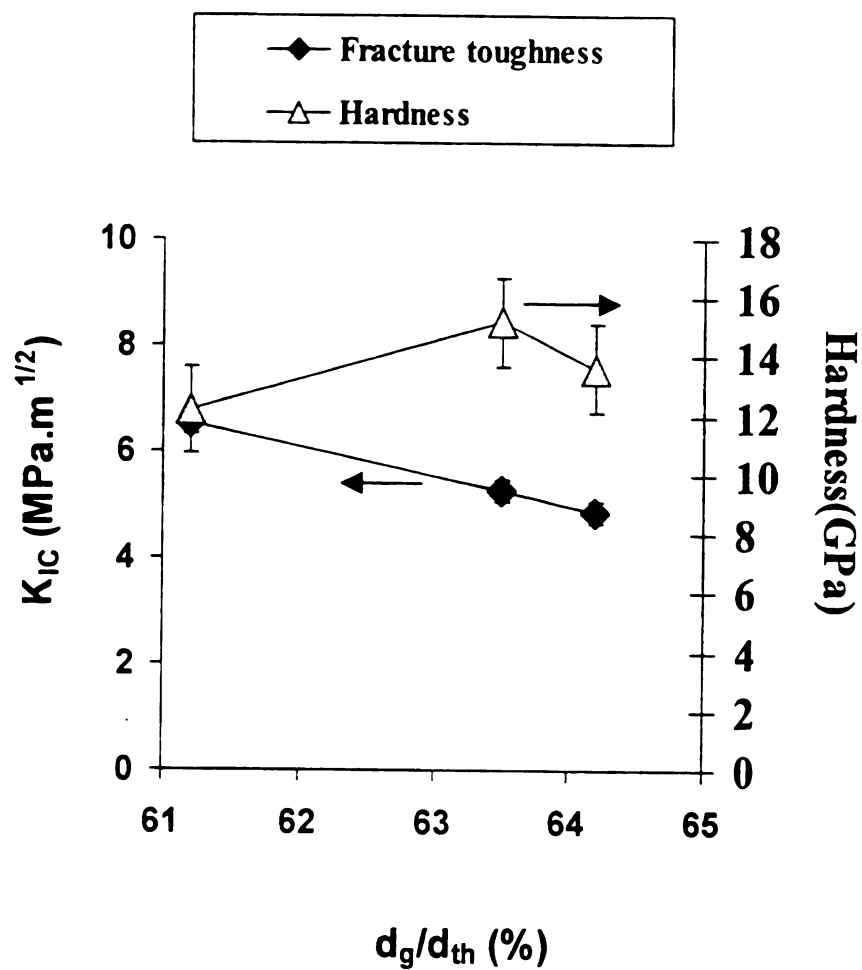


Figure 67 K_{IC} and hardness of sintered composites versus the green density of their green bodies, respectively (5-20 vol% SiC_w/Al_2O_3 , 0.001N KNO_3 , ball-milled, pH 11, 2.5 vol% polyelectrolyte, 0.5 wt% MgO and 2 wt% Y_2O_3 , sintered at 1600°C for 1h, nitrogen atmosphere).

CHAPTER 4 CONCLUSIONS

As the ethanol content increases, the absolute values of the zeta potential for both SiC_w and Al₂O₃ decrease. The iso-electric point likewise shifts for SiC_w to more basic pHs and to more acidic pHs for Al₂O₃ because ethanol does not ionize. This leads to a decrease in the predicted stability for both materials, as verified by sedimentation experiments. Ethanol and a mixture of ethanol and electrolyte reduce the dielectric constant of both suspensions. The zeta potential decreases due to the compression of the double layer. The stability ratio shows that the stability generally decreases as the ethanol content increases. But at pH<7, stability predictions indicate the interactions between SiC_w/SiC_w are more stable. This can be explained by assuming that the van der Waal's attractive energy, V_A , is higher in ethanol than in water [20]. Green body microstructure shows the SiC_w and Al₂O₃ to be well dispersed in the electrolyte and in the ethanol:electrolyte (1:1). The partially sintered microstructure again shows good dispersion of SiC_w.

Although the composite suspension is stable and codispersion of SiC_w and Al₂O₃ in the electrolyte and in a mixture of ethanol and electrolyte is good, densification was inhibited by the SiC whisker network effect. Comparing these observations with the results from the aqueous system, the sintered density of 10 vol% SiC_w/Al₂O₃ composites which were slip cast from a mixture of ethanol and electrolyte increased slightly from $2.84 \pm 0.08 \text{ g/cm}^3$ (~73% TD) to $2.92 \pm 0.08 \text{ g/cm}^3$ (~75% TD). This small change in density after adding ethanol indicated that ethanol was not sufficiently able to eliminate the formation of the whisker networks.

The combined use of different approaches has been proved successful in producing dense SiC_w/Al₂O₃ composites from aqueous suspensions. First, whiskers were ball milled to reduce the aspect ratio and to reduce the occurrence of whisker networks. Second, sintering aids were added to create a grain boundary liquid phase that relaxed the back stresses resulting from the network effect. Third, a polyelectrolyte was used to control the surface chemistry and to stabilize the mixed SiC_w/Al₂O₃ suspension and sintering aids, Y₂O₃ and MgO. Polyelectrolyte is able to reverse the zeta potential or shift the iso-electric point of alumina powders as shown by zeta potential results. For nonaqueous suspensions, further research should be directed to creating compatible processing ranges by choosing suitable sintering aids and an appropriate polyelectrolyte to match the stable pH ranges of Al₂O₃ and SiC_w.

Homogeneous SiC_w/Al₂O₃ green bodies with densities of 2.55±0.07 g/cm³ (~65% TD) were obtained. Bulk densities of 3.80±0.06 g/cm³ (96% TD), 3.79±0.06 g/cm³ (97% TD), and 3.40±0.07 g/cm³ (89% TD) were obtained at 1600°C under nitrogen flow for composite samples containing 5, 10 and 20 vol% SiC whiskers, respectively. Bulk densities of the 10 vol% SiC_w/Al₂O₃ composites were 3.79±0.06 g/cm³ (97% TD) at pH 11 and 3.66±0.07 g/cm³ (94% TD) at pH 4, respectively. pH 11 was determined to be the optimum processing pH value for SiC_w/Al₂O₃ composites with sintering aids (2 wt% Y₂O₃ and 0.5 wt% MgO) and 2.5 vol% polyelectrolyte (ammonia salt of polymeric carboxylic acid). pH 11 was selected according to the compatibility for all the components and the stability for the suspension system. The final microstructures revealed homogeneous and near fully densified composites containing 10 vol% SiC whiskers (97% TD).

The effects of the SiC whisker aspect ratio, the content of Y_2O_3 and polyelectrolyte were examined. The whisker aspect ratio reduction had a more dramatic effect on achieving dense composites in 20 vol% SiC whisker in comparison to 5 or 10 vol% SiC whisker composites. High densities with 10 vol% SiC whisker were attainable without aspect ratio reduction. Sintered densities increased as Y_2O_3 content increased. For 5 and 10 vol% SiC_w/Al_2O_3 , respectively, the densities remained almost constant at Y_2O_3 addition greater than 0.5 wt% and 2 wt%, respectively. 2.5 vol% polyelectrolyte stabilized the suspensions and resulted in high densities of the composites. However, further addition of polyelectrolyte past the adsorption saturation limit served to leave excess polyelectrolyte in suspension and this excess polyelectrolyte lowered the densities of the composites due to depletion flocculation.

The hardness of composites changes closely as density changes. The higher density results in a higher hardness value. The processing which produces the best densification of composites also produces the highest hardness. The fracture toughness only depends on the vol% and the length of the SiC whiskers and their interaction with the alumina matrix. The fracture toughness values are higher when the composites have higher non-ball-milled whisker loadings. Although the hardness decreased as whisker loading increased due to the whisker's ability to inhibit densification, the fracture toughness increased as the whisker loading increased. The fracture toughness of Al_2O_3 was remarkably improved with increasing whisker content. The fracture toughness of the 20 vol% SiC_w/Al_2O_3 composite was twice the fracture toughness of the Al_2O_3 matrix. The fracture toughness of the 20 vol% SiC_w/Al_2O_3 composite decreased from 7.3 ± 0.2 $MPa \cdot m^{1/2}$ to 6.3 ± 0.2 $MPa \cdot m^{1/2}$ after ball milling SiC whiskers.

REFERENCES

REFERENCES

- [1] P. F. Becher and G. C. Wei, *Am. Ceram. Soc. Bull.*, 63, C-267-69 (1984).
- [2] G. C. Wei and P. F. Becher, *Am. Ceram. Soc. Bull.*, 64[2], 298-304 (1985).
- [3] T. N. Tiegs and P. F. Becher, *Am. Ceram. Soc. Bull.*, 66[2], 339-42 (1987).
- [4] R. Rice, p126-135 in *Advanced Ceramic Processing and Technology*, Edited by J. G. P. Binner, Vol.1, NOYES PUBLICATIONS, Park Ridge, New Jersey, 1990.
- [5] F. F. Lange, B. I. Davis and I. A. Aksay, *J. Am. Ceram. Soc.* 66, 407-08 (1983).
- [6] S. Lio, M. Watanabe, M. Matsubara and Y. Matsuo, *J. Am. Ceram. Soc.* 72[10], 1880-84 (1989).
- [7] B. V. Deryaguin and L. Landau, *Acta Physicochim. URSS*, 14, 633 (1941).
- [8] E. J. W. Verwey and J. T. G. Overbeek, *Theory of the Stability of Lyophobic Colloids*, Elsevier, Amsterdam, 1948.
- [9] J. T. G. Overbeek, in H. R. Kruyt (Ed.), *Colloid Science*, Vol. I, Elsevier, Amsterdam, 1952.
- [10] J. Lyklema, *Advan. Colloid Interface Sci.*, 2, 65-114 (1968).
- [11] P. Sarkar and P. S. Nicholson, *J. Am. Ceram. Soc.*, 79[8], 1987-2002 (1996).
- [12] S. N. Heavens, p262 in *Advanced Ceramic Processing and Technology*, Edited by J. G. P. Binner, Vol.1, NOYES PUBLICATIONS, Park Ridge, New Jersey, 1990.
- [13] G. Gouy, *J. Phys.*, 9(4), 457, (1910); *Ann. Phys.*, 7(9), 129 (1917).
- [14] D. L. Chapman, *Phil. Mag.*, 25(6), 475 (1913).
- [15] R. Hogg, T. W. Healy and D. W. Fuerstenau, *Trans. Faraday Soc.*, 62, 1638 (1966).
- [16] B. A. Wilson and M. J. Crimp, *Langmuir*, 9, 2836-43 (1993).
- [17] B. V. Derjaguin, *Kolloid-z*, 69, 155 (1934).
- [18] B. V. Derjaguin, *Acta Physicochim. URSS*, 10, 33 (1939).
- [19] H. Kallmann and M. Willstatter, *Naturwiss.*, 20, 952 (1932).

- [20] A. Bleier, J. Am. Ceram. Soc., 66, C79 (1983).
- [21] J. T. G. Overbeek, In Colloid Science Volume 1: Irreversible Systems; Elsevier, New York, 1952.
- [22] R. Hogg, T. W. Healy and D. W. Fuerstenau, Trans. Faraday Soc. 62,1638 (1966).
- [23] R. J. Hunter, Foundation of Colloid Science, Vol.1, p419, Clarendon Press, Oxford, 1987.
- [24] R. J. Hunter, Zeta Potential in Colloid Science, Academic Press, New York, 1981.
- [25] D. E. Brooks, J. Colloid Interface Sci. 43, 670, 687, 700, 714 (1973).
- [26] P. C. Hidber, T. J. Graule and L. J. Gauckler, J. Am. Ceram. Soc., 78[7], 1775-80 (1995).
- [27] R. W. O'Brien, J. Fluid Mech. 71, 190 (1986).
- [28] R. W. O'Brien, J. Fluid Mech. 81, 212 (1990).
- [29] M. J. Crimp, Colloidal Characterization of Silicon Carbide and Silicon Nitride. M.S. thesis, Case Western Reserve University, 1985
- [30] J. Cesarano III and I. A. Aksay, J. Am. Ceram. Soc., 71[f12] 1062-67 (1988).
- [31] J. Homeny, W. Vaughn and M. K. Ferber, Am. Ceram. Soc. Bull., 66[2], 333-38 (1987).
- [32] J. R. Porter, F. F. Lange and A. H. Chokshi, Am. Ceram. Soc. Bull., 66[2], 343-47 (1987).
- [33] S. M. Smith, J. P. Singh and R. O. Scattergood, J. Am. Ceram. Soc., 76[2], 497-502 (1993).
- [34] H. Liu, M. E. Fine and H. S. Cheng, J. Am. Ceram. Soc., 77[1], 179-85 (1994).
- [35] T. N. Tiegs and D. M. Dillard, J. Am. Ceram. Soc., 73[5], 1440-42 (1990).
- [36] C. Hu and M. N. Rahaman, J. Am. Ceram. Soc., 76[10], 2549-54 (1993).
- [37] M. D. Sacks, H. Lee and O. E. Rojas, J. Am. Ceram. Soc., 71[5], 370-79 (1988).
- [38] A. Takashi, T. Yasuhiro, M. Yohtaro and Y. Eiichi, J. of Ceram. Soc. of Japan, 100[1167], 1297-303 (1992).

- [39] C. Cheng-Chih, Y. Fu-Su, Y. S. C. Max, Proc. Third 93 Int. Offshore Polar Eng. Conf. 380-85, 1993.
- [40] A. L. Stuijts, p1 in Ceramic Microstructure'76; Edited by R. M. Fulrath and J. A. Pask, Wesview Press, Boulder, 1977.
- [41] G. Y. Onoda and L. L. Hench, Ceramic Processing Before Firing, Wiley, New York, 1978.
- [42] A. Roosen and H. K. Bonen, J. Am. Ceram. Soc., 71, 250 (1988).
- [43] A. O. Boschi and E. Gilbart, p75 in Advanced Ceramic Processing and Technology, Edited by J. G. P. Binner, Vol.1, NOYES PUBLICATIONS, Park Ridge, New Jersey, 1990.
- [44] Data provided by the manufacturers (Tokai Carbon Co. of Tokyo, Japan, Sumitomo Industries, New York and Rhone-Poulenc Basic Chemicals Company)
- [45] B. A. Wilson, M. S. Thesis, "Prediction of Colloidal Suspension Stability for SiC/Si₃N₄ and FeAl/Al₂O₃ Fiber Systems Using Material and System Parameters", Michigan State University, 1992.
- [46] E. D. Case, Private Communication.
- [47] G. R. Anstis, P. Chantikul, B. R. Lawn, and D. B. Marshall, J. Am. Ceram. Soc., 64 [9], 533-43 (1981).
- [48] A. G. Evans and E. A. Charles, J. Am. Ceram. Soc., 59 [7-8], 371-72 (1976).
- [49] A. G. Evans, pp. 112-35 in Fracture Mechanics Applied to Brittle Materials. Edited by S. W. Freiman. Am. Soc. Test. Mater. Spec. Tech. Publ. 678, 1978.
- [50] J. P. Singh, K. C. Goretti, D. S. Kupperman, J. L. Routbort and J. F. Rhodes, Advanced Ceramic Materials, 3[4], 357-60 (1988).
- [51] D. W. Richerson, Modern Ceramic Engineering: Properties, Processing and Use in Design, M. Dekker, New York, 1992.
- [52] B. I. Lee and U. Paik, Ceramic International, 19, 214 (1993).
- [53] W. H. Tuan, E. Gilbart and R. J. Brook, J. Mat. Sci. 24, 1062-68 (1989).
- [54] S. J. Barclay, J. R. Fox and H. K. Bowen, J. Mat. Sci. 22, 4403-06 (1987).
- [55] T. Garino, J. Am. Cer. Soc. 75[3], 514-18 (1992).

- [56] R. K. Bordia and G. W. Scherer, pp872-86 in *Ceramic Transactions, Vol. 1, Ceramic Powder Science II, B*. Edited by G. L. Messing, E.R. Fuller, and H. Hausner. American Ceramic Society, Westerville, OH, 1988.
- [57] F. F. Lange, *J. Mater. Res.*, 2[1], 59-65 (1987).
- [58] J. V. Milewski, *Adv. Ceram. Mater.*, 1[1], 36-41 (1986).
- [59] K. T. Faber and A. G. Evans, *Acta Metall.*, 31[4], 565-76 (1983).
- [60] K. J. Konsztowicz, *Ceram. Eng. Sci. Proc.*, 11[7-8], 695-708 (1990).
- [61] O. Sudre and F. F. Lange, *J. Am. Ceram. Soc.*, 75[3], 519-24 (1992).
- [62] O. Sudre, G. Bao, B. Fan, F. F. Lange, and A. G. Evans, *J. Am. Ceram. Soc.*, 75[3], 525-31 (1992).
- [63] E. M. Levin, C. R. Robbins and H. F. McMurdie, *Phase Diagrams for Ceramists*, The American Ceramic Society, Ohio, pp165, Figure 2586, 1969.
- [64] K. R. Karasek, S. A. Bradley, J. T. Donner, H. C. Yeh, J. L. Schienle and H. T. Fang, *J. Am. Ceram. Soc.* 72[10], 1907-13 (1989).
- [65] T. Graule, P. Hidber, and L. J. Gauckler, pp. 299-305 in *Euro-Ceramics, Vol. II, Basic Science and Processing of Ceramics*. Edited by G. Ziegler and H. Hausner. Deutsche Keramische Gesellschaft e. V., Koeln, Germany, 1993.
- [66] Information provided by the manufacturer (Rohm and Haas Company).
- [67] *CRC Handbook of Chemistry and Physics*, ed. by D. R. Lide, CRC Press, 1990
- [68] P. Hidber, T. Graule, and L. J. Gauckler, pp. 247-54 in *Handbook on Characterization Techniques for the Solid-Solution Interface*. Edited by J. A. Adair, J. A. Casey, and S. Venigalla. American Ceramic Society, Westerville, OH, 1993.
- [69] Y. K. Baek and C. H. Kim, *J. Mat. Sci.*, 24, 1589-93 (1989).
- [70] S. M. Smith, J. P. Singh and R. O. Scattergood, *J. Am. Ceram. Soc.*, 76[2], 497-502 (1993).
- [71] P. C. Hidber, T. J. Graule, and L. J. Gauckler, *J. Am. Ceram. Soc.*, 79[7], 1857-67 (1996).
- [72] Dept. of Materials Science and Mechanics, Michigan State University, MSM 250 Lab Manual, 1995.

[73] M. D. Sacks, H. W. Lee and O. E. Rojas, Ceram. Eng. Sci. Proc. 9 [7-8], 741-54 (1988).

[74] H. W. Lee and M. D. Sacks, J. Am. Ceram. Soc., 73[7], 1894-1900 (1990).

MICHIGAN STATE UNIV. LIBRARIES



31293018017313